TECHNISCHE
UNIVERSITÄT
WIEN

VIENNA
UNIVERSITY OF
TECHNOLOGY

DIPLOMARBEIT

Development and Test of the Cooling System for the ATLAS Hadron Tile Calorimeter

ausgeführt am
Atominstitut
der österreichischen Universitäten
und am
CERN, Genf

unter der Anleitung von
Ao. Univ. Prof. Dr. Christian Fabjan

durch

Gerolf Schlager

Matrikelnummer 9525067
geboren am 24. Mai 1977 in Salzburg
Pyhrnstrasse 43, A-4563 Micheldorf

Genf, am 8. September 2002

Kurzfassung

Der ATLAS Detektor ist ein Universalexperiment für Proton-Proton Kollisionen, der für den Large Hadron Collider (LHC) am CERN gebaut wird. Der ATLAS Tile Hadron Kalorimeter (Tilecal) wird verwendet um die Energie von Jets mit einer Auflösung von $\Delta E/E = 50\%/\sqrt{E} \oplus 3\%$, für $\mid \eta \mid < 3$ zu messen.

Diese Diplomarbeit präsentiert Ergebnisse von Versuchen mit Prototypen des Tilecal Kühlungssystems, die im Zuge meines Aufenthaltes im Rahmen des 'Technical Student Program' am CERN durchgeführt worden sind. Die gewonnenen Erkenntnisse tragen massgeblich zum Design des endgültigen Kühlungssystems des ATLAS Tile Kalorimeters bei.

Das Verhalten des Kühlungssystems, das für die Kalibration der Tilecal Module verwendet wird, wurde für verschiedene Parameter wie Temperaturstabilität und Betriebssicherheit geprüft. Ausserdem wirkte ich bei der Analyse des Signalverhaltens des Kalorimeters für unterschiedliche Kühlwassertemperaturen mit. Die Resultate legten die notwendigen Rahmenbedingungen hinsichtlich Temperaturstabilität während des Betriebes von ATLAS fest.

In weiteren Versuchen ermittelte ich den Einfluss der Umgebungstemperatur auf das Kühlungssystem und auf die vorgesehenen, nicht isolierten Kühlungsrohre. Durch den ersteren wurde ein Einfluss der Umgebungstemperatur festgestellt und konnte minimiert werden. Der andere führte zur endgültigen Festlegung des verwendeten Rohrtyps für die Kühlung in Tilecal.

Weiters konnte der Leistungsverbrauch der Elektronik in den Tilecal Modulen erstmals mit endgültigen Komponenten von mir gemessen werden. Es war mir auch möglich die Effizienz des Kühlungssystems und die ideale Strömungsgeschwindigkeit des Kühlwassers während des Betriebes zu ermitteln. Diese Tests ermöglichten eine bessere Abschätzung des Bedarfs eines Kühlungssystems für das ATLAS Myon Spektrometer.

In Hinblick auf zukünftige Wartungsarbeiten untersuchte ich das Temperaturverhalten im Inneren der Tilecal Module bei abgeschalteter Kühlung. Ausserdem ermittelte ich die Absoluttemperaturen von wichtigen elektronischen Komponenten während des Betriebes.

Ein Kühlungsprototyp in Originalgrösse wurde eigens entworfen und gebaut um vorgesehene Komponenten zu testen, Berechnungen zu überprüfen und ein Kontroll- und Überwachungssystem zu entwickeln. Ich wirkte mit an den elektrischen Installationen, an der Entwicklung eines Überwachungssystems und an der Analyse genommener Daten.

Zusätzlich war ich während der Testbeam Perioden im Jahr 2002 verantwortlich für das verwendeten Tilecal Kühlungssystem. Ich übernahm Arbeitsschichten und half weiters mit, ein Überwachungssystem für die Niederspannungsversorgung der Module zu entwickeln und einen Alarm für die Hochspannungsversorgung der Photovervielfacher zu implementieren.

Die Ergebnisse dieser Arbeit wurden bereits teilweise in einer 'ATLAS Internal Note' [32] veröffentlicht und eine weitere Veröffentlichung in Form einer 'Internal Note' folgt im Herbst 2002.

Abstract

The ATLAS detector is a general-purpose experiment for proton-proton collisions designed to investigate the full range of physical processes at the Large Hadron Collider (LHC). The ATLAS Tile Hadron Calorimeter is designed to measure the energies of jets with a resolution of $\Delta E/E = 50\%/\sqrt{E} \oplus 3\%$, for $\mid \eta \mid < 3$.

This thesis presents the detailed studies which were carried out with prototypes of the Tilecal cooling system during my year as technical student at CERN. The results will be used to validate and to determine the final design of the cooling system of the ATLAS Tile calorimeter.

The performance of the cooling unit built for the calibration of Tilecal modules was evaluated for various parameters like temperature stability and safety conditions during operation. Additionally I contributed to the analysis of the calorimeter response for different cooling temperatures. These results determined the constraints on the operation conditions of the cooling system in terms of temperature stability that will be needed during ATLAS operation.

Furthermore I carried out tests to evaluate the effect of ambient temperature on the cooling system and on the foreseen non-isolated cooling pipes. Due to the first test a dependence on ambient temperature was found and could be minimised. The latter test resulted in the final decision of the type of tube which will be used for the final cooling system.

In another test I measured the total power dissipated by the electronics of the Tilecal modules using for the first time final components. I was able to determine the efficiency of the cooling system and the ideal flow rate during real operation conditions. These tests also allowed to better define the needs of a cooling system for the ATLAS muon chambers that will be located nearby.

For future maintenance purposes of Tilecal I studied the temperature increase inside the Tilecal modules with the cooling disconnected. Additionally I studied the absolute temperatures in the front end electronics of the Tilecal modules during normal operation and without cooling.

A special full-scale prototype of the Tilecal cooling system was designed and installed to test the forseen components, to check the calculations for pressure and flow, to develop the control system and to study the performance stablitity during several months of operation. I participated in the electrical installation, in the development of the control system and in the analysis of data taken during the operation of the system.

Besides I was responsible for the cooling system during the three Tilecal beam calibration periods in 2002. I participated actively in the testbeam program in the form of shifts and helped to implement a monitoring system of the low voltage power supplies and several alarms for the high voltage of the photomultipliers.

The results of this thesis are already partially published in an ATLAS internal note [32] and another note will be published in autumn 2002.

Acknowledgement

I am most grateful to my two supervisors Ana Maria Henriques Correia and Chris Fabjan. Chris Fabjan awakened my interest for coming to CERN and regularly gave me a push to the right direction. I thank him for having an open ear for my problems and providing help in his straightforward way. Ana guided me through my year as technical student. She always had time for me and gave me advice and motivation whenever I needed it. It was a great pleasure to work in her group.

Very special thanks go to Philippe Grenier. He helped me with my first steps in the scientific world and gave me the feeling that I can accomplish something. He also showed me that work can be a funny if you are with the right people. Thank you, Philippe!

I also owe many thanks to Fernando Varela Rodriguez. We discussed a lot and he never stopped teaching me things I didn't know. I think the real reason he taught me so much was to make sure that I don't come too often and ask him something! Moreover now I know when to come for a Spanish dinner if it 'starts' at 8h.

A lot of thanks to Pierre Bonneau who never became tired of my questions, specially during the 'hot phase' of my thesis. And also thanks to Stephane Berry for helping when I needed him.

I would like to thank Amelia Maio and Lluis Miralles with whom I shared the office in the last year. They kept motivating me by showing interest in the work I did and they were always open for discussions about physics, engineering, flowers or olives. Thanks for the company!

Many thanks to Tomas Davidek who explained me a lot about Tilecal, linux and latex and who patiently waited for me on the way up the Jura!

Also many thanks to Calin Alexa for the endless discussions about life, music, the best way to drink tequila, art and everything else.

I am very grateful to the ATLAS Tilecal community giving me the possibility to spend an extremely interesting year at CERN. Special thanks to Rupert Leitner, Stanislav Nemecek, Agostinho Gomes, Richard Teuscher, Andrei Karioukhine and Bob "I've got a job for you" Stanek. All of them gave me the feeling to be part of the team and were always open for questions. Thank you very much!

I also want to thank the many friends I had here at CERN. Without them

Contents

x

Chapter 1

LHC and experiments

1.1 The Large Hadron Collider

Already in the mid-1980's, before LEP was operating, scientists around the world started to think about an accelerator which would be capable to exceed the energies provided by LEP in order to probe even deeper into the properties of matter. Finally, in 1994, the construction of CERN's Large Hadron Collider (LHC) was officially approved. This year marks the birth of the world largest and most powerful accelerator which will provide proton-proton collisions at energies 10 times greater and collision rates 100 times higher than any previous machine. LHC will be installed in the existing LEP tunnel. According to the current schedule the LHC is planned to be operational in the year 2007.

1.1.1 Design Parameters

The LHC is a proton-proton collider with a total collision energy in the centre of mass of 14 TeV and a designed luminosity of 10^{34} cm^{-2} s^{-1} [1]. It will be installed in the existing 27 km LEP tunnel and is scheduled to be operational in 2007. It will also provide heavy ion collisions (Pb) with a centre of mass energy of more than 1000 TeV.

Since the LHC will accelerate two proton beams moving in opposite directions, two separate beam pipes are needed. They are both combined in a so-called 'two-in-one' design, whereby the two beam pipes and their corresponding sets of coils are inserted in a unique structure and in a single cryostat.

In order to reach the desired energies very high magnetic fields have to be applied. In existing accelerators like the Tevatron (Fermilab) and HERA (Desy) NbTi superconductor magnets are used and cooled with normal liquid helium to temperatures slightly above 4.2 K. But the resulting magnetic fields of ~ 4 T are too weak for the LHC. The only way to reach the required fields of above 8 T and still to be able to keep the well-proven fabrication methods of NbTi superconductors is to cool the magnets at much lower temperature (< 2 K). Therefore
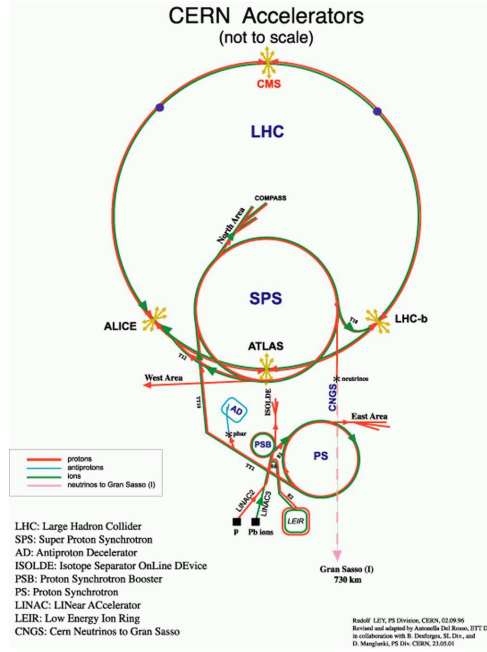
Figure 1.1: *Overview over the CERN accelerator facilities. Before the particles are finally injected into the LHC they are pre-accelerated in other accelerators.*

the superconducting NbTi magnets of LHC will be cooled with superfluid helium at 1.9 K and a maximum operational field of 8.4 T can be reached. In total 1232 dipole magnets will be used each with a length of approximately 14.2 m.

Production rate of particles

The production rate (R) of particles is a statistical process and depends basically on two factors: On the kind of particles and their energy (represented by the cross section - σ) and the luminosity (L) following the formula [3]

$$R = \sigma L \tag{1.1}$$

The luminosity is defined by the beam parameters:

$$L = \frac{1}{4\pi} \frac{N^2 f}{\sigma_x \sigma_y t} \tag{1.2}$$

N - the number of protons per bunch, f - the fraction of bunch positions containing protons, t - the time between bunches, σ_x and σ_y - the transverse dimensions of the Gaussian beam profiles (horizontal and vertical).

All those parameters have to be optimised in order to get a satisfying production rate of the processes of interest. LHC is designed to work with a bunch
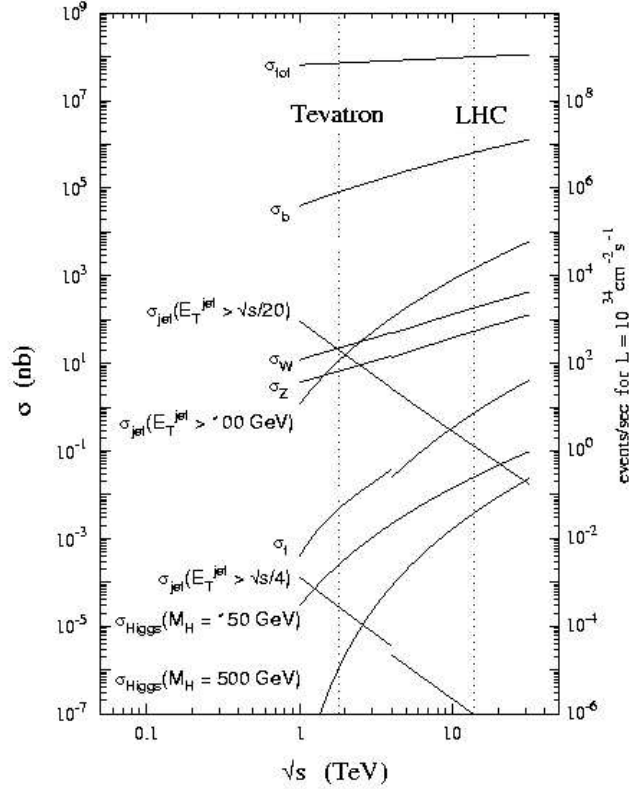
Figure 1.2: *Expected cross sections of selected channels for proton-proton collisions as a function of the centre of mass energy.*

crossing time of $t = 25$ ns and each bunch will contain around $N = 11^{10}$ protons. With 80% of the total number of bunch positions filled ($f = 0.8$) and a bunch dimension of some μm a final luminosity of 10^{34} cm^{-2} s^{-1} can be reached. Taking the cross section of the proton-proton collisions into account there will be about 23 interactions in the centre of the detectors per bunch crossing.

This high rate environment makes great demands on the different techniques and technologies used for the four LHC detectors.

1.1.2 Physics expected at the LHC

One of the major goals of LHC is to search for the Higgs Boson. But also searches for supersymmetric particles, high precision measurements of Standard Model parameters and studies of CP-violation are on the schedule [6]. Some of the major physic topics are listed below.

Higgs particle

In the Standard model particles receive their mass via the Higgs mechanism. According to this, the whole space is filled with a 'Higgs field', and by interacting with this field particles obtain their masses. The Higgs field has at least one particle associated with it, the Higgs Boson.

Direct searches have excluded a Higgs boson mass below 114.3 GeV [1] [2] and theory requires it not to be heavier than ~ 1 TeV making the whole mass range accessible for LHC. Depending on the mass of the Higgs there are different signatures which can be observed. Some of the best experimental signatures for observing the Higgs are expected to be:

- for $m_H < 120$ GeV

$$H \rightarrow \gamma\gamma$$
$$H \rightarrow b\bar{b}$$

- for $m_H < 800$ GeV

$$H \rightarrow ZZ^{(*)} \rightarrow 4l$$
$$H \rightarrow ZZ \rightarrow ll\nu\bar{\nu}$$

- for $m_H \sim 1$ TeV

$$H \rightarrow WW \rightarrow l\nu jj$$
$$H \rightarrow ZZ \rightarrow lljj$$

Supersymmetry (SUSY)

Supersymmetry is an extension of the Standard Model where every particle has a supersymmetric partner. If SUSY exists many of the supersymmetric particles like squarks and gluinos are expected to be produced at the LHC.

High-precision top quark measurements

The LHC has a significant potential of performing high-precision top quark measurements. Even at moderate luminosity during the first years of operation (10^{33} cm^{-2} s^{-1}), about 10^7 $t\bar{t}$ pairs will be produced per year which provides excellent statistics for high-precision measurements.

B-physics

Although not particularly designed for it, LHC will work as a b-quark factory. The available statistics will allow a very wide programme of b-quark physics to be performed. One of the LHC experiments - LHCb - is specially dedicated to b-physics.

---

[1] at 95% confidence level

1.1.3 Experiments at the LHC

In total four experiments will be installed at the LHC accelerator: ATLAS, CMS, ALICE and LHCb.

ATLAS and CMS are general-purpose proton-proton detectors with similar physical goals but different design. The main difference lies in the magnet system which strongly influences the geometry of the detectors. ALICE and LHCb are two specialised detectors. ALICE is specialised on heavy ion (Pb-Pb) collisions and LHCb focuses on B-physics and the connected CP-violation.

More details about the detectors can be found in the technical design reports: for ATLAS [6], for CMS [7], for ALICE [8] and for LHCb [9].

CMS

The **C**ompact **M**uon **S**olenoid (CMS) is also a multi-purpose experiment for proton-proton collisions. With a length of 22 m and a height of 15 m CMS is smaller than ATLAS. Nevertheless its weight is almost two times the weight of ATLAS, namely 12500 t. The detector will be built around a 13 m long superconducting solenoid with a bore of 5.9 m and a nominal magnetic field strength of 4 T, leading to a compact design of the muon spectrometer and giving the detector its name **Compact** Muon Solenoid.

ALICE

ALICE (**A L**arge **I**on **C**ollider **E**xperiment) is a general-purpose heavy-ion detector designed to investigate Pb-Pb collisions. With ALICE it will be possible to study the physics of strongly interacting matter and the quark-gluon-plasma. That will give us a better view about our universe as it was shortly after the big bang. An interesting aspect of ALICE is that it will reuse parts of the L3 experiment which was running at LEP

LHCb

LHCb is designed to study CP violation and other rare phenomena in decays of B mesons. These studies are not only interesting for elementary particle physics but also for cosmology, in order to explain the dominance of matter over antimatter in our universe. LHCb can work at much lower luminosity (10^{32} cm^{-2} s^{-1}) than the nominal luminosity of LHC. Therefore it is possible to reach its full physics potential already in the beginning of LHC operation.

ATLAS

The ATLAS experiment is explained more in detail in the following section. The cooling system of the ATLAS Hadron Calorimeter (Tile Calorimeter) is subject

of this thesis.

1.2   The ATLAS detector

The ATLAS (**A T**oroidal **L**HC **A**pparatu**S**) detector is a general-purpose experiment for proton-proton collisions designed to investigate the full range of physical processes at the Large Hadron Collider (LHC) ([6], [10]). With its length of 45 m and its height of 22 m it is one of the largest and most elaborate particle physics experiments ever built. Its main parts are the Inner Detector, surrounded by a super-conducting solenoid, the Calorimeters and the Muon Spectrometer with its gigantic superconducting air-core toroids. All those components together will have a weight of 7000 t. It is designed to work at high luminosity (10^{34} cm^{-2}s^{-1}) and beam crossings every 25 ns. To meet the high requirements of this environmental conditions highly sophisticated technologies and specialised materials are required. The start of operation is planned for 2007.

Major focus of interest will be the origin of mass. The detector optimisation is therefore guided by issues such as sensitivity to the largest possible Higgs mass range. Other important objectives are the search for heavy W- and Z-like objects, for supersymmetric particles, for compositeness of the fundamental fermions, as well as the investigation of CP violation in B-decays, and detailed studies of the top-quark. Furthermore the detector can cope with a broad variety of possible physics processes and is expected to have a high potential for the discovery of new, unexpected physics.

The predefined objectives resulted in the following basic design criteria.

- Very good electromagnetic calorimetry for electron and photon identification and measurements, and additionally full-coverage hadronic calorimetry for accurate jet and missing transverse energy (E$_T{}^{miss}$) measurements;

- High-precision muon momentum measurements at the highest luminosity using the external muon spectrometer alone;

- Efficient tracking at high luminosity for high-p$_T$ lepton-momentum measurements, electron and photon identification, τ-lepton and heavy-flavor identification, and full event reconstruction capability;

- Maximum geometrical coverage

- Triggering and measurements of particles at low-p$_T$ thresholds, providing high efficiencies for most physics processes of interest at LHC;

Information about the overall detector concept can be found in the ATLAS TDR for Technical Co-ordination [5] and in the (already older) ATLAS technical
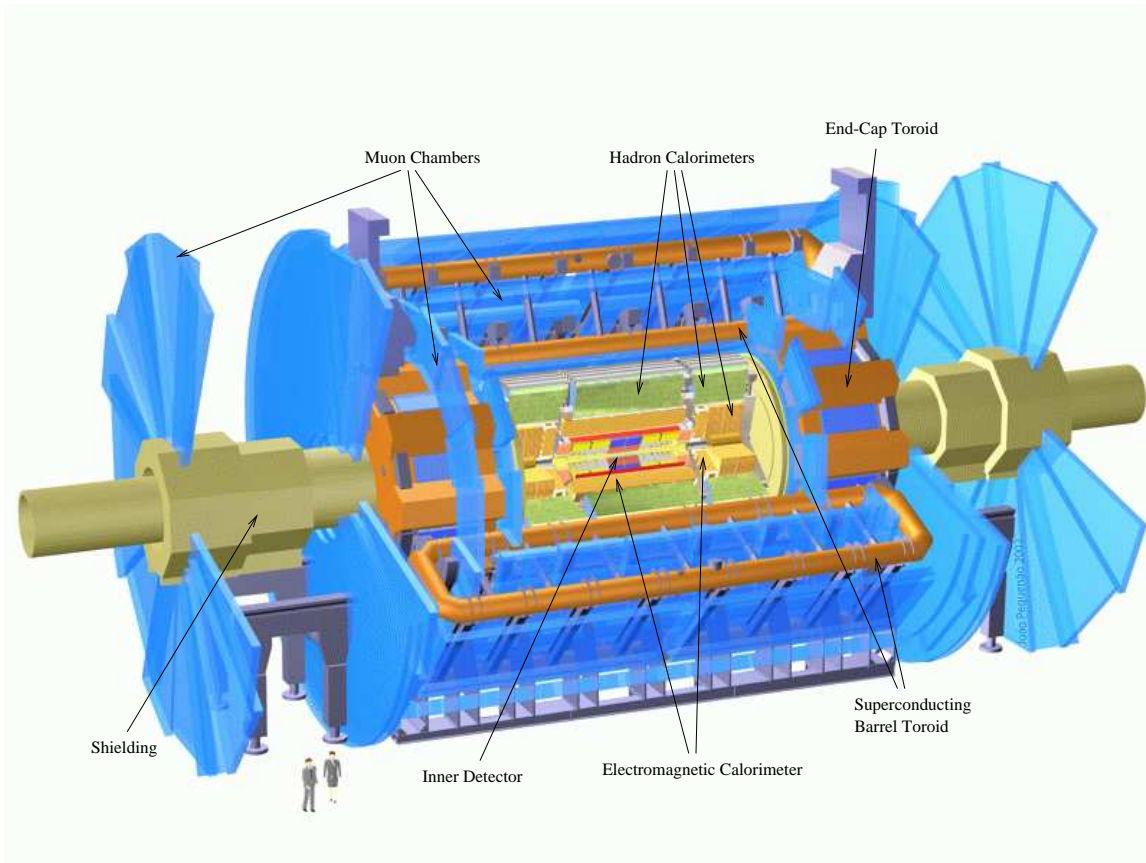
Figure 1.3: *Overall layout of the ATLAS detector. With its length of 45 m, its height of 22 m and its weight of 7000 t it is one of the largest and most elaborate particle physics experiments ever built.*

proposal [6]. More detailed information about the ATLAS subsystems is presented in the Technical Design Report (TDR) of each subsystem ([11], [12], [13], [14], [15], [16]).

1.2.1 Inner Detector

The ATLAS Inner Detector consists of three different types of detectors. At the inner radii two high-resolution detectors are used to perform high-precision measurements whereas at the outer radii continuous tracking elements are installed. The three parts of the inner detector are contained in the central solenoid which provides a nominal magnetic field of 2 T. Its purpose is to provide pattern recognition, momentum and vertex measurements and electron identification. The Inner Detector is shown in figure 1.4.

Given the momentum and vertex resolution requirements and the very large
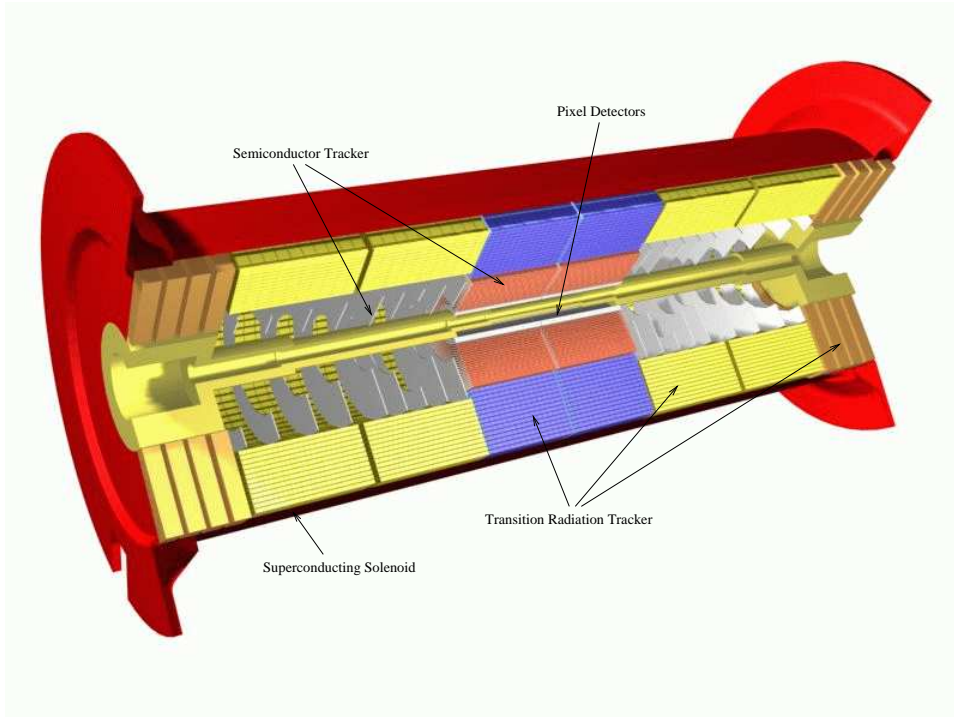
Figure 1.4: *Cut through the ATLAS Inner Detector. It consists of two different high-resolution detectors at the inner radii (Pixel Detector, Semiconductor Tracker (Silicon Strip Detector)) and continous tracking elements (Transition Radiation Tracker) at the outer radii.*

track density at the LHC, fine-granularity detectors are needed to be able to work with sufficient precision. Therefore semiconductor tracking detectors were chosen, applying pixel and silicon microstrip (SCT) technologies. Since the amount of material should be minimal and because of the high costs the number of precision layers must be limited. At the outer radii a straw tube tracker (TRT) is implemented to provide continuous track-following with little material per point and at low costs. A typical particle track crosses three pixel layers and eight strip layers (equal to four space points). Additionally around 36 tracking points are provided by the straw tubes. Although the straw tubes have a lower precision per point compared to the silicon trackers, they compensate that by a large number of measurements and a higher average radius. Those techniques combined give a robust pattern recognition and a very good resolution.

The outer radius of the Inner Detector cavity is 115 cm and its total length is 7 m. It is divided into one barrel part and two identical end-caps on either side. In the barrel, the high-precision layers are arranged in concentric cylinders around the beam axis. In the end-caps they are mounted on discs perpendicular to the beam axis. Similarly the straw tubes are adjusted parallel to the beam

axis in the barrel and radially in the endcaps. The layout of the Inner Detector provides a full tracking coverage over $\eta \geq 2.5$ [2]

Pixel Detector

The pixel detector consists of three barrels at radii of 4 cm, 10 cm and 13 cm and five discs on each side between radii of 11 cm and 20 cm. A total of 140 million pixels, each 50 μm in Rϕ direction and 300 μm in z, will provide the required resolution for the highly crowded LHC environment. Since the pixel detector is the innermost component its readout chips have to withstand over 300 kGy of ionising radiation and over $5\mathrm{x}10^{14}$ neutrons per cm^2 during 10 years of operation.

Silicon Strip Detector

The silicon strip detector (SemiConductor Tracker - SCT) in the barrel part is mounted on carbon-fibre cylinders at radii of 30.0, 37.3, 44.7 and 52.0 cm. In the end-caps they are mounted in up to three rings onto nine wheels. The 61 m^2 of silicon detectors, with 6.2 million readout channels have a resolution of 16μm in Rϕ direction and 580 μ in z. Tracks can be distinguished if seperated by more than $\sim$ 200 μm.

Transition Radiation Tracker

The transition radiation tracker (TRT) is divided into a barrel section and several wheels in each end-cap. It consists of 420 000 straws, each with a diameter of 4 mm. Transition-radiation photons are created in a radiator between the straws and are used for electron identification. The drift-time measurement gives a spatial resolution of 170 μm per straw and two independent tresholds. These allow the detector to distinguish between transition-radiation hits and tracking hits. The TRT is operated with a special Xe-CO$_2$-CF$_4$ gas mixture. A primary concern was to obtain good performance at high occupancy and counting rates. This was achived with a small straw diameter and with isolation of the sense wires within individual gas volumes.

1.2.2 Magnet System

The ATLAS superconducting magnet system consists of a central solenoid (CS) providing the magnetic field for the Inner Detector and of three large air-core toroids generating the magnetic field for the Muon Spectrometer. The magnets are indirectly cooled by helium at 4.5 K which is provided by a central refrigeration plant located in the side cavern.

---

[2]The polar angle measured from the beam axis (Θ) is usually expressed in terms of pseudo-rapidity: $\eta = -ln(tan\frac{\Theta}{2})$

The CS is positioned in front of the EM calorimeter and has to be as thin as possible in order to achive the desired calorimeter performance. Therefore the CS is integrated in the LAr vacuum vessel, eliminating two additional vacuum walls. The nominal strenght of its central field is 2 T with a peak magnetic field at the superconductor of 2.6 T. It is energized by a 8 kA power supply.

The three air-core toroids are divided into one barrel toroid (BT) and two end-cap toroids (ECT). Each toroid consists of eight racetrack, double-pancake coils assembled symetrically around the beam axis. The coils of the barrel toroid are integrated in individual cryostats whereas the end-cap toroids are placed in one large cryostat each. The peak magnetic fields on the superconductors in the barrel toroid and end-cap toroid are 3.9 and 4.1 T respectively. The toroid coil system is powered by a 21 kA power supply.

To achive the desired high magnetic fields an aluminium-stabilised NbTi superconductor is used. It is housed in the center of an aluminium alloy casing to provide sufficient mechanical strenght. To avoid overheating of the coils an adequate and proved quench protection system has been designed.

1.2.3   Muon Spectrometer

The ATLAS muon spectrometer measures the magnetic deflection of muon tracks in the three large superconducting air-core toroid magnets. The layout is shown in figure 1.5. For this measurement it uses two types of trigger chambers and two types of high-precision tracking chambers.

A major constraint for the design of the muon spectrometer was the expected high level of particle flux in LHC. Trigger and reconstruction algorithms had to be optimized for the high radiation backgrounds, mostly neutrons and photons, produced from secondary interactions in the calorimeters, shielding material, beam pipe and LHC machine elements. The level of particle flux together with the selected benchmark processes defined the requirements for the spectrometer such as

- very good intrinsic resolution

- high rate capability

- adequate ageing properties

- sufficient granulatrity

- radiation hardness

The magentic field for the muon spectrometer can be seen consisting of three parts. In the barrel region ($| \eta | \leq 1.0$) the magnetic field is produced by the large barrel toroid. In the end-cap region ($1.4 \leq | \eta | \leq 2.7$) the tracks are bent
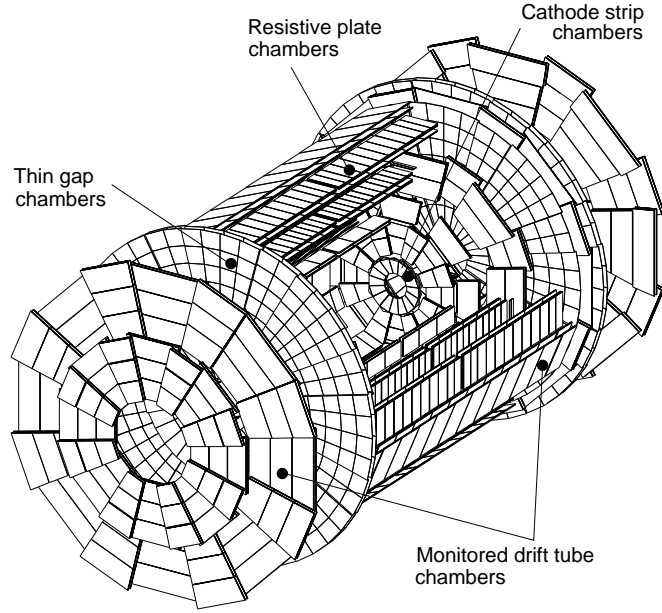
Figure 1.5: *The layout of the muon spectrometer is shown. It uses four different chamber technologies to measure the deflection of muon tracks in the magnetic field created by the three superconducting air-core toroids.*

by two smaller end-cap magnets. The region between $1.0 \leq |\eta| \leq 1.4$ is called transition region. There the magnetic bending is provided by the combination of the other two magnetic fields.

In the barrel region the muon chambers form three cylinders concentric with the beam axis. They are positioned at radii of about 5, 7.5 and 10 m. The end-cap chambers are arranged in four vertical discs at distances of 7, 10, 14 and 21-23 m from the interaction point. The outer muon chambers define the size of the ATLAS detector.

The high-precision muon track measurement is provided by the Monitored Drift Tubes (MDT) over most of the η-range. Only at large η and close to the interaction point, Cathode Strip Chambers (CSC) are used because of the demanding rate and background conditions. For the trigger system Resistive Plate Chambers (RPC) are used in the barrel and Thin Gap Chambers (TGC) in the end-cap regions. They cover the range $|\eta| \leq 2.4$. The trigger chambers serve three main purposes:

- identification of the bunch crossing and therefore requiring a better resolu-

tion than the LHC bunch spacing of 25 ns

- a trigger with well-defined p_T cut-off in moderate magnetic fields

- measurement of the coordinate in the direction orthogonal to the one measured by the precision chambers, with a resolution of about 5-10 mm

Monitored Drift Tube chambers

The MDT chambers consist of a 30 mm diameter aluminium tube with a central W-Re wire. They are operated at 3 bar absolut pressure with a non-flammable mixture of Ar-CO_2. They provide a maximum drift time of ~ 700 ns, excellent ageing properties and a singel-wire resolution of ~ 80 μm. The tube lenghts vary from 70 to 630 cm and the tubes are positioned orthogonal to the R-z plane in both the barrel and end-cap region. That allows a high-precision measurement of the axial coordinate (z) in the barrel and the radial coordinate (R) in the transition and end-cap region.

Cathode Strip Chambers

The CSCs are multiwire proportional chambers with symmetric cells. The cathode is segmented into strips orthogonal to the anode wires. Due to the avalanche effect around the anode wire, charge is induced into the cathode and by charge interpolation between neighbouring strips a high-precision measurement can be accomplished, resulting in resolutions better than 60 μm. The chambers are operated with a non-flammable mixture of Ar-CO_2-CF_4. Advantages of the CSC are small electron drift times, good time resolution, good two-track resolution and low neutron sensitivity. The measurement of the transverse coordinate is performed by the second cathode which consists of strips parallel to the anode wires.

Resistive Plate Chambers

The RPCs consist of a narrow gap formed by two parallel resistive plates. The gap is filled with non-flammable gas based on $C_2H_2F_4$. Through a high electric field between the plates, primary ionisation electrons are multiplied into avalanches and form a current of typical 0.5 pC. The signal is read out via capacitive coupling of metal strips on both sides of the chamber. Similar to the CSCs the cathode strips of one side are orthogonal to the ones on the other side to achieve a two coordinates measurement. Advantages of the RPCs are a simple mechanical structure as well as good transmission properties of the readout strips. Terminators on both ends avoid signal reflections resulting in excellent intrinsic time resolution.

Thin Gap Chambers

The TGCs are similar to multiwire proportional chambers but have slightly different dimensions. The chambers are operated with a highly flammable gas mixture of CO_2-nC_5H_{12}, therefore adequate safety precautions have to be taken. The electric field configuration and the small dimensions provide a short drift time and thus a good time resolution. Other advantages are the small sensitivity to mechanical deformations which lowers the costs, small dependence of the pulse height on the incident angle and nearly Gaussian pulse height distribution.

Alignement

The alignment of the muon spectrometer is another crucial point that has been taken care of. To achive the required momentum resolution a stabilisation of the dimensions and positions of the chambers at the 30 μm level has to be provided. However this is not possible over the large dimensions of the muon spectrometer. Therefore an optical alignment system was developed to monitor the chamber deformations and positions. This data will be used later for correction in the offline analysis.

1.2.4 Electromagnetic Calorimeter

The Electromagnetic (EM) Calorimeter, like other subdetectors, is divided into a barrel part ($| \eta | < 1.4575$) and two end-caps ($1.375 < | \eta | < 3.2$). It is a lead - Liquid Argon (LAr) calorimeter, highly granular and using accordion-shaped Kapton electrodes. The barrel calorimeter consists of two identical half-barrels, separated by a small gap at z = 0 whereas the two end-caps are divided into two coaxial wheels.

The main requirements for the LAr calorimeter are:

- large rapidity coverage to maintain excellent acceptance

- optimal segmentation for good electron and photon identification, position resolution and small electronic noise and pile-up contributions

- adequate dynamic range from 35 MeV to 3 TeV per cell

- excellent energy resolution

- sufficient calorimeter thickness to avoid shower leakage

- high angular resolution to measure the shower direction

To achieve the requirements for the high precision measurement in the region $| \eta | < 2.5$ the first sampling ($\sim$6 radiation lengts (X_0)) of the calorimeter is segmented into very narrow strips and plays the role of a 'preshower' detector.

13

With a pitch of ~ 4 mm in the η direction the preshower detector enhances the particle separation and provides a precise position measurement in η. The other two samplings as well as the end-caps have a coarser granularity, still satisfying the physics requirements.

The barrel EM calorimeter is placed inside a barrel cryostat, which surrounds the Inner Detector. The central solenoid which provides the magnetic field for the Inner Detector is integrated in the barrel cryostat in order to minimize the material in front of the EM calorimeter and to achieve the desired calorimeter performance. As a consequence the total material seen by an incident particle before the EM clorimeter is about 2.3 X_0 at $\eta = 0$ and increases with η because of the particle angle. The end-cap EM calorimeters are contained in two end-cap cryostats together with the hadronic end-cap EM calorimeter and the forward calorimeter. The total thickness of the EM calorimeter in the barrel and in the end-cap regions is > 24 X_0 and > 26 X_0 respectively.
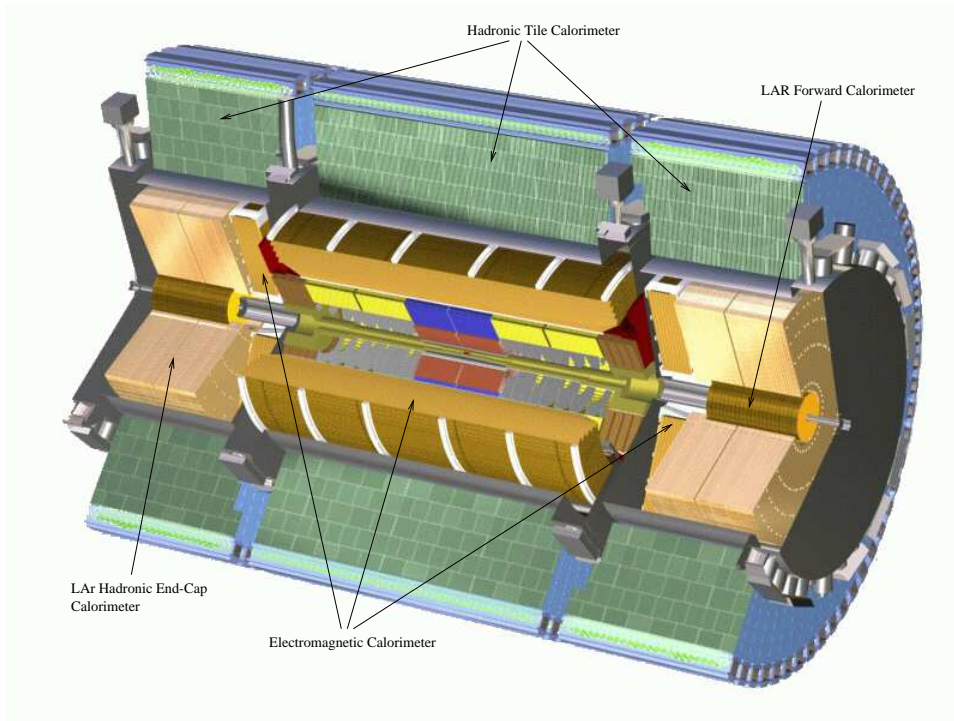
Figure 1.6: *Overview of the calorimeter system in ATLAS. Electromagnetic and Hadronic Calorimeters are shown. In the inner part the Inner Detector with its components is also visible.*

1.2.5 Hadronic Calorimeters

The Hadronic Calorimeters are adapted to the varying requirements and radiation environments in ATLAS. Therefore there are three different hadronic detectors, namely the Tile Calorimeter, the LAr Hadronic End-cap Calorimeter (HEC) and the LAr Forward Calorimeter (FCAL). HEC and FCAL were chosen for the larger pseudorapidities where higher radiation resistance is needed because of the intrinsically radiation-hard LAr technology.

The major goals of the hadronic calorimetry are:

- to identify jets and measure their energy and direction

- to measure the total missing transverse energy (E_T^{miss})

- to enhance the particle identification of the EM calorimeter by measuring quantities such as leakage and isolation

One important parameter to achieve this goals is the hadronic calorimeter thickness. Measurements and simulations showed that the total thickness of 11 interaction lenghts (λ) is sufficient to reduce puch through to the muon system and provide good containment for hadronic showers.

Tile Calorimeter

The Tile Calorimeter covers the range of $|\eta| < 1.6$. It uses a sampling technique with iron as absorber and scintillating tiles as active material. The tiles are placed perpendicular to the beam axis and are staggered in depth. The periodical structure consists alternately of a 3 mm thick tile and a 14 mm thick iron plate. Two sides of the scintillating tiles are read out by wavelength shifting (WLS) fibres into two separate photomultipliers (PMT).

The calorimeter is divided into one barrel and two extended barrels, each of the three made up of 64 modules. The gap between barrel and extended barrel provides space for cables, feedthroughs and service pipes. A more detailed description of the Tile Calorimeter is given in chapter 2.

LAr Hadronic End-Cap Calorimeter

The HEC covers the region $\sim 1.5 |\eta| < 3.2$. It is a copper - LAr calorimeter with parallel-plate geometry. Each HEC consists of two independend wheels of outer radius 2.03 m. The wheel nearer to the interaction point is built out of 25 mm copper plates whereas the second wheel which is farther away has a coarser granularity and uses 50 mm plates. Each wheel is made out of 32 modules. The weight of the first wheel is 67 tons, the second wheel has 90 tons. In summer 1999 the intrinsic energy resolution for pions was measured in the testbeam [17]:

$$\frac{\sigma}{E} = \frac{(76.2 \pm 0.9)\%}{\sqrt{E_0(GeV)}} \oplus (6.68 \pm 0.09)\% \qquad (1.3)$$

LAr Forward Calorimeter

The FCAL is designed to work at the range $3.1 < |\eta| < 4.9$, very close to the beam pipe. Therefore it has to cope with a particularly high level of radiation. It consists of a metal matrix with regularly spaced longitudinal channels filled with concentric rods and tubes. The rods are at positive high voltage while the matrix and the tubes are grounded. The FCAL is divided into three sections, the first one made of copper and the other two made of tungsten. The number of channels is 3584 for the total of both sides.

Chapter 2

ATLAS Hadron Calorimeter - Tilecal

2.1 Principles of calorimetry

In high energy physics a calorimeter is a device which measures the energy of incident particles. In principle the particles are absorbed by a large block of matter and their energy is transfered to the absorber. A part of the absorbed energy creates a signal which can be measured [18].

Because of its interaction with matter (electro-magnetic, strong or sometimes weak interaction) a high energy particle entering a calorimeter produces secondary particles with lower energy. If the energy of the produced particles is high enough a third generation of particles can be created, etc. The result is a particle shower or cascade which will propagate through the calorimeter. Once the energy of the particles falls below the threshold to produce new ones the remaining energy is transferred to the absorber via other processes like ionisation or excitation. A small fraction of this deposited energy is used to produce a detectable signal which is ideally proportional to the energy of the incoming particle and can be measured.

The important role of calorimeters in high energy physics can be understood on the basis of the following properties:

- The energy deposition by the shower development is a statistical process. The number of produced particles is in average proportional to the energy of the incident particle $<n> \sim <E>$. The resulting resolution behaves like

$$\frac{\sigma}{E} \sim \frac{\sqrt{n}}{n} = \frac{1}{\sqrt{n}} \sim \frac{1}{\sqrt{E}} \qquad (2.1)$$

  That means that the resolution improves with increasing energy with $1/\sqrt{E}$.

17

- Due to the propagation of the particle shower, the necessary depth of the calorimeter increases only with the logarithm of the energy of the incident particle $D \sim \ln E$. This allows a rather compact design of calorimeters.

- Calorimeters can detect charged as well as neutral particles.

- Calorimeters are 'fast' detectors. Signals can be read out between ~ 10 to 200 ns which allows operation at high particle rates and usage as selective trigger of events.

- A full geometric coverage of the calorimeter allows the measurement of missing transverse energy E_{miss}^T.

- The segmentation of the calorimeter gives additional spatial information about particles.

- The shower development is different depending on the nature of the incident particle and the materials used for the calorimeter.

2.1.1 Calorimeters

In general one has to distinguish between electromagnetic and hadronic calorimeters.

Electromagnetic and hadronic calorimeters

Electromagnetic calorimeters are optimised for particles like electrons and photons which create electromagnetic showers in the material. Those particles are absorbed and measured by the calorimeter but other particles like hadrons can easily pass it.

Therefore the electromagnetic calorimeter is usually followed by a hadronic calorimeter which is designed to measure the energy of hadrons. Unlike electromagnetic showers, in which the evolution of the shower undergoes a few well-understood processes, hadronic showers are rather complicated.

In detectors like ATLAS one can find both the electromagnetic and the hadronic calorimeters. This allows an optimised energy measurement for all produced particles according to their intrinsic properties and behaviour.

Homogeneous and sampling calorimeter

From the construction point of view a calorimeter can be built in two different ways: As a homogeneous calorimeter or as a heterogeneous (sampling) calorimeter.

Homogeneous calorimeter: Signals in homogeneous calorimeters are produced homogeneously in all their volume. Usually they are built out of specially grown crystals. Their important advantage is their high energy resolution which is also the reason that they are frequently used for high precision measurements.

Sampling calorimeter: Sampling calorimeters consist of alternating layers of passive (absorber) and active material. The absorber material (Fe, Pb, ...) has the task of absorbing most of the energy of particles and can be optimised for the detector requirements. In the active material (scintillators, gases, ...) a signal is produced by passing particles which can be measured and used to reconstruct the particle energy. Advantages of the sampling calorimeters are the very compact design and therefore a significant reduction in volume and price and the high effective density and the segmentation possibilities which allow excellent spatial resolution and therefore also better particle identification. A disadvantage is the lower energy resolution because only a small fraction of the incident particle energy is used to form a signal.

The Tile calorimeter is a sampling calorimeter.

2.1.2 The hadronic shower

The hadronic shower is very similar to the electromagnetic shower. The main difference is the more complex physics of hadron interactions [19]. The shower development in a hadronic cascade is governed by interactions between hadrons and nuclei of the absorber medium. Two main types of hadronic interactions with different time scales can be distinguished during evolution of the cascade:

- The interaction of a high energetic incident hadron with an absorber nucleus causes multiple production of secondary particles. The result is a fast development of the cascade with a typical time scale in the order of 10^{-22} s. The produced particles are mainly $\pi^{\pm}$ and π^0 but if the energy is sufficient also fast protons, neutrons and heavier nuclear fragments like α's are produced. The nucleus (or its remnants) is left in an excited state.

- The second phase is characterised by a slow and low energetic decay of excited nuclei produced in the previous phase within a time scale of about 10^{-18} s. The nucleus successively evaporates nucleons (thermal neutrons, protons, α's) and emits γ's during nuclear transitions. For very heavy elements like Uranium also nuclear fission may occur.

Some produced particles, like π^0, γ, η^0 and $e^{\pm}$ trigger an electromagnetic shower. Therefore a hadronic shower in general also consists of an electromagnetic component, its fraction fluctuating from event to event since the production of those particles depends on statistics.

Hadrons deposit their energy in the absorbing material basically in four different components:

- Electromagnetic component, mainly photons.

- Invisible energy due to nuclear breakup (binding energy) or particles that excape the detection (muons, neutrinos).

- Ionisation energy loss of charged particles.

- Low energy neutrons.

The fraction of the invisible energy can be as high as 40% of the total deposited energy. This fraction is lost for calorimetric purposes since it does not contribute to the detector signal.

2.1.3 The e/h ratio and calorimeter compensation

As already mentioned a hadron shower includes a hadronic and an electromagnetic component. Therefore the initial energy of the primary hadron initiating the shower is shared among two components [19]:

$$f_{em} = \frac{E_{em}}{E} \quad \text{and} \quad f_h = \frac{E_h}{E} \tag{2.2}$$

with

$$f_{em} + f_h = 1 \tag{2.3}$$

The two fractions f_{em} and f_h fluctuate from event to event depending on the number of π^0s produced.

Additionally the average fraction of the electromagnetic component in a hadronic shower $< f_{em} >$ increases with energy [25]:

$$< f_{em} >= 0.11 \ln E \quad (E \text{ in GeV}) \tag{2.4}$$

Since a part of the hadronic component cannot be detected (nuclear breakup), the signal of the electromagnetic component (e) is in general bigger than that of the non-electromagnetic (h) component giving a ratio of $e/h > 1$. Consequently also the signal produced by incident electrons (e) is in general bigger than that produced by hadrons (π) at the same energy, quantified with $e/\pi > 1$.

The e/h ratio cannot be measured directly but can be deduced from the energy dependent e/π ratio. Taking into account the average fraction of energy used for π^0 production ($< f_{em} >$), the following relation between the e/π ratio and the e/h ratio can be found:

$$\frac{e}{\pi}(E) = \frac{e}{e < f_{em} > + h(1 - < f_{em} >)} = \frac{e/h}{1 + (e/h - 1)0.11 \ln E} \qquad (2.5)$$

The equation shows that if $e/h = 1$ the ratio e/π is also equal to one and becomes energy independent. Then the hadronic signal is not dependent any more on the fluctuations of $< f_{em} >$.

In the case $e/h = 1$ the calorimeter is called *compensated*. A ratio $e/h \neq 1$ has the following implications on the calorimeter performance:

- The energy resolution of the calorimeter is influenced by the fluctuation of π^0 production ($< f_{em} >$).

- The signal distribution for monoenergetic hadrons is not gaussian.

- The calorimeter signal is not linear proportional to the incident hadron energy.

- The energy resolution improves with the energy in a more complex way than $1/\sqrt{E}$ (see 2.1.4).

- The e/π ratio depends on the energy.

To achieve compensation either the response to the non-electromagnetic component of the shower has to be increased or the response to the electromagnetic part of the shower has to be decreased.

A possibility to increase the calorimeter response to the hadronic component is the choice of special materials which enhance the detection of slow neutrons. Uran can be used as absorber or materials which contain hydrogen (e.g. plastic scintillator) can be used for the active components in the calorimeter. On the other hand it is also possible to reduce the electromagnetic component by using special configurations of absorbers. Additional tuning of the e/h ratio can be done by changing the active/passive layer volume ratio (so-called sampling fraction) [20].

Another possibility are off-line corrections. If the granularity of the calorimeter is sufficient the hadronic and the electromagnetic shower can be distinguished. Thus the electromagnetic component can be separated and appropriate weighting factors can be applied [26].

2.1.4 Energy resolution

The development of a hadronic shower is a statistical process where the deposited energy is proportional to the number (n) of produced particles [20]. Therefore the intrinsic accuracy improves with increasing energy as

$$\frac{\sigma_{samp}}{E} = \frac{a}{\sqrt{E}} \tag{2.6}$$

Typical values for hadronic sampling calorimeters are $a = 50 - 100\%$.

A second component is due to electronic noise effects and decreases with E:

$$\frac{\sigma_{noise}}{E} = \frac{b}{E} \tag{2.7}$$

A third component is due to calibration errors, non-uniformities and non-linearities of PMT's, ADC's, etc. This contribution is energy independent:

$$\frac{\sigma_{syst}}{E} = c \tag{2.8}$$

Combining all three components, the energy resolution of a calorimeter is given by the following expression:

$$\frac{\sigma}{E} = \frac{a}{\sqrt{E}} \oplus \frac{b}{E} \oplus c \tag{2.9}$$

where $\oplus$ is the quadratic sum operator.

2.2   The Tile Calorimeter

The Tile calorimeter (Tilecal) is a non-compensated sampling calorimeter made out of steel and scintillating tiles, as absorber and active material respectively, in a ratio of approximately 4 to 1. Its major task will consist in identifying jets and measuring their energy and direction, as well as to contribute to a good E_T^{miss} measurement. This is not an easy task at LHC since the large centre of mass energy (14 TeV) requires good performance over an extremely large dynamic range extending from a few GeV, deposited by traversing muons, to several TeV per cell due to jets.

The calorimeter will also improve the particle identification of the electromagnetic calorimeter. The segmentation of $\delta\eta \times \delta\phi = 0.1 \times 0.1$ allows an efficient hadron leakage cut, needed for electron and photon identification. The granularity of the calorimeter will additionally allow to minimise effects due to the non-compensation and to restore linearity of the energy response to hadron showers by weighting techniques at the level of 1–2 %.

A large fraction of the radiation produced by the high interaction rate of the order of 10^9 interactions per second per collision point will be absorbed by the Tile Calorimeter. Therefore the used materials and the front-end electronics have to be radiation tolerant to the expected dose to ensure operation during the lifetime of the experiment.
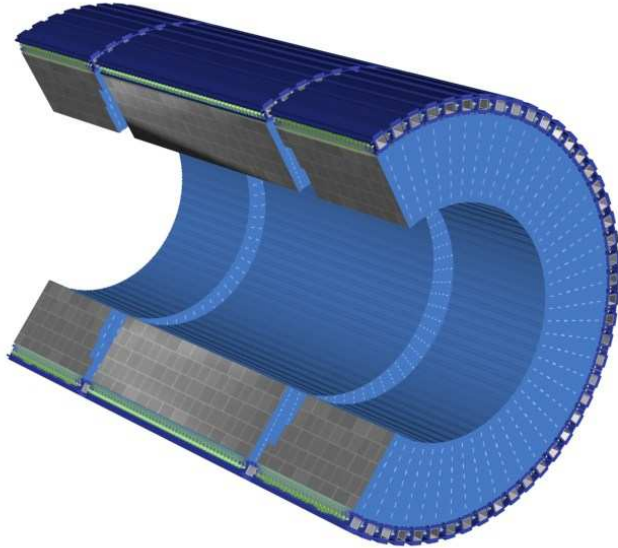
Figure 2.1: *View of the ATLAS Hadron Calorimeter (Tilecal). It is divided in three sections, one barrel and two extended barrels on either side. Each section consists of 64 azimuthal modules which are independent from each other.*

Additionally the calorimeter has to absorb all radiation but muons in front of the Muon Spectrometer, thus requiring a thickness of about 11 λ (including other sub-detectors placed in front of the Tile Calorimeter) at $\eta = 0$.

Finally, the calorimeter will form part of the ATLAS level-1 (LVL1) trigger system. Therefore a fast readout system is required.

Detailed information about the Tile Calorimeter can be found in [14].

2.2.1   Mechanics

The Tilecal is a laminated steel structure with pockets at periodic intervals to contain the scintillating tiles. The highly periodic structure allows the construction of a large detector by assembling smaller sub-modules together. It is a self-contained unit with the readout electronics being fully contained within the calorimeter. In addition to the function as absorber, the steel structure also provides the magnetic flux return yoke for the ATLAS solenoid.

The calorimeter consists of a cylindrical structure with an inner radius of 2.28 m and an outer radius of 4.23 m. It is subdivided into three sections, into a 5.64 m long barrel part covering $| \eta | < 1$ and two 2.65 m long extended barrels on each side, extending the rapidity coverage to $| \eta | < 1.6$. Each section consists of 64 independent azimuthal wedges called modules, illustrated in figure 2.1. The total weight is about 2900 tons. Between the three sections there

are gaps of 70 cm which are only partially instrumented with the Intermediate Tile Calorimeter (ITC). These gaps provide space for cables and services (e.g. cryogenics) for the innermost detectors.

Each of the modules is built out of repeating elements called sub-modules which are again built out of periods. A central barrel module consists of 19 such sub-modules whereas the extended barrel modules only of 10. A period has four layers. The first and the third layer consists of large trapezoidal steel plates (master plates), 5 mm thick and spanning the full radial dimension of the module. In the second and fourth layer, smaller trapezoidal steel plates (spacer plates), 4 mm thick, are glued periodically to the master plates with epoxy, providing space for the scintillating tiles between them.

Two holes are located on the radial axis of each spacer, in the corresponding master plates and in each tile. These are used to insert small tubes for calibration purposes.

A rigid girder at the outer radius and a 10 mm front plate at the inner radius provide structural integrity and allow the modules to be joined to a self supporting cylinder. The girder also houses the PMTs and the front-end electronics and additionally provides sufficient steel cross section for the solenoidal field flux return.

Attached to the girder there is a rugged steel box called *finger*. The finger was initially introduced in the design in order to provide continuity of the magnetic field between barrel and extended barrels. Additionally it will house the LV power supply for the front end electronics.

2.2.2 Optics

Ionising particles crossing the tiles induce the production of light in the scintillator tiles with wavelengths in the UV range. This light is subsequently converted to visible blue light by scintillation additives and propagates through the tile to its edges. There it is absorbed by WaveLength Shifting (WLS) fibres, placed on both sides of the tiles, and shifted to a longer wavelength, chosen to match the sensitive region of the PMT photocathode. A fraction of the light in the fibre is captured and propagated via total internal reflection to the PMT where it is detected. Between the fibres and the photocathode a light mixer is placed to optimise detection uniformity.

In all calorimeters of this type constructed so far, the tiles are placed orthogonal to the particle trajectories, which makes the readout of the light difficult while maintaining detector hermeticity. In the case of Tilecal this problem is solved with scintillating tiles which are placed perpendicular to the colliding beam.

The scintillator tiles are wrapped in a special material called Tyvek to protect the surface and to improve the response uniformity. A total of approximately 460000 tiles in 11 different sizes is required. They are produced by injection molding for reasons of cost and the required high production rate. Optically
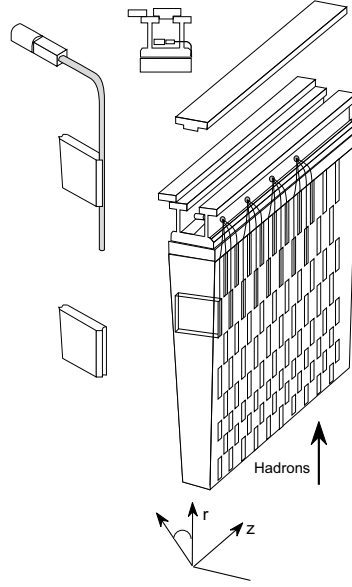
Figure 2.2: *Principle of the Tile Calorimeter design. The scintillating tiles are inserted in a rigid steel structure and staggered in depth. WaveLength Shifting (WLS) fibres run radially along both sides of the module and guide the light produced in the tiles to the PMTs situated in the girder.*

transparent granulated polystyrene is used as a base material with the addition of two scintillation additives (1.5% PTP and 0.04% POPOP).

The WLS fibres have a diameter of 1 mm and are doped with a fast (< 10 ns decay time) shifter which absorbs the blue light from the scintillator tiles and emit it at longer wavelength. The fibre ends opposite to the PMTs are aluminised by a sputtering technique to increase the light yield. In total 640000 fibres are required to build Tilecal, giving a total length of about 1120 km.

As shown in figure 2.3 the modules are segmented in cells and towers. The cells are made by grouping the fibres, coming from the respective tiles, together in the same bundle which is read out by a PMT. Each cell is read out by two PMTs, one on each side of the module. There are three independent radial sampling depths in total, with a granularity of $\delta\eta = 0.1$ for the two inner samplings and $\delta\eta = 0.2$ for the outer one. The thickness of the samplings at $\eta = 0$ is 1.9 λ, 4.2 λ and 1.5 λ respectively.

2.2.3 Electronics and Read-out

All front-end electronics and photomultipliers are mounted on so-called drawers which are movable and can be inserted into the girder, located at the outer radius of the modules. There are always two drawers combined to a 3 m long unit, called
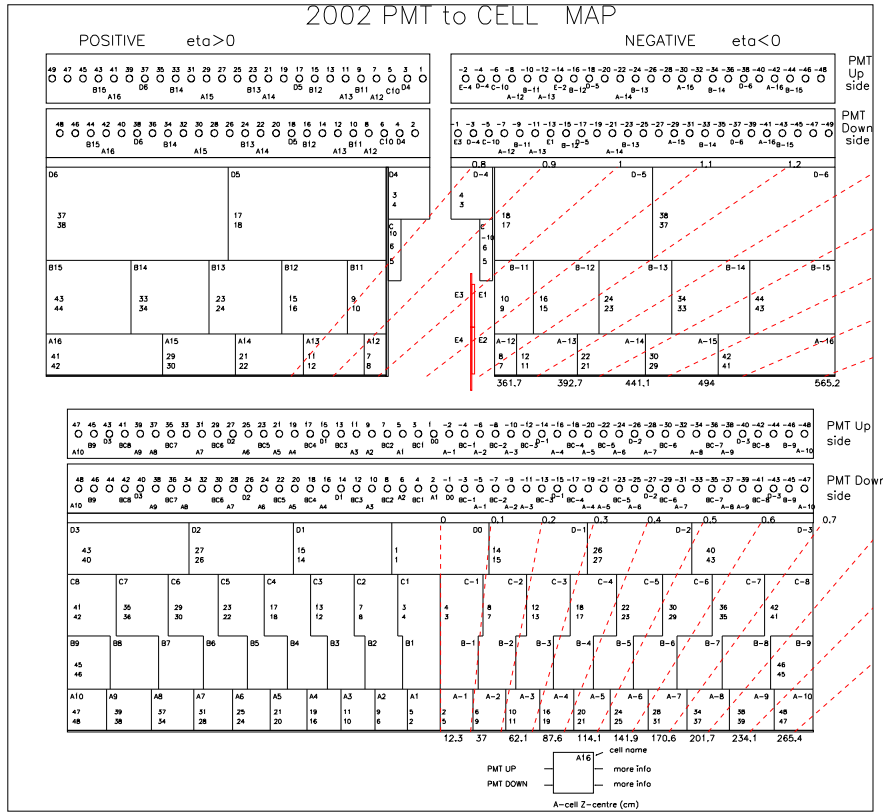
Figure 2.3: *Cell layout of both extended barrel modules and a barrel module. Each cell is read out by two PMTs, one on each side of the module. There are three radial sampling depths A, BC and D. The dashed lines are η lines spaced by δη = 0.1. The circles in the girder represent the positions of the PMTs.*

superdrawer. One such superdrawer is needed to read out an extended barrel module, whereas the barrel modules have two superdrawers inside their girder. On the external side of the superdrawers a so-called patch panel is installed. It represents the boarder to the outside and is equipped with connectors for all the services needed inside the girder.

Each drawer houses up to 24 PMT blocks and contains electronics to provide the HV levels required for the operation of the elements of the PMT block and to process the signals induced by physics and calibration events. In total 10140 PMTs are used in Tilecal. The electronics boards are connected by motherboards on the top and on the bottom sides of the drawers. An overview of the layout can be seen in figure 2.4.

Since the Tile Calorimeter will be part of the level-1 (LVL1) trigger its readout electronics have to be fast in order to cope with the bunch crossing time of 25 ns. In this intervals signals from 2000 trigger towers have to be sent to the
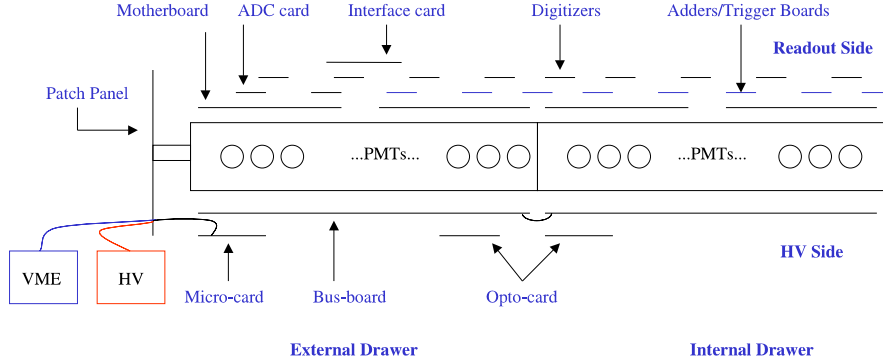
Figure 2.4: *Layout of the electronics in a superdrawer. They are separated into a readout part on one and a HV part on the other side. The Patch Panel is used to connect services like power supply, trigger cables, cooling pipes, etc.*

LVL1 system and locally buffered during the decision time of $\sim$2.5 μs. When LVL1 has accepted an event, the data are read out, processed and stored in readout buffers (ROBs) for use by the LVL2 trigger and the Event Filter (EF).

Furthermore the electronics have to cope with a large dynamic range starting from 0.35 GeV per cell deposited by muons to 1.5 TeV per cell deposited by jets.

Other constraints are the very limited space for the electronics, the residual magnetic field and radiation. Calculations show that the magnetic fields will be below 20 Gauss in the region of the front end electronics. The most sensitive components are the PMTs and their individual HV regulation system, which have to be designed and shielded to meet the requirements. Monte Carlo simulations of radiation levels showed that the iron of the hadronic detector itself considerably reduces radiation levels inside the girders. Nevertheless radiation tolerant electronics have to be used.

Temperature stability is another important issue and has to be maintained within to 1°C. A dedicated cooling system was developed for the front-end electronics to evacuate the dissipated heat. Additionally the large iron mass of the Tile Calorimeter contributes to the temperature stability.

PMT block

The function of a PMT block is to convert light signals from the scintillating tiles into electronic signals. Each PMT block contains a light mixer which is the interface between fibre bundle and PMT photocathode, a photomultiplier tube, a HV divider and a 3-in-1 card. The PMT blocks are located in holes inside the rigid aluminium structure of the drawers and are shielded with a mu-metal cylinders to provide magnetic shielding of up to 200 Gauss in any direction.

Light mixer: PMTs usually have large variations in response over their photo-cathode surface. Therefore the light mixer has the task to mix the light coming from the fibres in order to avoid any correlation between the position of the fibre and the area of the photocathode which receives the light.

PMT: Intensive evaluation of different PMTs has been carried out to find a suitable model which matches the requirements concerning points like quantum efficiency, dark current, rise time, non-linearity, useful photocathode area and size. It was found that the Hamamatsu R7877 is the best choice, its main features are:

- 8 stages (dynodes)

- Gain of 10^5 at 650 V

- Active photocathode area 324 mm^2

- dark current < 100 pA

- quantum efficiency at 480 nm 17 %

- metal channel dynodes

3-in-1 card: As the name is already indicating the 3-in-1 card consists of three main components with the following tasks:

- Pulse shaping and accommodation of the large dynamic range

- Charge injection calibration

- Slow integration of the PMT signals for monitoring and calibration

To avoid noise the 3-in-1 card is directly connected to the PMT via the HV divider which works as a socket and provides the different HV levels for the dynodes of the PMT. The current pulses from the PMTs are shaped and converted to a voltage signal on the 3-in-1 card. Then the signal is split in two, one of them is going directly to the trigger boards, the other one is transmitted to the fast digitisers for further processing.

Other electronic components

ADC integrator card: It is used to read out the signal induced by the Cs source. A special ADC is used which is able to read continuous currents.

Digitiser card: The digitiser cards digitise the shaped pulses coming from the PMT on a 25 ns basis. It also buffers the signals while the LVL1 decides if the signal is accepted or discarded.

Interface card: The interface card works as interface to the outside. It brings in the 25 ns clock via an optical fibre, provides external communication and also sends the signals from the digitisers.

Micro card: The HV regulation is done by the micro card. It has stored all the settings required for the operation of the PMTs and also handles the communication to a VME crate used to control the HV.

Opto Boards: Using a regulation loop the opto boards set the correct HV on the corresponding PMT. They receive the correct settings by the micro card.

Adder / Trigger board: The Adders work with analogue signals and provide two output signals:

- Groups of 5 PMTs are arranged in trigger towers which correspond to the path of passing particles. The adder board performs a fast summation over the signals of the 5 PMTs which gives a fast information about the deposited energy.

- The Adders also sum over all signals of the PMTs of the third sample (D). This provides a fast muon trigger.

2.2.4   Calibration

In order to relate the digitised signal at the end of the readout chain to the corresponding energy deposited in the calorimeter a *calibration factor* has to be applied. This factor must be measured for every channel and its channel-to-channel variations have to be kept as low as possible. Since due to ageing or radiation damage the set of calibration factors can change over the lifetime of the detector and they have to be monitored in order to correct for their variations in time.

It is foreseen for Tilecal to carry out an absolute calibration of 12% of the modules in a particle beam. The rest of the modules will then be intercalibrated by means of a movable Cs source which will be explained later.

It is crucial for a good calorimeter performance that the temperature of the electronics is the same during the calibration periods and in the ATLAS cavern. Therefore two cooling station prototypes have been constructed which are used to cool the electronics at a stable temperature during times of calibration. Performance tests with this prototypes are presented in detail in chapter 4.

In general the read-out chain of the signal can be separated into three stages. Each stage can be effected by deterioration with time and therefore has to be monitored. The three stages and possible effects are:

- **Production of light in the scintillating tiles and propagation through the WLS fibres:** Radiation damage and ageing of fibres and scintillators can change their light yield. Such changes are typically slow and can be monitored by inducing light of known characteristics with the help of a radioactive source.

- **Conversion of the light into a current at the PMT:** Due to gain drift and deterioration of gain or quantum efficiency the photomultiplier response may change. Injecting a well known light pulse at this stage helps monitoring such processes.

- **Read-out and processing of the calorimeter signal:** Ageing of electronic components can result in non-linearity. This can be monitored by injecting a defined charge into the electronics and comparing it with the signal given at the end of the read-out chain.

Therefore the Tilecal intercalibration and monitoring strategy is based on several tools:

- The ^{137}Cs calibration system

- The laser system

- The Charge Injection system

- The Minimum Bias Events monitoring system

The ^{137}Cs calibration system

The intercalibration of the modules and the monitoring of the light yield of fibres and tiles will be performed by the Cs system. Every scintillating tile is traversed by a hollow tube through which a gamma source (^{137}Cs, 5 mCi) can be sent by means of a hydraulic system. The radiation of the Cs source induces a defined current in the PMTs while passing the tiles. This allows to check the quality and uniformity of the optical system.

The Cs system also allows cell-to-cell calibration to obtain the same average response in all cells. According to the average induced signal the high voltages of the PMTs are set in order to provide uniform response over the whole calorimeter.

Additionally the Cs source system is used to monitor the long term stability of the optics. Cs source runs will be performed periodically to maintain the overall energy calibration of the cells. Those runs can be carried out during shut-down periods of the detector.

Laser system

A YLF solid-state laser transmits light pulses directly into the PMT via a separate clear fibre. Having a wavelength of 480 nm and a pulse width of 15 ns the light signal is very similar to a signal produced by particles. Several attenuation filters (non-attenuated, 10 times attenuated, 100 times attenuated) provide the possibility to monitor the response of the PMTs over the full dynamic range and to check for gain drift or variations in quantum efficiency.

Charge Injection System

The Charge Injection System (CIS) is located on the 3-in-1 card. It mainly consists of two capacitors, 5 pF and 100 pF, which can be used to send a defined charge into the read-out electronics. In this way the read-out chain can be tested on linearity which may deteriorate due to the ageing of components.

Monitoring of minimum bias events

This diagnostic tool is based on the background noise produced by inelastic proton-proton collisions at small momentum transfers. This type of events, called Minimum Bias events (MB), induce a quasi-DC current in the PMTs and can be used to continuously monitor the response of the calorimeter. The rate of energy deposition by MB events depends on the LHC luminosity and the cell location. Monitoring MB events can be used complementary to Cs source scan because it does not require the beam to be off.

2.2.5   Performance

The detector performance has been measured in both stand-alone operation and combined test of the electromagnetic LAr and the Tile Calorimeters. The combined test have been carried out in 1994 and 1996 ([21], [22],[26]) whereas the stand-alone tests with prototypes and later with module zero started already in 1993. In all cases the response to charged hadrons, electrons and muons has been studied.

The combined tests for a pion beam in the energy range of 20 to 300 GeV gave the following resolution [26]:

$$\frac{\sigma}{E} = \frac{(41.9 \pm 1.6)\%}{\sqrt{E}} \oplus (1.8 \pm 0.1)\% \oplus \frac{(1.8 \pm 0.1)\text{GeV}}{E} \qquad (2.10)$$

Tests with module 0, the first production module of Tilecal, were performed and the response to pions with energies from 10 to 400 GeV has been measured. The result for the resolution was the following:

$$\frac{\sigma}{E} = \frac{(52.0 \pm 0.6)\%}{\sqrt{E}} \oplus (4.1 \pm 0.1)\% \qquad (2.11)$$

Comparison between electrons and pions allowed to determine a value of the calorimeter response to electromagnetic and hadronic components of the shower. With the measured ratio e/π it was found that $e/h = 1.362 \pm 0.006$ [27].

The response to muons has been extensively studied. In particular, the response in the three samples of the Tile Calorimeter as a function of the pseudo-rapidity has been measured. The ability of a clean muon measurement above the noise level allows additional contribution to the muon identification at the trigger and analysis level. For 100 GeV muons the signal was in general separated by more than six standard deviations from the noise.

Also the response uniformity of the module as a function of η and ϕ was studied with muons. The results showed a uniformity within 2%.

Another point of interest were the photostatistics. It was found that in average 70 photoelectrons are generated in the photocathode of the PMT per GeV. This high photostatistics assure a good separation of muons from noise [28].

2.2.6   Status of the construction of Tilecal

The construction and instrumentation of 64 (of 64) barrel modules and of 118 (of 128) extended barrel modules is completed. The missing extended barrel modules will be ready in December 2002.

The mass production of the superdrawers (including electronics) is planned to start in October 2002 with a maximum rate of 16 per month. In September 2002 almost 10% of the superdrawers had been completed. The end of production is scheduled for December 2003.

Chapter 3

The ATLAS Tilecal cooling system

Electronic devices are influenced by temperature. This circumstance makes a adequate cooling system essential for any unit which has integrated electronics. Especially for highly sophisticated instruments like particle detectors where reproducibility is an important factor, stable temperatures and therefore a reliable cooling system is a crucial point. Since the ATLAS detector will be one of the most delicate and advanced devices in the world the necessity for a reliably working cooling system is not surprising.

3.1   The ATLAS Calorimeter Cooling Project

The ATLAS Calorimeter Cooling Project has been set up to provide a common framework for the cooling of the ATLAS calorimeter electronics, both for the Tile Calorimeter and for the LAr Calorimeter. Its aims are to develop submodules of the cooling system and to test critical components of the 'Leakless Cooling System v.2' and the preparation of technical specification documents to be used in the procurement of the various components for mass production.

From a cooling point of view the Tilecal and LAr calorimeter will be quite different:

- Tilecal will dissipate approximately 77 kW. Four partitions, each with 64 modules (one module ≡ 300 W) including superdrawer electronics and low voltage power supply, have to be cooled.

- LAr will dissipate 255 kW. Crates and power supplies (2x16 for the barrel, 2x13 for the End Cap) have to be cooled.

Nevertheless the same type of cooling system, the Leakless System v.2, is planned to be used for both. Also other LHC detectors like ALICE intend to use this system.

3.1.1 Strategy for Tilecal

Although similar cooling systems are already running in other experiments, the huge dimensions of ATLAS and the severe environment (high radiation, magnetic fields, inaccessible), call for a full-scale test to verify calculations and design. For Tilecal the approach to the final cooling system consists of three main steps:

1. The construction and performance analysis of prototype cooling units for the calibration of the Tilecal modules.

2. A full-scale hydraulic test with final components.

3. Magnetic field and radiation tests with the final components.

The construction of the prototypes and the full-scale hydraulic test setup was done by the CERN ST/CV group which is also responsible for the construction of the final Tilecal cooling system. The performance evaluation of the prototypes and the full-scale test took place during the year 2001/02 and is subject to this thesis. The last missing point at this stage of the project, the magnetic and radiation tests, are planned to be performed in autumn 2002.

One of the cooling unit prototypes is located at CERN in building 887 (H8 beam area) where 12% of the Tilecal modules are calibrated with a particle beam. It is successfully working since the summer 2001 beam period. Another cooling unit prototype is placed in building 175 where Cs intercalibration of all the modules will take place. The full-scale test is placed in building 185. The performance of the prototype units and the full-scale test setup is discussed in detail in chapter 4 and chapter 5, respectively.

3.2 Requirements for the Tilecal cooling system

There are several requirements for the design of the cooling system of the Tile Calorimeter [29]:

- A constant temperature of the electronics over a long period has to be ensured. The heat produced has to be removed efficiently. Specially temperature sensitive components like the PMT and in particular its gain have to remain stable within 0.5%.

- The temperature of the drawer material (cast aluminium) must be as close as possible to the girder temperature. The girder is a large iron mass which will be at ambient temperature.

- Safety of the system is very important. There must not be any liquid leaks in the circuit because the electronics are packed inside a closed space using high and low voltages. A leak would have fatal consequences for the Tile Calorimeter but also for other ATLAS subsystems.

- Cooling must be provided for each of the 256 superdrawers and their corresponding low voltage power supply.

- Flexible connections are needed between certain components because they have to be removable (internal / external drawer, superdrawer / patch-panel, patch-panel / outside world).

- Space is very restricted inside the girder therefore the cooling tubes and the connectors have to small enough.

- The system must be simply and quickly connected and disconnected without leaks at superdrawer level because of the access to the electronics.

- The temperatures, specially of the PMTs, should be uniform inside the superdrawer. The creation of a 'hot' side and a 'cold' side should be avoided.

- The global costs of the cooling system have to be considered, including its impact on the drawer design.

- The chosen system must have been experimentally demonstrated under real conditions.

- The cooling temperature has to be the same for the calibration in the test-beam, the calibration with the Cs source and in the ATLAS cavern.

The chosen solution for Tilecal is the so-called Leakless Cooling System v.2 (LCS) ([29], [30]) which fits all the requirements.

3.2.1 The Leakless Cooling System

For ATLAS the Leakless Cooling System v.2 (LCS) was adapted. This system is specially designed to avoid dangerous leakage of liquid. In principle the LCS is a closed system working with sub-atmospheric pressures. Since the pressure in the cooling pipes is lower than the atmospheric pressure a leak in the circuit does not result in leakage of cooling water but air will be sucked in. This additionally allows to detect leaks in the system because it implicates an increase in pressure which can be monitored.

The LCS is used for applications where leakage would have fatal consequences, like in the case of Tilecal where sensible electronic components have to be cooled. In Tilecal demineralised water was chosen as the cooling liquid.

The operating principle shown in figure 3.1 is the following: Cooling liquid (in the case of Tilecal demineralised water) is held in a storage tank (3) which is kept under sub-atmospheric pressure by a vacuum pump (2). The liquid is transported to the heat exchangers (1) by a pump (4). For safety reasons a discharge valve (5) is installed on the tank to avoid overpressure. The pressure
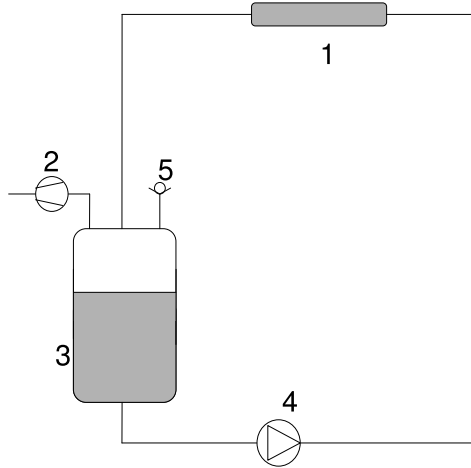
Figure 3.1: *Principle of the Leakless Cooling System v.2. The circuit is kept under sub-atmospheric pressure by a vacuum pump (2) to avoid leakage of the cooling liquid. The pump (4) transports the liquid to the heat exchanger (1) and then back into the storage tank (3). To avoid overpressure a discharge valve (5) is installed for security reasons.*

in the various points of the circuit depends on the head losses and hydrostatic pressures. An implemented control logic monitors the pressure and supervises the correct operation of the system.

The LCS has already been used successfully in the L3 experiment over more than 10 years without any water leaks being observed.

3.3   Layout of the Tilecal cooling system

3.3.1   Design Parameters

It is planned to install the cooling station, consisting mainly of a water tank, a refrigeration unit, a water pump and pneumatic pressure regulators, on the floor of the cavern UX15, where ATLAS will be located [29]. Pipes, some of them going up to ∼15 m height, will distribute the cooling water to the 256 superdrawers and their corresponding low voltage power supplies in the fingers. To minimise the amount of pipes but still to maintain optimal operation of the LCS the calorimeter will be divided into several sectors, each with a maximum pressure head of 2 to 3 m. The barrel will be divided into 12 sectors, each extended barrel
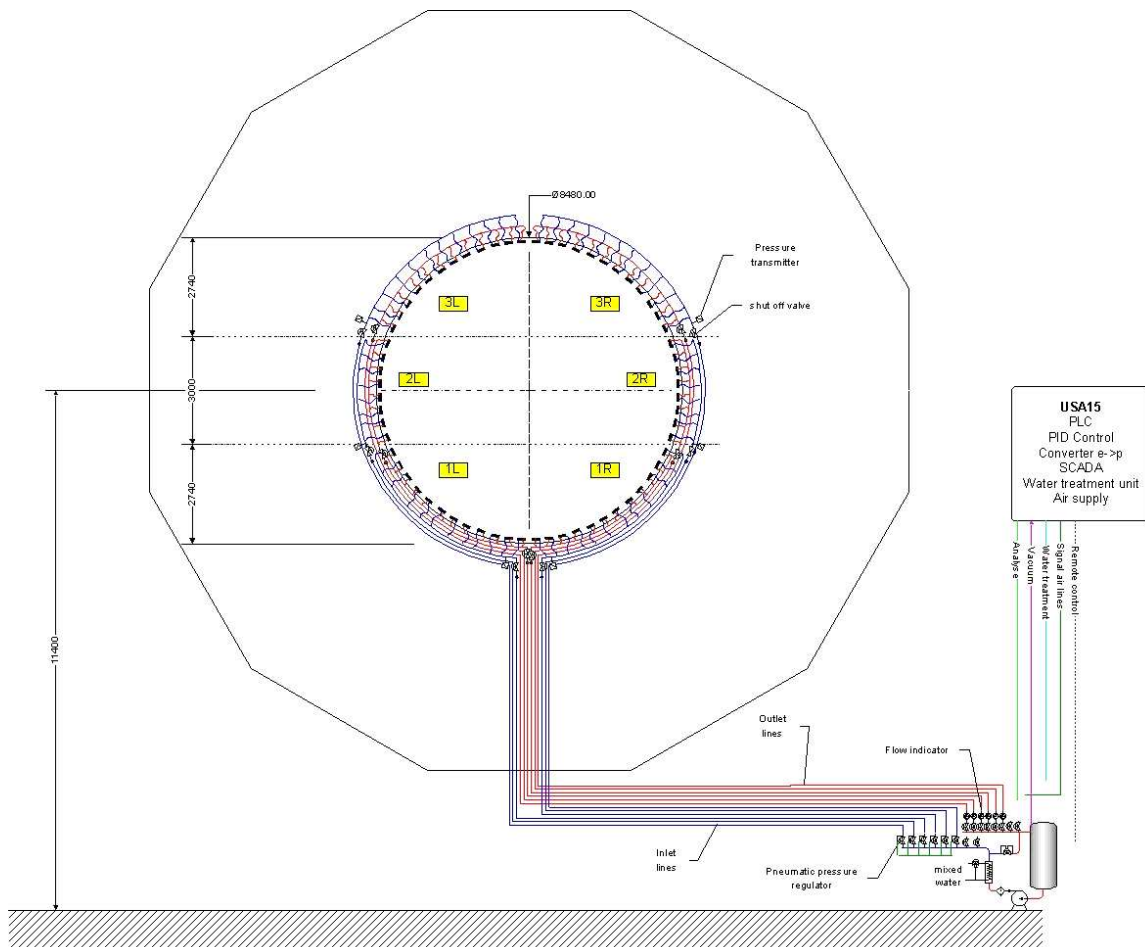
Figure 3.2: *Layout of the cooling system and the piping for half of the barrel of the Tile Calorimeter. Both halves of the barrel are divided into 6 sectors, each one connected to the cooling station via an inlet and an outlet pipe. The sectors include 8 respectively 12 modules. Each sector will be equipped with an isolation valve and a pressure transmitter, both controlled by the PLC in the side cavern.*

Figure 3.3: *Layout of the cooling system and the piping for one extended barrel of the Tile Calorimeter. Like in the case of the barrel there are 6 sectors which are connected to the cooling station via inlet and outlet pipes. The sectors include 8 respectively 12 modules. Each sector will be equipped with an isolation valve and a pressure transmitter, both controlled by the PLC in the side cavern.*

into 6 sectors. Each sector will be equipped with a pressure transmitter and isolating valves to be able to monitor the pressure ins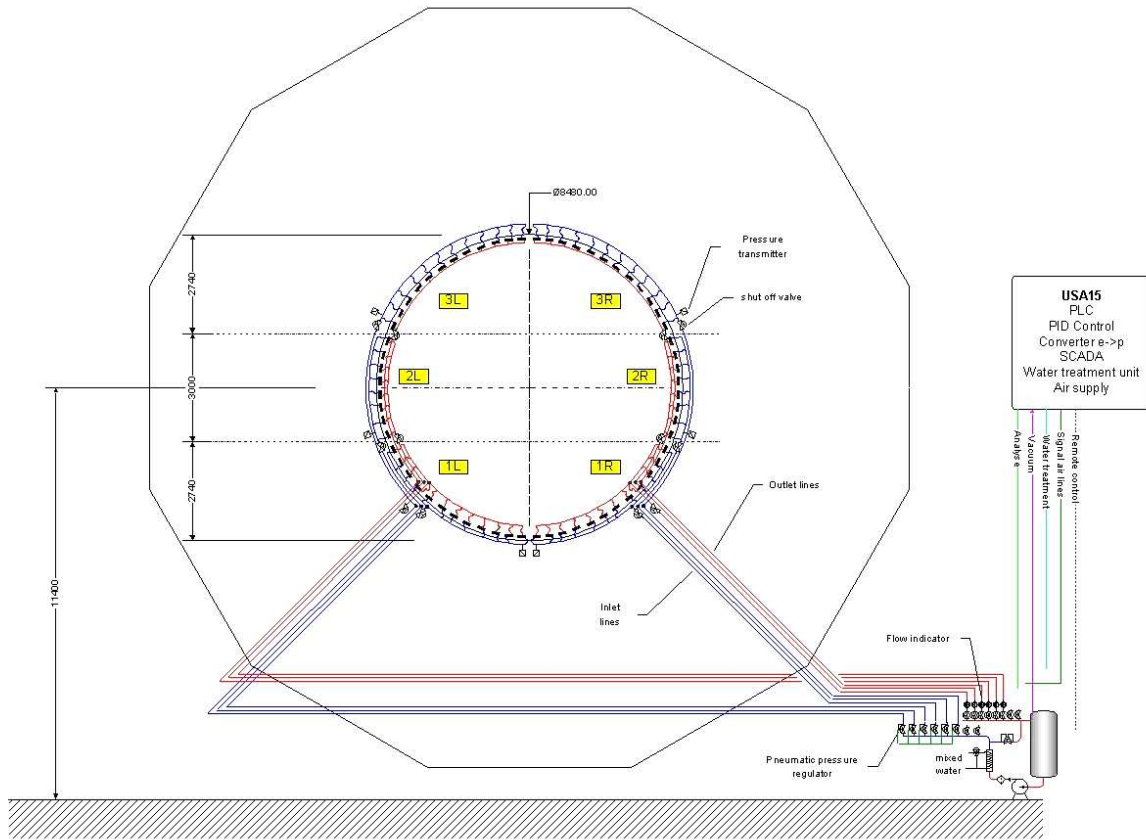ide the circuit and in case of maintenance or problems to isolate the respective sector. One sector will feed 8 to 12 superdrawers and their corresponding low voltage power supplies. From a cooling point of view a superdrawer and its corresponding low voltage power supply represent one unit which is fed by one cooling channel.

The inlet pipes, from the water pump in the cooling station to the arrival to the corresponding sector, are designed to have overpressure (1 to 2 bar). The distribution pipes inside a sector and inside the modules will work with sub-atmospheric pressure (0 to -0.8 bar).

Based on theoretical assumptions and measurements of electronic prototypes, the Tilecal cooling system was designed to be capable of extracting 300 W per cooling channel and to keep a ΔT between input and outlet of the module of 2°C. 200 W are expected to be dissipated by the electronics in the superdrawer and 100 W by the low voltage power supply in the finger. Since the Tile Calorimeter consists of 128 extended barrel modules and 64 barrel modules, the power the cooling system can extract is:

$$128 * 300 + 64 * 2 * 300 = 77kW \qquad (3.1)$$

To reach an efficiency of 100% for a cooling system is not possible. First of all the connection between the cooling and the warm medium will always have a certain thermal resistance. Secondly the isolation of the warm medium cannot be perfect what results in heat loss to the surrounding area.

3.3.2   Cooling principle

The cooling principle is based on two independent circuits, a primary and a secondary one, as it can be seen in figure 3.4. The primary circuit is the CERN mixed water cooling circuit, supplying water at 14/16°C for CERN installations. The secondary circuit is a closed circuit working with demineralised water. The water is transported from the cooling station to the modules and back. The secondary circuit is cooled by the primary circuit via a plate heat exchanger. A bypass and a regulating valve operated by the PLC is installed in the primary circuit in order to control the water temperature of the secondary circuit.

3.3.3   Cooling inside the modules

Inside the superdrawers the cooling is implemented by two crossed circuits (figure 3.5) to ensure a certain temperature uniformity between along the drawer. The water is flowing through stiff tubes (duralumin) which are glued into grooves with aluminium-loaded glue. The connections between two drawers, the return loop at the inner end and the connection to the patch panel are ensured by flexible plastic tubes.
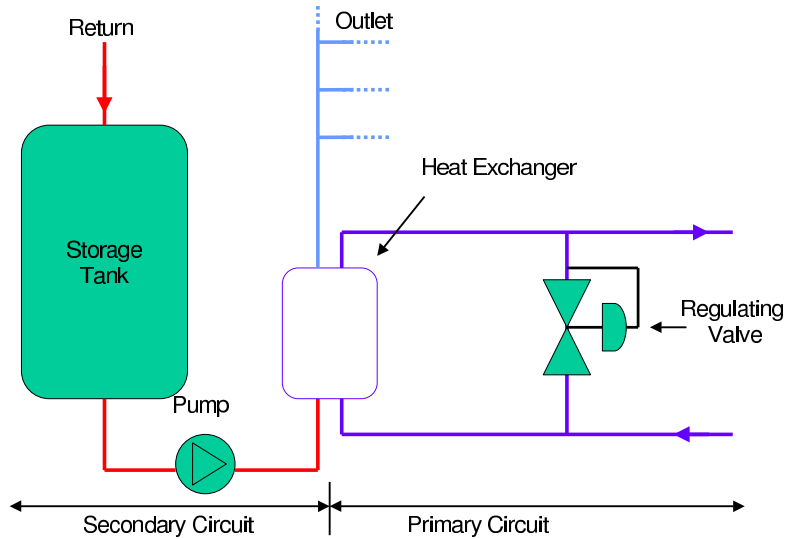
Figure 3.4: *The cooling principle of the final Tilecal cooling station. The system is divided into two circuits, primary and secondary. The primary circuit supplies water at $14/16°C$ and is coupled with the secondary circuit via a heat exchanger. The secondary circuit delivers the cooled water to the modules. Via a regulating valve a bypass in the primary circuit is opened/closed in order to control the water temperature in the secondary circuit.*

3.3.4 Control and readout

Because of the restricted space and the severe environment in UX15, other components of the cooling station will be installed in the side cavern USA15, specially built for the services of the ATLAS detector. Those components include a PLC (Programmable Logic Controller) as the control unit, a vacuum system, a water treatment unit including water analysis, an e-p converter, an air supply for the pneumatic system and an auto tuning PID controller to regulate the water temperature. The PLC and the PID will run largely independent and will use closed-loop controls to operate the cooling system. The PLC is responsible for the general operation of the system whereas the PID controls only the temperature of the cooling water.

The PLC will be interface to the general Detector Control System (DCS) using the OPC standard described in [4]. Additionally another system will be implemented to perform passive monitoring of parameters of the cooling system like the status of valves and pumps or temperatures and pressures at different locations. This secondary monitoring system will be fully integrated in the DCS and will use the standard DCS tools following the ATLAS DCS vertical slice [31] which is defined as the full readout chain from the sensor to the operator

40
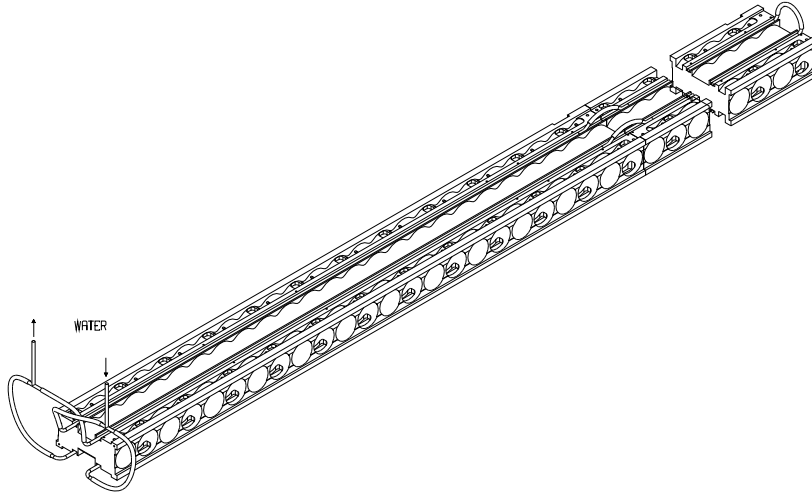
Figure 3.5: *The routing of the cooling tubes inside the superdrawers . A crossed circuit setup is chosen to ensure temperature uniformity. For the straight sections a stiff duralumin tube is glued into grooves of the casted aluminium drawer. For the connections between two drawers and from the drawer to the patch panel as well as for the return loop on the inner end flexible plastic tubes are used.*

interface (ELMB, CANopen OPC server and PVSS-II). First implementations have already been realised for the monitoring of the parameters of the cooling system which is installed for the calibration of the Tilecal modules with beam particles. These implementations are described more in detail in chapter 4.

An overview of the Tilecal cooling system is given in table 3.1.

3.3.5   Cooling temperature

In order to find the optimal value for the temperature of the cooling water, several tests have been carried out. Two main considerations have to be taken into account: On one side the temperature in the superdrawer has to be low enough to assure good performance of the electronics, which was found to be valid for temperatures below 45°C.

The other consideration is connected with the condensation of water. If the cooling temperature is lower than the dew point, water can condensate on the electronic boards and create dangerous short-circuits. The dew point is dependent on the humidity and the ambient temperature and therefore on the environmental conditions in the ATLAS cavern and the buildings where the calibration takes place. It was finally proposed that the temperature in the superdrawers should always be higher than 14°C [29].

---

[1]A barrel module is read out by two superdrawers and an extended barrel module by one.
[2]One sector includes 8 or 12 modules

Characteristics of the ATLAS Tilecal cooling system	
Cooling liquid	demineralised water
Cooling liquid temperature	18°C
Primary Circuit	mixed water 14/16°C
Number of cooling stations	1
Total power of cooling system	77000 W
Power dissipation of one superdrawer & LV	300 W
Number of superdrawers to be cooled [1]	4 x 64
Number of cooling channels	24
Number of cooling sectors [2]	24
Total length of piping	2200 m
Control of cooling station	PLC
Monitoring of cooling parameters	ELMB – PVSS–II
Manpower Piping/Welding/Mechanics	2061 h
Manpower Electricity/PLC/Test/Documentation	848 h
Total cost	CHF 350000

Table 3.1: *A summary of the characteristics of the Tilecal cooling system is given. More details about the cost evaluation can be found in appendix A.*

The final decision was to keep the cooling water temperature at 18°C in order to provide good operational conditions for the electronics and to avoid condensation inside the superdrawers.

Chapter 4

Performance of the prototype cooling stations for the Tilecal module calibration

4.1 Introduction

A new prototype cooling station (figure 4.2) for the calibration of Tilecal modules was installed in the H8 beam zone where it already worked successfully in the summer calibration period 2001. Only 12% of the modules can be calibrated in the H8 beam area due to beam time constraints. Therefore an identical cooling station (figure 4.1) will be used in building 175 for the calibration of all the modules with a Cs source. Also the second unit was already successfully operated in several performed tests.

In both prototype cooling systems the *Leakless Cooling System* ([29],[30]) is implemented. It uses sub-atmospheric pressure to prevent the cooling liquid from leaking.

The final cooling system of the Tile Calorimeter will be based on the results of the tests performed with the prototype stations presented in this chapter.

4.2 The Cooling System

In the following section a detailed description of the cooling station used for the calibration of Tilecal modules with beam particles is given. This station is fix installed in the H8 test beam area. The second cooling station is constructed in the same way but movable and located in another building.

The cooling system consist of the cooling unit, the piping and the cooling monitoring system including software and hardware components. It is designed

Figure 4.1: *Cooling station used for the Cs calibration of the Tilecal modules. The unit is independent and movable.*

to evacuate 2 kW, hence six super-drawers can be cooled simultaneously. For most of the cooling tests a nominal cooling temperature of 18°C and a flow of 60 l/h was applied. The subsystems are described in the following sections [30].

As the low voltage power supply in the fingers is not yet available an external, non-cooled source was used. Tests with the finger low voltage supply will follow once it is available.

4.2.1 Cooling unit

The cooling unit is placed under the scanning table, utilising a flexible suspension which provides its horizontal position despite the movement of the table. It consists of various components which will be described in detail. Two separate circuits can be distinguished. The primary (fridge) circuit and the secondary circuit. The principle of the cooling unit is shown in figure 4.3.

The returning water is first collected in the storage tank. Then it passes the resistor heater and the heat exchanger before it is again fed into the circuits. In the heat exchanger the water is cooled by the fridge circuit, which is always working at constant power. A temperature sensor at the outlet controls the water temperature and is connected to the PID controller. Whenever needed the PID activates the resistor heater in order to keep the water temperature stable at the setpoint.

It should be added that in times when ecological awareness should be naturally, this cooling principle is not adequate. Cooling the liquid and then heating it again could be easily avoided with the implementation of a bypass with a regulating valve. The flow would get separated into two channels, one being cooled by
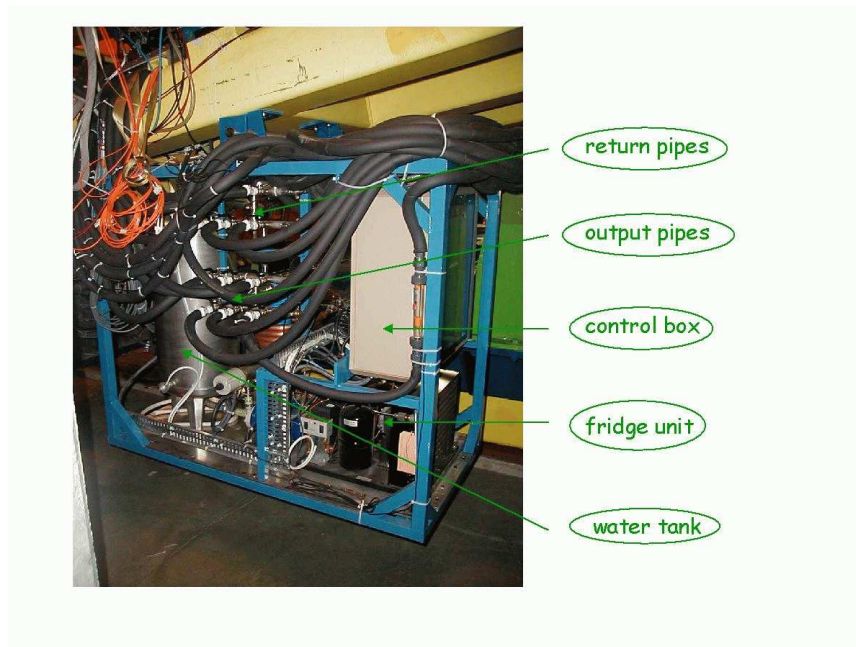
Figure 4.2: *Cooling station used for the calibration of Tilecal modules with beam particles. The station is fix installed on a scanning table in the H8 beam area.*

the fridge circuit and the other one bypassing it. Behind the fridge the channels would be merged again. Instead of a resistor heater, the regulation valve would be used to regulate the temperature.

Cooling liquid

The cooling liquid is demineralised water at 18°C. Since aluminium heat exchangers and cooling screens are used, the corrosion must not be underestimated. Therefore a demineralisation filter is included in the circuit. In the final prototype for the ATLAS detector the corrosion rate of the water will be analysed in regular intervals which still have to be determined. This can be done by the use of spectroscopy or electro-chemical analysis.

Storage tank

The storage tank contains the water which is distributed to the modules. It has a capacity of 80 litres and the level can be checked by a visual liquid level. The returning water from the modules is first collected in the storage tank before it is again fed into the circuit. In normal operation there is sub-atmospheric pressure of approximately -500 mbar in the tank. This sub-atmospheric pressure is maintained by a vacuum pump which is connected to the top of the tank
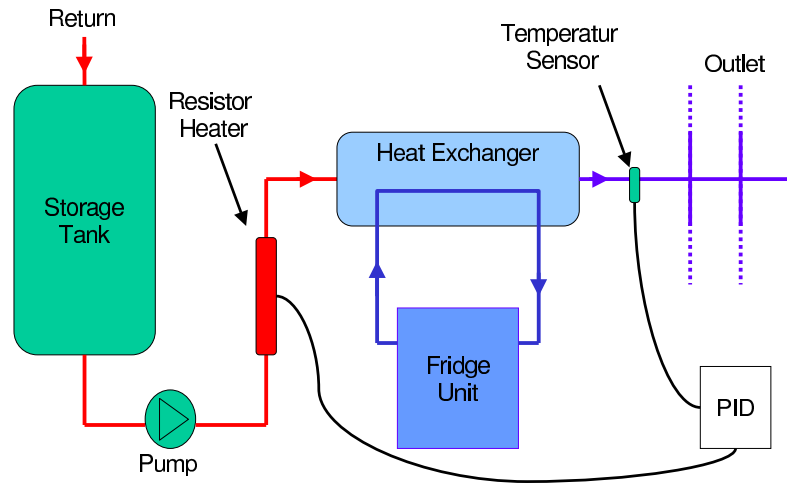
Figure 4.3: *Principle of the cooling. The water is collected in the tank and then transported to the resistor heater and the heat exchanger. In the heat exchanger the water is cooled by the fridge circuit which is working with constant cooling power. The current in the resistor heater is controlled by the PID. It also monitors the water temperature at the outlet with a temperature sensor and activates the resistor heater in order to keep the water temperature stable.*

and which is activated by a pressure switch as soon as the pressure exceeds the setpoint of -400 mbar.

Fridge circuit

The main parts of the fridge (primary) circuit are a coaxial evaporator, an air-cooled condenser, a hermetic compressor and a refrigerating tank. It works with the same principle as any fridge in a household. Using the refrigerating liquid R134a (HFC) it is designed for a power of 2000 W. The achievable evaporative temperature is +10°C and the condensing temperature +40°C. The fridge circuit is connected to the secondary circuit via heat exchanger. A standard filter dryer and a sight glass control the humidity of the liquid.

Resistor heater

To regulate the temperature of the cooling water a 3000 W electrical resistor heater is used. Following the circuit, the water is first heated by the electrical heater and then cooled down by the fridge. The heater is controlled by a PID which will be explained later.

PID

The auto tuning PID controller is the 'temperature-brain' of the cooling unit. It steadily controls the water temperature at the output of the cooling unit and regulates the electric heater according to these values to keep the output temperature as stable as possible. The temperature sensor for the controller is a standard Pt100 which is placed on the manifold of the cooling output. The PID offers a wide range of user defined settings like cycle-time, ramp, integral time, etc.. The initial setup was done manually and the sensor selection (Pt100) and the Output Device (Solid State Drive) was chosen. The other settings can be defined automatically by an auto-tune program which has to be executed while the cooling system is running. During an auto-tune the temperature is decreased and increased periodically and the response of the cooling system is monitored. When the program has finished the PID selects suitable values according to the monitored behaviour of the cooling system. The most important setpoint is the temperature setpoint of the cooling system. During cooling tests it was always set to 18°C.

If the cooling setup is changed e.g. superdrawers are added or removed, it is advisable to rerun the auto-tune program because intrinsic properties of the behaviour of the cooling system might have changed. Whenever electronics has to be cooled while the auto-tune program is started, the 'Tune at Setpoint' program should be used instead of the simple 'Tune' program. 'Tune at Setpoint' keeps the periodic change of the cooling temperature around the setpoint. The normal 'Tune' program would decrease the temperature too much and dew water could be created inside the superdrawers which is harmful for the electronics.

Circulator pump

The circulator pump is situated between the storage tank and the electric heater and its task is to keep the cooling water circulating. It is equipped with a variable speed control. This gives the possibility to keep a constant output pressure regardless how many superdrawers are connected to the cooling. The most frequent failure of pumps is the leakage of the shaft seal which would be catastrophic during a run-period of the ATLAS detector. Therefore a magnetic drive pump will be used for the ATLAS detector to avoid this problem.

PLC

The Programmable Logical Controller is used to control all logical operations of the cooling unit. It is responsible for the procedures that are described in the next section like stopping the whole system if the vacuum pump is activated for more than 20 minutes.

Run mode

At start-up the vacuum pump is activated if the pressure in the storage tank is not low enough. Once the pressure has reached the nominal value the vacuum pump is switched off and the system changes to running mode. In this mode the circulator pump, the fridge circuit and the electrical heater are activated. In case of a leak there will be an air-intake because the secondary circuit is at sub-atmospheric pressure. This air-intake raises the pressure in the storage tank. The vacuum pump will be activated and the circulator pump will be stopped to cut off the water flow. If the vacuum pump is running for more than 20 minutes the whole system is stopped and has to be reset.

Another crucial safety measure is the use of a discharge valve between the output and the return manifold. It provides a minimal flow between output and return even in case that all six channels are closed. This is important to avoid formation of ice in the evaporator. Furthermore this valve controls the differential pressure.

4.2.2 Cooling monitoring system

The cooling monitoring system is part of the Detector Control System (DCS) which was developed for the calibration period of the Tilecal modules in summer 2001 [32]. This DCS uses the same standard tools as foreseen for the final DCS of the ATLAS experiment and merges the Tilecal subsystems, namely the low voltage, the high voltage, the scanning table and the cooling system.

The DCS is used for monitoring and controlling the running parameters and the operational conditions of the modules and also provides communication to external systems like the SPS accelerator.

In general the DCS consists of two parts called the "Back-End" and the "Front-End" (FE) of the detector subsystem. For the BE the commercial Supervisory Control And Data Acquisition (SCADA) system PVSS-II has been selected. It runs on standard PCs and collects the data from the FE components. Furthermore it offers functions like data processing, execution of control procedures, alert handling, archiving, etc.

For the FE a general purpose I/O concentrator called "Embedded Local Monitor Board" (ELMB) has been developed by the central DCS team. It is equipped with 64 ADC channels and digital I/O functions, is radiation tolerant and can work in strong magnetic fields. Its low power consumption allows it to be remotely powered via the CANbus. Additionally the ELMB is a low-cost device, which is crucial since in ATLAS alone approximately 5000 are needed. Also the other three LHC experiments will use this technology.

In the test beam area a 80 m long CAN bus connects the ELMB to a NI-CAN II interface card which is installed in a PC in the control room. The ELMB is powered remotely from the control room via the bus by a 9 V DC power supply.
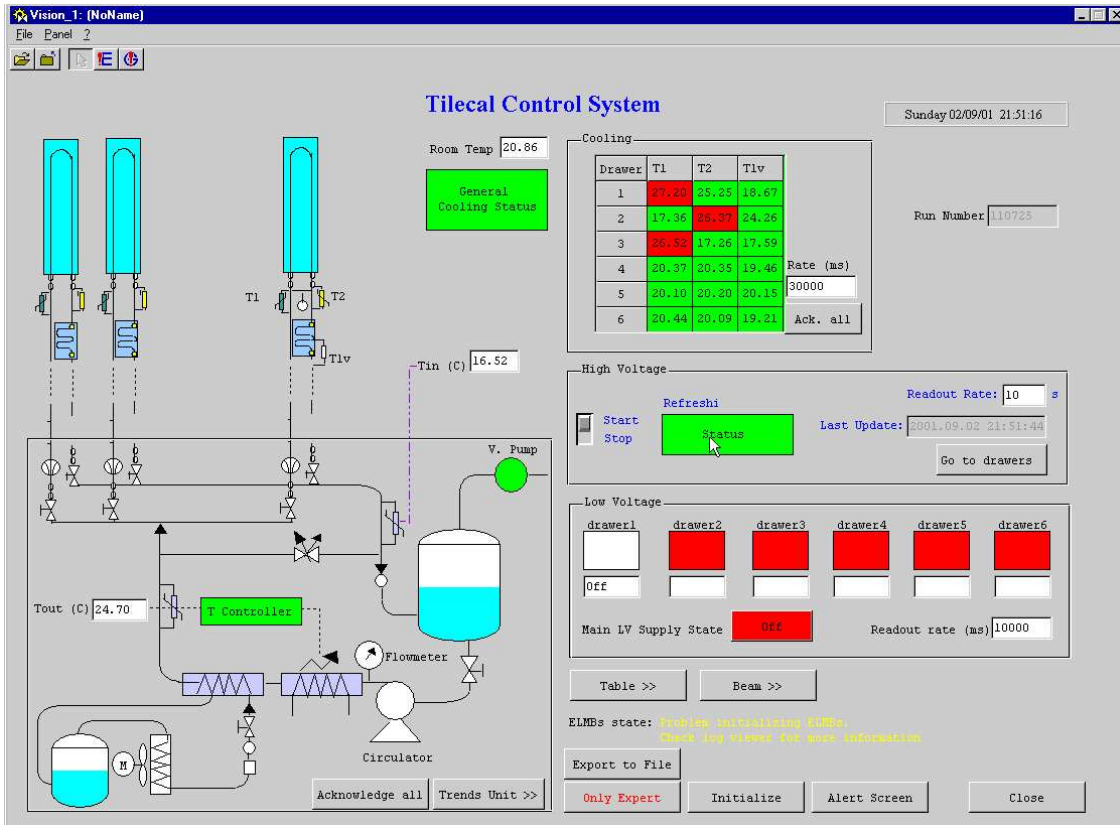
Figure 4.4: *The main panel of the PVSS application for the cooling system in the H8 beam area. The signals of all the temperature sensors are displayed on it. Via double-click it is possible to access the trend of the temperature of interest during the last few hours, days or even months.*

The chosen high-level communication protocol for its readout is CANopen. This protocol is also frequently used by the automobile industry because it is very insensitive to electronic noise. The interface between PVSS and CANopen is realized with a CANopen OPC server (OLE for Process Control) which was developed by the ATLAS DCS team.

The PVSS main panel for the operator in the control room is shown in figure 4.4. The displayed temperatures are refreshed every ten seconds. By a simple mouse click on the temperature of interest a trend panel opens which visualises the archived data. In this way it is possible to check the trend of the temperatures during the last hours, days and even months. Alerts are also displayed on this panel and warn the operator from malfunctions of the system.

Major tasks

Three major tasks have to be performed by the cooling monitoring system:

- Monitoring of the temperature sensors placed along the cooling pipes.

- Read out the seven temperature probes which are placed inside the drawer.

- Monitoring of all states and alarms concerning the cooling unit.

All the data is finally collected by PVSS-II, stored to the PVSS-II historical database and transferred to the DAQ for offline analysis. The possibility to access the database remotely has been implemented via a dedicated web interface. It allows SQL-queries to the PVSS-II database from any web browser and also offers the feasibility to download the values as an ASCII file. The SQL-queries can be performed for a specific time interval and specific temperatures.

Alarms

Already in 2001 three different kinds of general alarms had been implemented in PVSS. One alarm controls the water temperatures outside the modules. If the temperature increases or drops more than a certain threshold, the corresponding temperature starts to blink in red. The other alarm triggered a simple pop-up window whenever the HV dropped below a certain value. The third alarm is activated when the vacuum pump runs longer than a certain amount of time. This would indicate a leak in the system.

In the summer period 2002 an additional more sophisticated alarm for the HV was implemented. The new alarm distinguishes between a breakdown of the HV and small changes in the stability of the HV values. The current values are permanently compared with the nominal ones and whenever variations are recorded the alarm is triggered. A table also indicates exactly if a whole superdrawer or a single PMT is affected by the problem. Combined with an acoustic signal it

50

provides an excellent supervision of the HV values and was used with very good performance in the August 2002 calibration period.

4.2.3 Experimental setup in the test-beam area
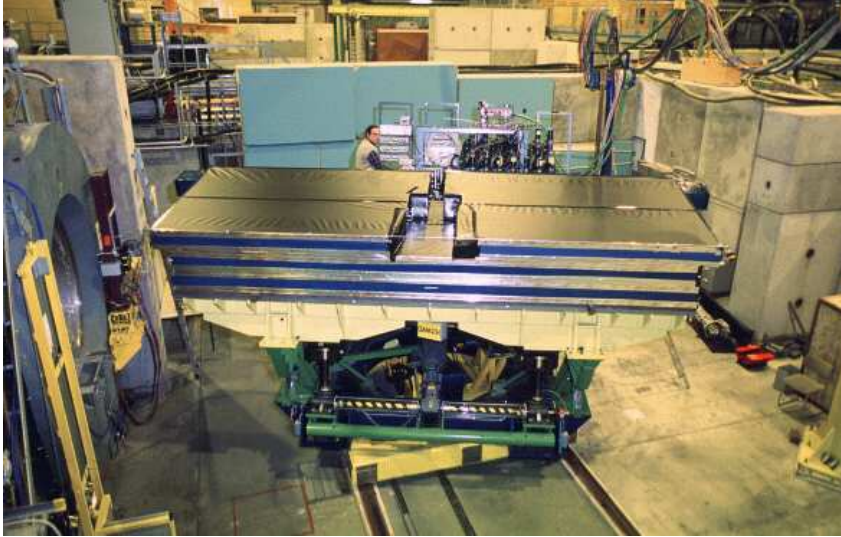
Figure 4.5: *The picture shows the setup of the Tilecal modules in the beam area where they are calibrated with a particle beam. Four modules (2 barrel, 2 extended barrel) are placed on the movable scanning table which can be remotely controlled from the control room. Behind the modules the low voltage supplies are installed in several racks because the final low voltage supplies are not yet available. During run the beam particles enter from the left side of the picture (through the big round magnet).*

In the testbeam area up to six superdrawers can be operated simultaneously. To be operational each superdrawer has to be supplied with HV, LV and cooling. The modules are mounted on a hydraulic table which makes it possible to change the angle and position of the modules relative to the incident beam. The beam mainly consists of electrons with a strong contamination of pions and muons. Additionally to the beam it is possible to use a laser source or the Charge Injection System (CIS) to test the electronic readout.

The setup in the testbeam area is shown in figure 4.5 and figure 4.6.

Temperature sensors outside the modules

Each superdrawer is fed by a separate cooling circuit coming from the cooling station. Each circuit is equipped with three temperature sensors. One sensor at
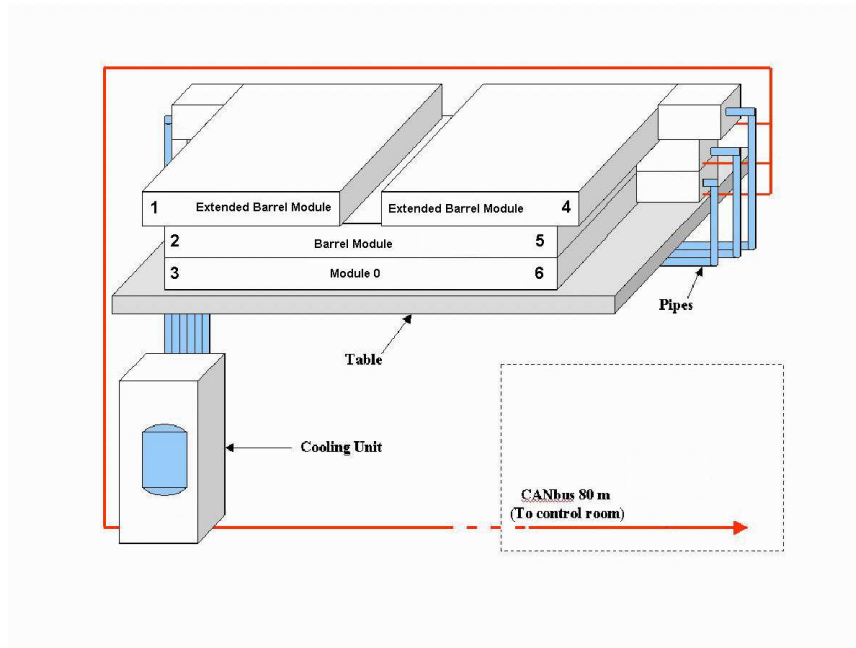
Figure 4.6: *The layout of the modules in the testbeam area is shown. The cooling unit is placed below the scanning table and pipes are connected to each one of the superdrawers. Since barrel modules comprise two superdrawers (one on each side of the module) and extended barrel modules one, there are in total six superdrawers that have to be cooled. Consequently there are six cooling circuits numbered, as shown on the figure, from 1 to 6. The parameters of the system are read out by a CANbus and the data is collected on a PC in the control room.*

the entrance of the superdrawer, one at the exit and one between the LV power supply and the superdrawer. Since the internal LV power supply was not yet available, the latter sensor is not used. In addition there are sensors at the outlet of the cooling unit (to measure the cooling water temperature) and at the return to the cooling unit.

All those temperature sensors are 10 kΩ NTCs that are in direct contact with the water and isolated from the ambient air. There is one more temperature sensor (a Pt100) on the outlet manifold of the cooling unit that is directly connected to the PLC controller and therefore cannot be readout by PVSS. The PLC uses it as the reference temperature to regulate the cooling water temperature according to the setpoint (18°C). The NTC sensors are read out over the chain ELMB - NI-CAN II interface card - OPC server - PVSS.

The NTC sensors were calibrated with an external temperature reference at 18°C. The measured temperature is connected to the resistance of the NTC with a formula which is provided by the manufacturer (a $= 9.577 \text{x} 10^{-4}$, b $= 2.404 \text{x} 10^{-4}$, c $= 2.341 \text{x} 10^{-7}$):

$$T = \frac{1}{a + b * ln((R_{NTC} + c * (ln(R_{NTC}))^3)} - T_{offset} \qquad (4.1)$$

Temperature sensors inside the modules

Additional to the described NTCs there are seven temperature sensors (also NTC) installed inside the superdrawers to measure the temperature of the electronics. They are located at different positions and measure the surrounding temperature of some key elements, like the PMT block, etc. A summary of those sensors and their position is given in table 4.1 and figure 4.7.
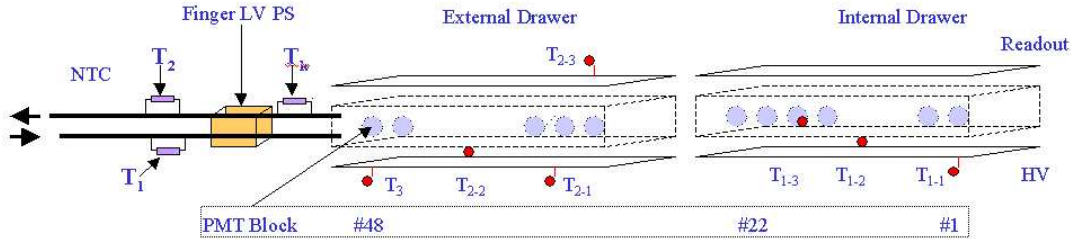
Figure 4.7: *Location of the seven temperature sensors inside the superdrawer. They measure the temperature of some key elements of the electronics. Each cooling circuit is additionally equipped with three temperature sensors: T_1, T_2 and T_{lv}. In the finger the internal LV power supply will be installed.*

T1_1	Internal High Voltage (HV) opto board temperature
T2_1	External HV opto board temperature
T1_2	Internal drawer temperature
T2_2	External Drawer temperature
T1_3	PMT block 22 temperature
T2_3	Interface card temperature
T3	HV micro card temperature

Table 4.1: *The names of the seven temperature sensors which are located inside the drawers and their position.*

The seven sensors are read out through the HV system [34] and subsequently from a Bridge View application. PVSS communicates with this Bridge View application via the Windows Shared Memory and finally stores the values in the PVSS database.

4.3 Stability of the cooling system

The measured signal of the Tile calorimeter depends on the temperature of its components. Therefore it is necessary to maintain a good stability of the cooling system. In general all the components of the readout chain (electronics, PMT, scintillators,...) are affected by temperature. But by far the most sensitive component is the PMT while all other components are only very little affected by temperature changes.

The gain of the PMTs has to remain stable within 0.5% during data taking. Previous measurements in the lab [36] showed a gain dependency of 0.2%/°C what results in the requirement that the temperature of the PMT has to remain stable within 2.5°C.

The stability of the cooling system in the H8 beam area has been monitored in the September 2001 calibration period [32] using temperature sensors inside and outside the superdrawers. During that period only two extended barrel modules were equipped with superdrawers, IFA-15 and IFA-24.

4.3.1 Temperatures outside the modules

Both modules have been monitored during a five days period. In figure 4.8 the temperatures of the sensors outside the superdrawers are presented. The temperature at the outlet of the cooling unit and at the inlet of the superdrawers are very similar because the 10 m long pipes which are used to connect the superdrawers to the cooling unit are well isolated.

As expected there is a difference between inlet and outlet of the superdrawers due to the extraction of heat produced by the electronics. This difference is 1.35 ± 0.05°C for IFA-15 and 1.25 ± 0.05°C for IFA-24 [32]. Since the LV power supply was not available for the test an increase of this difference to approximately 2°C is expected once the power supply is installed and cooled by the system.

Obviously all the temperatures follow the same fluctuations which are sufficiently small and caused by the regulation cycles of the cooling unit. In table 4.2 the mean values and their error is given.

A very good stability of 0.1°C (r.m.s.) could be observed during 5 days of data taking which is perfectly sufficient for the requirements of the electronics.

4.3.2 Temperatures inside the modules

Additionally the temperatures inside the superdrawer was monitored in the same five days period using the already described seven temperature sensors. The result for IFA-15 is shown in figure 4.9. All temperatures show a very stable behaviour. In particular the temperature sensor beside PMT 22 gives a mean value of 24.5°C with a r.m.s. of 0.1°C.
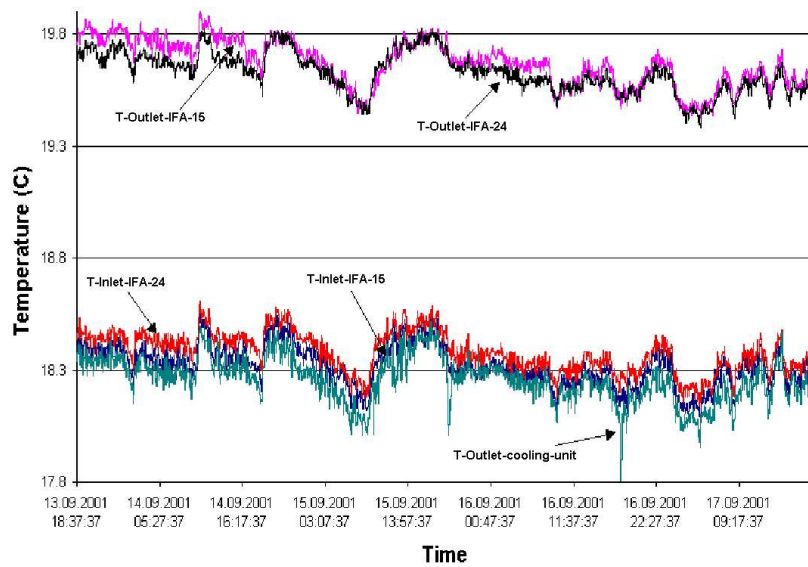
Figure 4.8: *Water temperatures at the outlet of the cooling unit and the inlet and outlet of the superdrawers of the modules IFA-15 and IFA-24 during a 5 days period in September 2001. The stability of the temperatures is 0.1°C (r.m.s.). The fluctuations are caused by the temperature regulation cycle of the cooling unit.*

Temperature	Average value and error (r.m.s.) (°C)
Outlet cooling unit	18.3 ± 0.1
Inlet IFA 15	18.3 ± 0.1
Inlet IFA 24	18.4 ± 0.1
Outlet IFA 15	19.7 ± 0.1
Outlet IFA 24	19.6 ± 0.1

Table 4.2: *The average cooling water temperatures and errors at the outlet of the cooling unit and at the inlet and outlet of the superdrawers of module IFA-15 and IFA-24 during a 5 days period in September 2001. The observed stability of $0.1°C$ (r.m.s.) is absolutely sufficient for the requirements of Tilecal.*

4.3.3 Conclusion

Taking into account these results the conclusion can be reached that the intrinsic stability of the cooling station is sufficient and the gain variations due to temperature fluctuations caused by the cooling unit are negligible.

4.4 Effects of the cooling temperature on the calorimeter response

In the beam period of summer 2001 a dedicated test was performed to evaluate the effects of temperature variation of the cooling water on the response of the Tile Calorimeter. The photomultipliers (PMTs) are the most sensible components in the Tilecal read-out regarding temperature fluctuations because their gain is strongly influenced by the temperature.

In order to evaluate the size of the effect, the cooling water temperature was varied stepwise and data was taken with a 180 GeV particle beam. Comparing the energy measurements of the particles at different temperatures gave the dependence of the read-out on the cooling temperature.

4.4.1 Study of the particle separation

The used particle beam consisted of three different kinds of particles: positrons, pions and muons. That gave the possibility to study the detector response for different particles.

To separate the particles usually the so-called *Cherenkov Cut* was used which is based on two Cherenkov counters placed in the beam line. Additionally the *Hadronic Cut* was developed which is based on the energy deposition of the particles in the different samples ($\equiv$depths) of Tilecal.
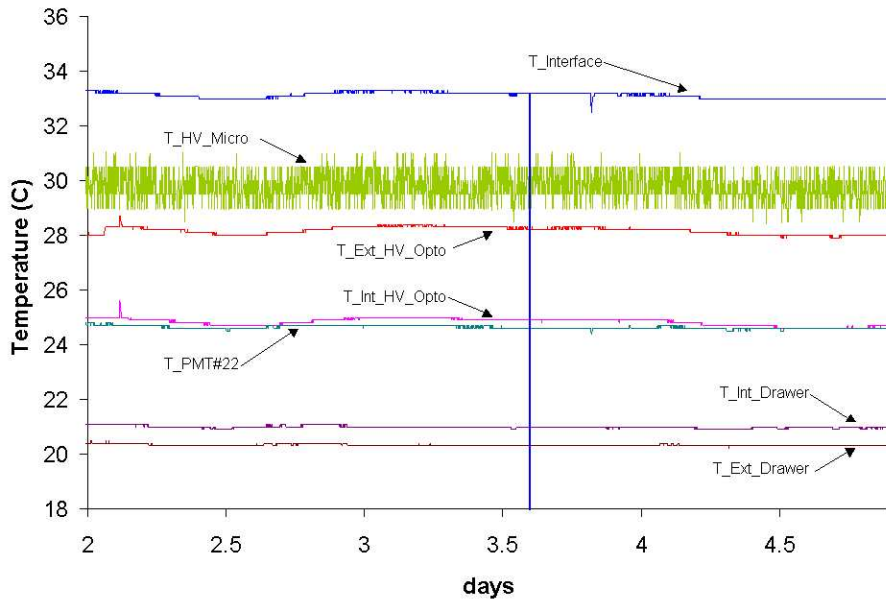
Figure 4.9: *The temperatures of the seven temperature sensors inside the super-drawer of module IFA-15 during the September calibration period. The calculated r.m.s. of the PMT temperature is $0.1°C$ in this period. For the other module, IFA-24, the same behaviour has been observed.*
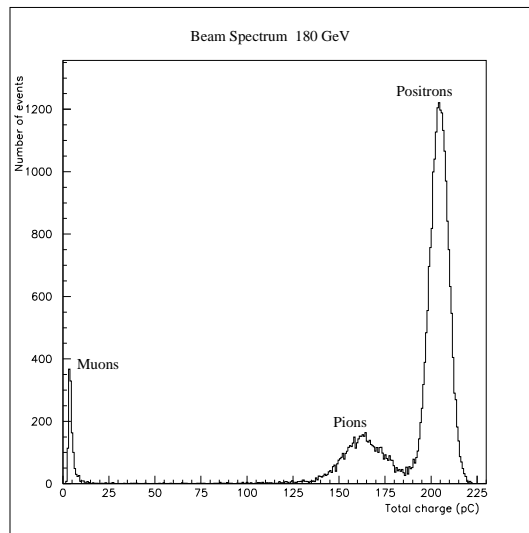
Figure 4.10: *Beam composition of the used 180 GeV particle beam. The three visible peaks correspond to muons, pions and positrons (from left to right). The measured charge has to be divided by a conversion factor of 1.2 to get the corresponding energy in GeV.*

Figure 4.10 shows the number of events versus the total charge deposited in the module is shown. The three visible peaks correspond to the three different kinds of particles: Positrons, pions and muons. The energy of the particles is represented by the charge they induce in the PMTs (in pC). A conversion factor of 1.2 is used to calculate the corresponding particle energy:

$$1 \text{ GeV} = 1.2 \text{ pC} \tag{4.2}$$

The beam contains mainly positrons, represented by the big peak with the centre at approximately 204 pC. The next peak at lower energies is the pion peak. The e/π ratio for 180 GeV is 1.13 and additionally pions create a larger shower than electrons and therefore a part of the shower is not contained in the module. The leftmost peak is the muon signal. Muons, as minimum ionising particles, interact very weakly with matter and loose very little energy while passing through the detector. One of the crucial requirements for Tilecal is the clear separation of the muon signal from the pedestal in order to contribute to the trigger performance of muon events.

Cherenkov Cut
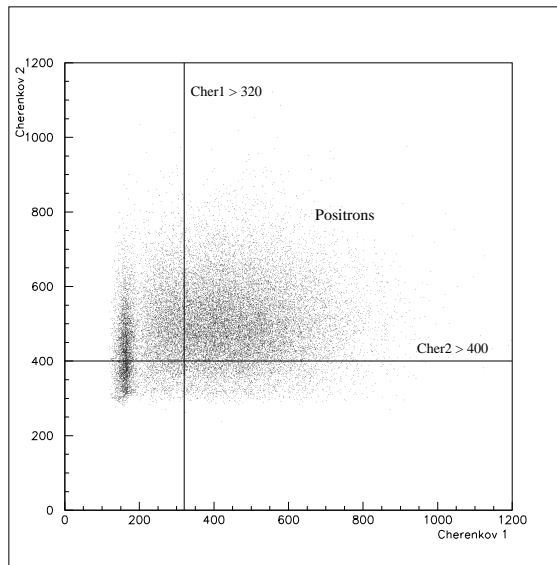
Figure 4.11: *Signal of Cherenkov counter 1 versus Cherenkov counter 2. The cut which was defined to separate positrons is indicated by the two lines. All events above those threshold energies are positrons. It is also visible that Cherenkov counter 2 did not work very well since there is no separation of positrons and pions visible.*
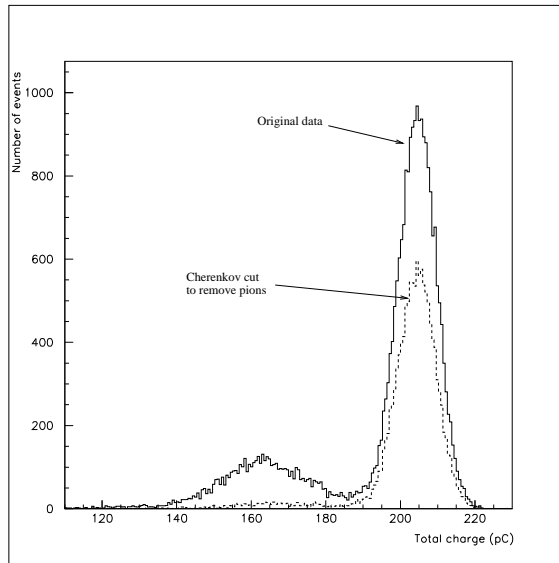
Figure 4.12: *Performance of the Cherenkov Cut. The plot shows the total measured charge in the calorimeter compared to the charge deposited by positrons separated with the Cherenkov Cut. When the cut is applied a lot of statistics is lost.*

The Cherenkov Cut used data obtained by the two Cherenkov counters placed in the beam line. They can be adjusted for specific particle separation by variation of the gas pressure inside the counters. In figure 4.11 the data of both Cherenkov counters is shown. Since positrons leave a higher signal in the counter they can be distinguished from pions.

But two problems occurred during this beam period. First of all the accuracy of the counters was deteriorating with high beam energies and for this run a high energy beam (180 GeV) was used. Secondly the counters were not properly adjusted for positron-pion discrimination. Hence the performance of this cut was rather bad, specially in terms of statistics.

Development of the Hadronic Cut

The Hadronic Cut is based on the fact that a pion shower is much larger and develops further than an electron shower. Electrons and pions were separated using a special cut on the ratio of energy that is contained in the first sample over the total deposited energy. Since electrons loose almost all their energy already in the first sample, they can be distinguished from pions which reach much further into the detector and distribute their energy over all three samples.

Figure 4.13 was the basis for the definition of the cut. The x-axis represents the fraction of energy that was deposited in the first sample, namely
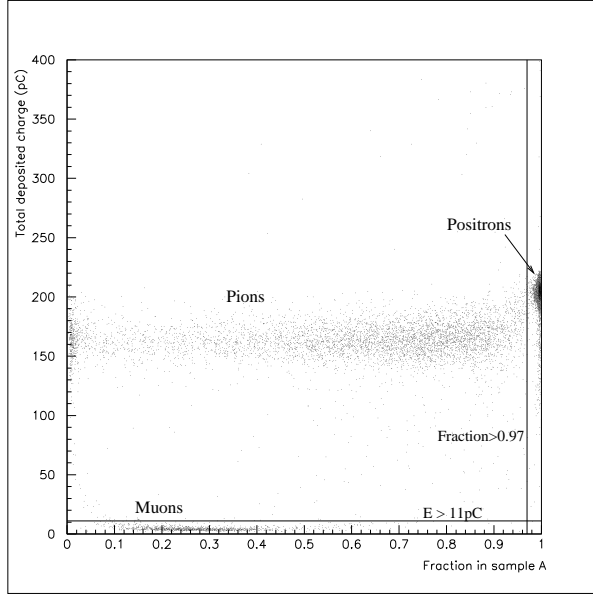
Figure 4.13: *The total measured charge over the energy fraction in sample A (energy in A / tot. energy) is shown. Each point represents one event. The Hadronic Cut to remove all particles except positrons is indicated with the two lines. An event is considered to be a positron if it deposits more than 97% of its energy in sample A and its total energy is higher than 11 pC ($\equiv$ 13 GeV).*

$$\frac{A}{A + BC + D} \tag{4.3}$$

(A, BC and D corresponds to the deposited energy in the respective sample) whereas the y-axis represents the total deposited energy in the module. Each point in the figure 4.13 is equivalent to an event. The electrons which loose most of their energy in the first sample are found on the right part of the figure because their value for A/(A+BC+D) is near to 1. Pions distribute their energy over all three samples and therefore show fractions less than one. Additionally their total deposited energy is lower than for the electrons because a fraction of the shower is lost outside the module. Muons loose their energy proportional to the length of their path through the detector. Since the way through sampling BC and D is longer than through A, their fraction-value is shifted to the left, to smaller values.

A study of the Hadronic Cut (figure 4.14) showed an excellent performance regarding particle separation and statistical yield. Therefore the Hadronic Cut was used for all further analysis.

Also a second possibility to implement a cut for positrons and pions was studied, following the paper [33]. This cut was based on the idea that a shower orig-

60
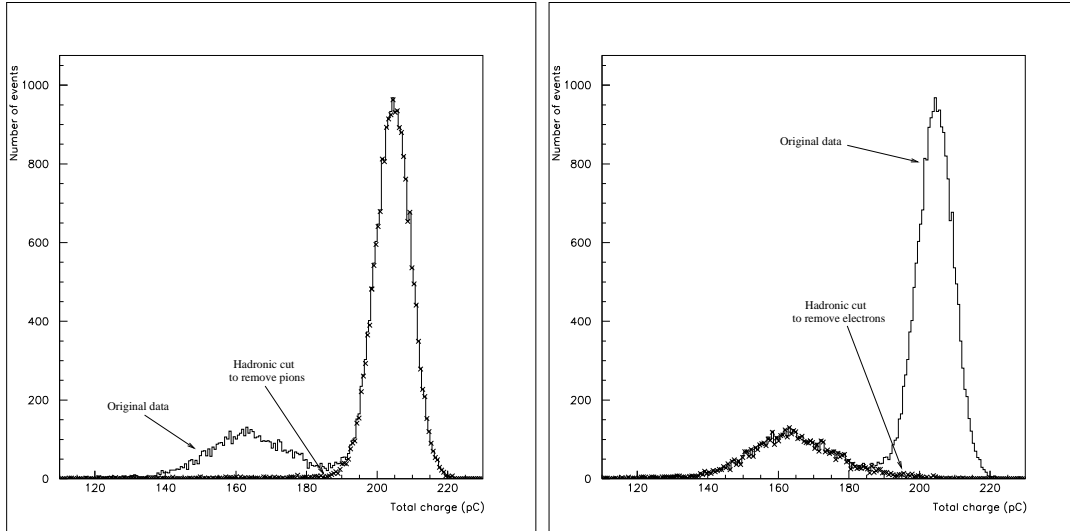
Figure 4.14: *Performance of the Hadronic Cut. The plots show the total charge measured in the calorimeter compared to the charge deposited by electrons (left) respectively pions (right) separated with the Hadronic Cut. The particle separation for both, the pions and the electrons works very well and high statistics are ensured. Therefore the Hadronic Cut was used for further analysis.*

inating from a pion triggers a signal in more PMTs than a shower of a positron. Therefore the number of PMTs with a signal above a certain threshold was computed for different events. It was found that in positron showers approximately 4 PMTs were involved whereas in pion showers more than 8 PMTs gave a significant signal. But the Hadronic Cut finally promised a better performance and a more straight forward implementation. Hence the idea with the number of PMTs was discarded.

4.4.2   Calorimeter response to a particle beam

In order to measure the variation of the calorimeter response the cooling temperature was varied stepwise in the range of 16°C to 22°C, at a constant flow of 60 l/h. After a stabilisation time of one to two hours the temperatures inside the drawer were measured.

Influence on the PMT temperature

All the seven temperature sensors inside the drawer showed similar behaviour as it can be seen in figure 4.15. In particular the temperature sensor which is placed beside PMT block 22 changed by approximately half the variation of the cooling water temperature.

61
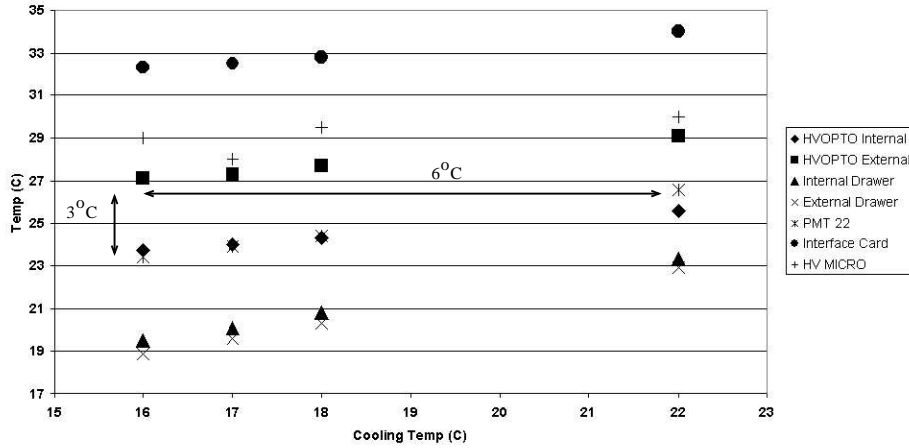
Figure 4.15: *The temperature of the seven temperature sensors inside the super-drawer is shown versus the temperature of the cooling water. Their behaviour is similar. It was found that the temperature of PMT 22 increases approximately $3^\circ C$ for a water temperature increase of $6^\circ C$.*
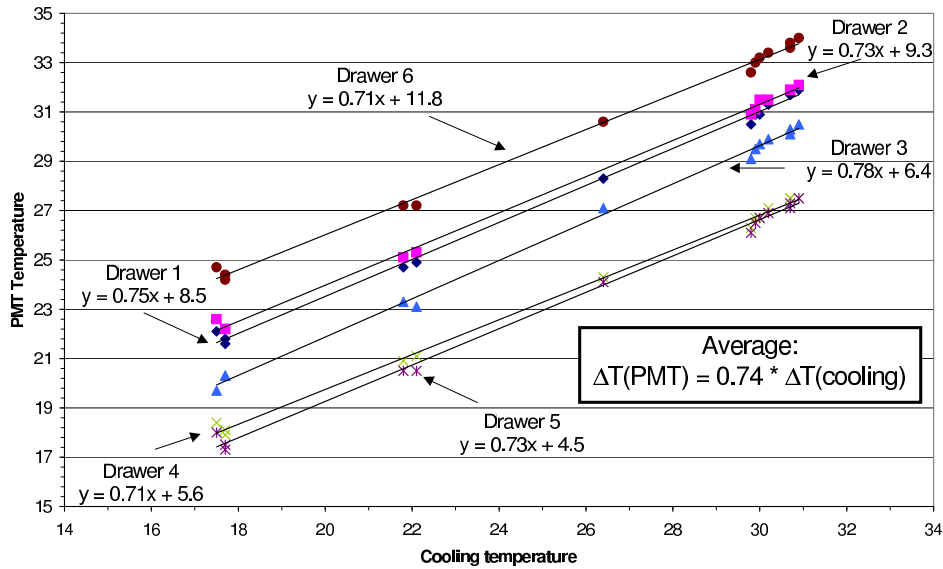
Figure 4.16: *The PMT block 22 temperatures of six superdrawers, calibrated in the August 2002 beam period are shown versus changing cooling water temperature. By computing the average behaviour the expression $\Delta T(PMT) = 0.74 * \Delta T(cooling)$ was found.*

Very recently August 2002 beam data was aquired for a bigger temperature range and for 6 superdrawers. The preliminary results are shown in figure 4.16. The results indicate the following relation between cooling water temperature and PMT temperature for the average of the 6 superdrawers:

$$\Delta T(\text{PMT}) = 0.74 * \Delta T(\text{cooling}) \tag{4.4}$$

Beam data

While the temperature of the cooling water was varied, a 180 GeV particle beam was directed to cell A14 to study the calorimeter response. This cell is read out by PMT 21 and PMT 22, the latter equipped with one of the seven temperature sensors. The data which was taken was used to compute the total measured energy for different PMT block temperatures.

Results

Figure 4.17 shows the variation of the total measured energy versus the temperature of PMT block 22 for positrons and pions. The dashed line represents a linear fit. Obviously the variation of the total energy and consequently the variation of the PMT gain is very similar for positrons and pions. This verifies that the PMT gain variation is the same for all photomultipliers since the shower of the pions effects several cells and several PMTs. The final relation between energy variation and temperature of the PMT block is given by:

$$\frac{\Delta E}{E} = 0.2\%/^{\circ}C_{PMT} \tag{4.5}$$

This result confirms previous measurements of PMT characteristics performed at a test bench [36].

Combined with the measurement that the PMT temperature changes by half of the variation of the cooling water temperature, the following relation for the gain variation of the PMTs is found:

$$\frac{\Delta G}{G} = 0.15\%/^{\circ}C_{cooling} \tag{4.6}$$

Conclusion

To ensure a PMT stability of 0.5%, the temperature variations of the PMT block have to be smaller than 2.5°C. This corresponds to a cooling water temperature stability of about 3.4°C. These results imply that only the cooling water is contributing to temperature fluctuations of the PMT blocks.
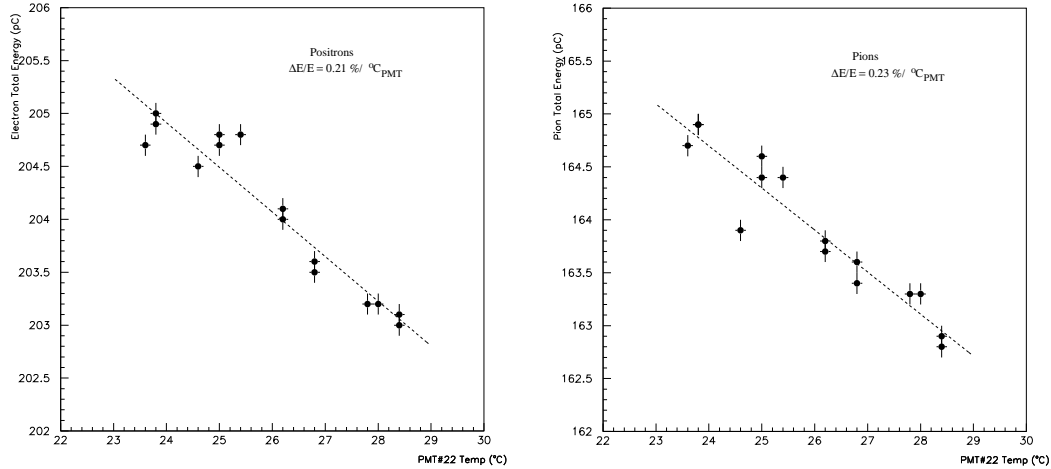
Figure 4.17: *Dependence of the total measured energy in a Tilecal module for a 180 GeV particle beam versus the PMT block temperature for positrons (left) and pions (right). The similarity of both linear fits show that the variation is more or less the same for all PMTs.*

4.4.3 Calorimeter response to Cs calibration

In August 2002 the calorimeter response versus temperature was studied by using the Cs calibration system (see 2.2.4). The cooling temperature was increased stepwise and finally the cooling was switched off. For each step a Cs-run was taken after a sufficient stabilisation time. The big difference to the preceding study with a particle beam (see 4.4.2) was that the response of all the 48 PMTs in the superdrawer could be measured. The scanned superdrawer was Module 0, positive η. As temperature reference the sensor beside PMT block 22 was taken.

When the Cs source passes the scintillating tiles, light is induced and read out by the PMTs. The signals are integrated for each tile-row in a cell and the average is computed. These values are used to compare the response for different temperatures.

The result is presented in figure 4.18. The temperature range from 19 to 39°C could be covered and the calorimeter response was normalised to the first measurement, represented by the circle without error bars. At each temperature two consecutive measurements were taken and the mean was formed. According to the linear fit the response changes like:

$$\frac{\Delta R}{R} = 0.18\%/°C_{PMT} \tag{4.7}$$

This result agrees with the measurement performed with the particle beam
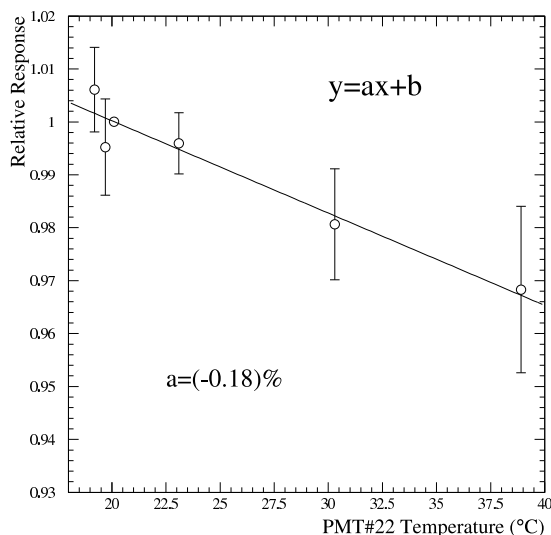
Figure 4.18: *The response of module 0, η+, for different temperatures using the Cs calibration system. The response is normalised to the first measurement, represented by the circle without error bars. With increasing temperature the response decreases. This outcome coincides with the result found in the study with the particle beam.*

which was presented in 4.4.2.

The error of the measurement is getting bigger for higher temperatures because the gains for each PMT change differently during a temperature increase.

4.5 Influence of the ambient temperature on the cooling water temperature

In a more detailed analysis of the cooling water temperature a dependency on the ambient temperature was found. This dependency could not be observed in the stability test because at that time the temperature difference between day and night was not so evident.

4.5.1 Dependency on the ambient temperature

Figure 4.19 shows a six days period in August 2001 with a very broad change of the ambient temperature between day and night. It is clearly visible that the cooling water temperature (T-cooling) follows this change at a smaller scale. In fact the change in August was
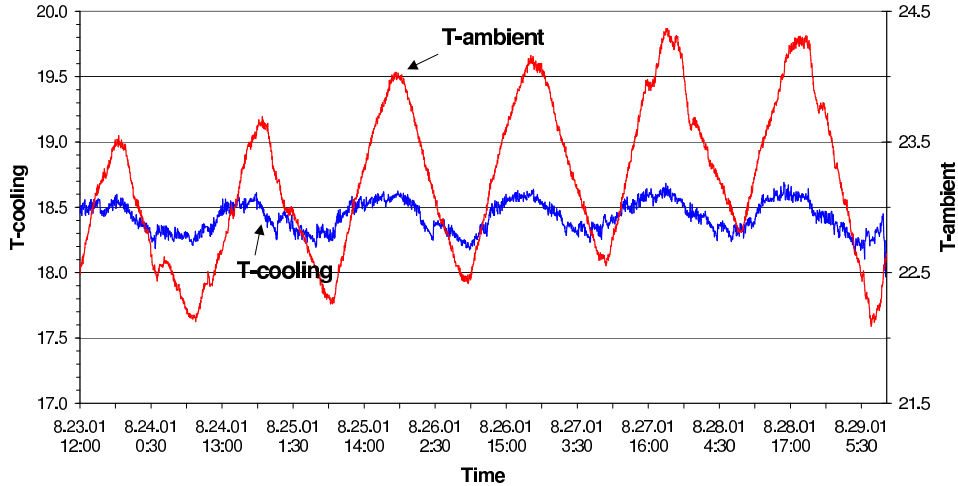
Figure 4.19: *The figure shows the ambient and the cooling temperature in a period in August 2001. Note that two different y-scales are used. The cooling temperature clearly follows the oscillation of the ambient temperature. The relation ΔT-cooling = 0.163° C / °C(ambient) was found for this period. Still the stability of the cooling unit is 0.1°C.*

$$\Delta T_{Cooling} = 0.163°C/°C_{ambient}. \qquad (4.8)$$

An influence of the ambient temperature is worrying because the calibration of the modules will be performed at different times in the year and in different buildings. Hence ambient temperature differences are preprogrammed and would influence the cooling temperature and consequentially the temperature in the superdrawers. In order to obtain good calibration results this influence should be minimised. On the other hand it has to be remarked that the influence of changes of the ambient temperature on the cooling water does not affect us in the ATLAS pit because there will be no such changes of the ambient temperature.

4.5.2 Evaluation of the size of the effect and solution

The next step was to try to get an overview of the influence of the ambient temperature over a broader temperature range. Therefore data from August, September and November 2001 was collected and an ambient temperature range from 13 to 24°C could be covered. Averaged over those months a change of the cooling water temperature of 0.11°C / °C(ambient) was found.

Following the performed measurements a range of ambient temperature in the order of magnitude of 10°C can be anticipated indoors between summer and winter. The resulting variation of cooling water temperature would be:

$$\Delta T_{Cooling} = 1.1°C \quad per \quad 10°C \Delta T_{ambient} \tag{4.9}$$

Although this is well inside the limit of 3.4°C which was found in the study of the calorimeter response (4.4) it was decided to further study this effect and to try to reduce the influence of the ambient temperature.
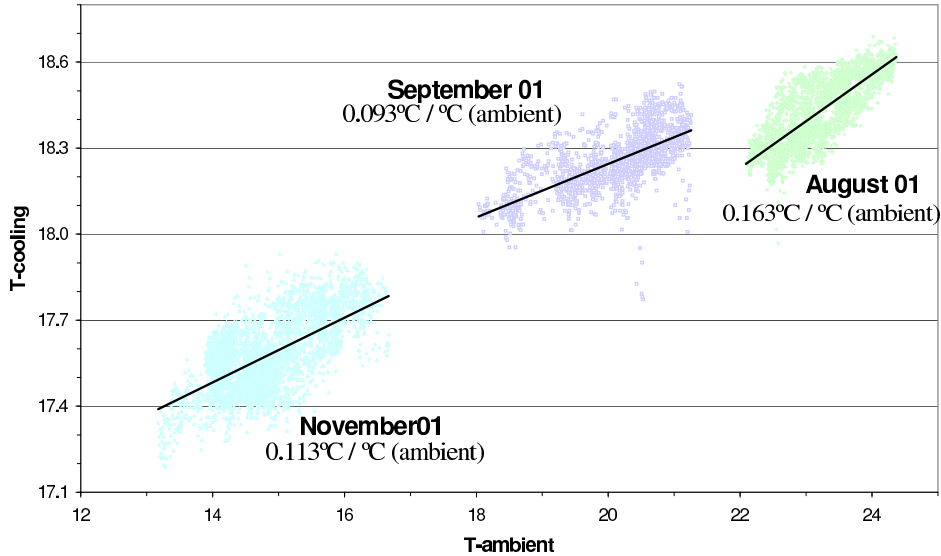
Figure 4.20: *The cooling water temperature versus the ambient for periods of several days in the three different months August, September and November is shown. An overall range of 11°C is covered which corresponds to the expected temperature gradient of the buildings between summer and winter. The dependence of the cooling water temperature is given for each month, the average dependence shows a change of 1.1°C per 10°C ambient temperature change.*

Figure 4.20 shows the behaviour of the cooling water temperature versus the ambient temperature. It gives an overview of the expected temperature gradient in the buildings for different seasons (August, September, November - in each month the temperatures where monitored during periods of several days).

After a closer investigation of the dependence it was discovered that the temperature sensor of the PID is the weak point in the system. This sensor is situated directly on the distribution manifold of the cooling unit and is read out by the PID which controls the temperature of the cooling water via an electrical resistance heater. As this sensor is only connected to the controller it cannot be read out by the PVSS application. The front part of the sensor sticks directly inside

the metal manifold and the rear part of its tube was exposed to the ambient air. As there was no insulation foreseen for this sensor it was very sensitive to ambient temperature changes.

After a proper insulation of the controller sensor and the surrounding manifold, new data was taken in January 2002. The result is shown in figure 4.21. A significant reduction of the influence of the ambient temperature could be obtained. The reduced dependence of the cooling water temperature on the ambient temperature after the improved insulation in January was

$$\Delta T_{Cooling} = 0.3°C \quad per \quad \Delta 10°C_{ambient} \tag{4.10}$$

That corresponds to a decrease of 73%. All values are summarised in table 4.3.

Month	Cooling water change per °C(ambient)
August	0.163°C
September	0.093°C
November	0.113°C
January (improved isolation)	0.027°C

Table 4.3: *Summary of the dependence of the cooling water temperature on the ambient temperature. With the improved isolation in January the influence could be minimised.*

4.6 Absolute temperatures inside the drawers

The absolute temperatures inside the superdrawers were checked in order to study if identic electronic components in different superdrawers show the same absolute temperatures. Additionally the temperature uniformity inside the modules could be derived.

4.6.1 Measurement of the temperatures

For the test the three modules (two extended barrel and one barrel module) which where calibrated in August 2001 were used. Hence four drawers were monitored. The test-beam setup for August is given in table 4.4.

To eliminate environmental influences which could cause different temperatures in the superdrawers, the monitored period was the same for all of them.

Figures 4.22 and 4.23 show the absolute temperatures for the two superdrawers of the barrel module during a 3 days period. The various temperatures are stable but differences in the absolute values can be observed. Those differences
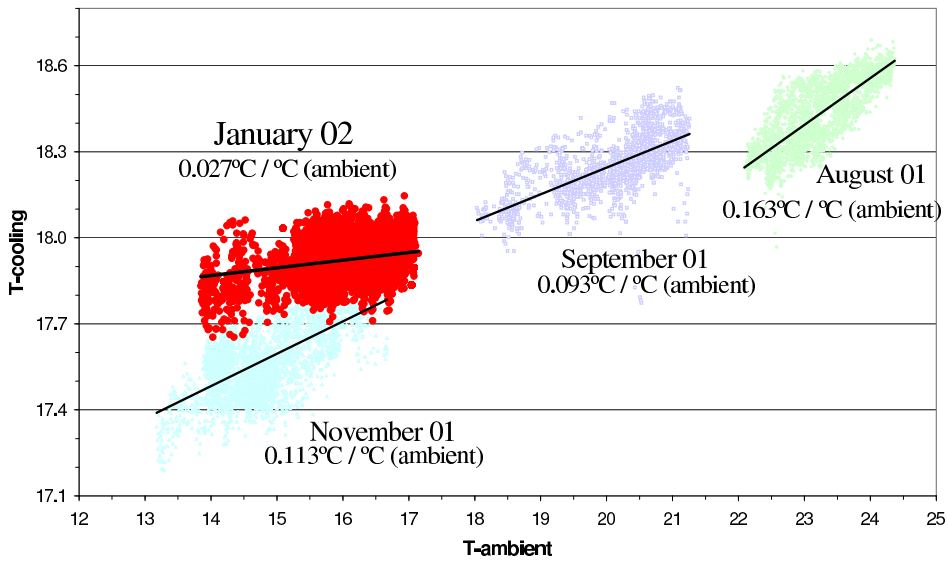
Figure 4.21: *Additional to figure 4.20 the data taken after the improvement of the isolation in January is shown. The influence of the ambient temperature could be reduced significantly by isolating the controller sensor and the surrounding manifold.*

Drawer 1 - IFA 38	ANL 15 - Drawer 4
Drawer 2 - JINR 18 - Drawer 5	
$\eta > 0$ - Module 0 - $\eta < 0$	

Table 4.4: *Setup of the monitored superdrawers and the associated modules that were calibrated in the August 2001 period.*

were surprisingly high although it is known from experience that the working temperature of e.g. PMTs can vary from piece to piece.

A summary of the data can be found in table 4.5. The largest differences were found for the PMT blocks and the interface cards, reaching values up to 4.8°C and 5.7°C respectively.

A reason for those temperatures differences could be a bad calibration of the temperature sensors. Since the sensors are merged with the electronics in the superdrawer it was not easily possible at CERN to calibrate or test them additionally. But since August the initial calibration method was improved.

It should not be forgotten that the differences of the absolute temperatures do not affect the final module performance because the modules will be calibrated individually and this calibration compensates the different temperatures.

69
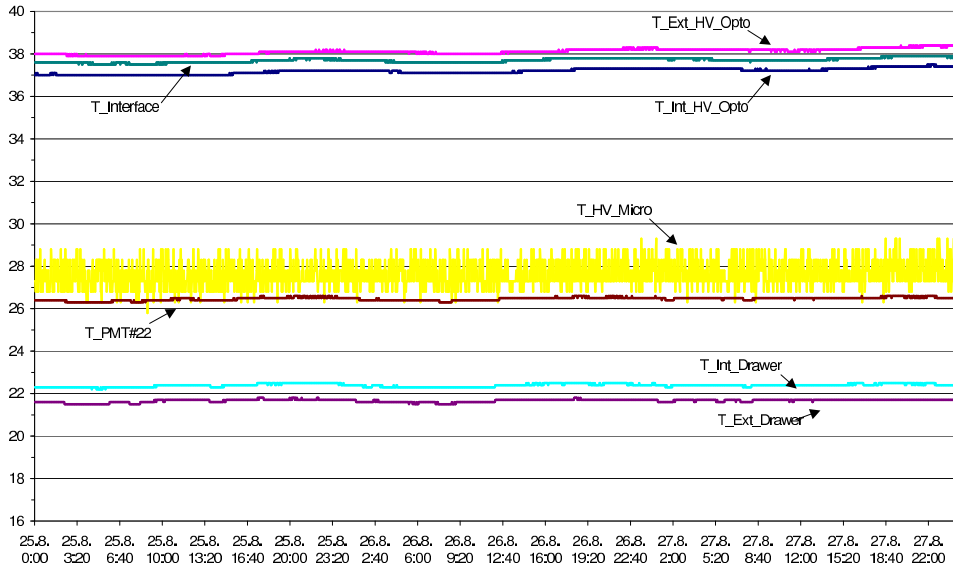
Figure 4.22: *Drawer 2, Module JINR 18, 3 days period. The temperatures of the seven sensors inside the drawer are shown. The stability is good but compared to figure 4.23 differences of the absolute temperature values can be seen.*
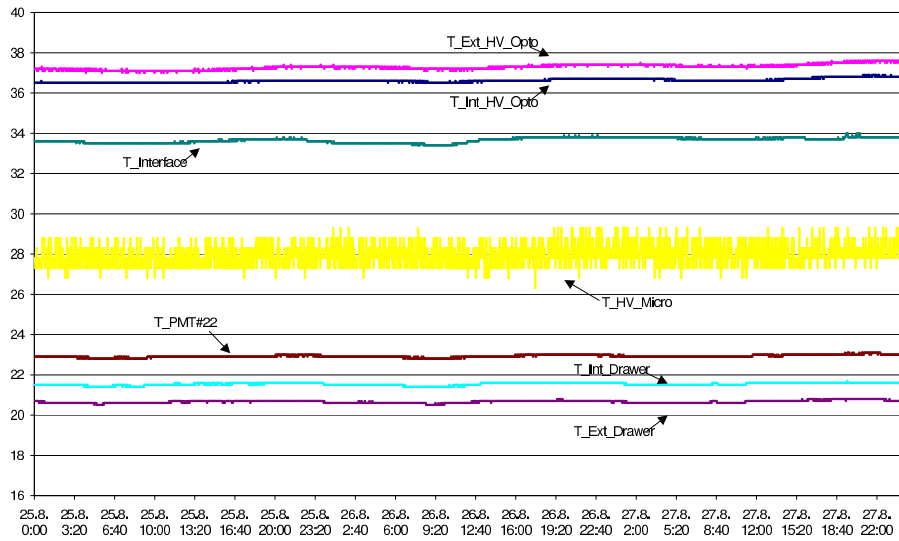
Figure 4.23: *Drawer 5, Module JINR 18, 3 days period. The temperatures of the seven sensors inside the drawer are shown.*

°C	Drawer 2	Drawer 1	Drawer 5	Drawer 4
Int-Opto	37	36.2	36.5	37.2
Ext-Opto	38	35.1	37.2	37.5
Int-Drawer	22.3	22.7	21.5	21.7
Ext-Drawer	21.6	20.2	20.6	20.9
PMT22	26.4	27.7	22.9	23.5
Interface	37.6	36.2	33.6	31.9
Micro	27.3	28.3	27.3	27.3

Table 4.5: *Overview over the mean temperatures of the seven sensors inside four different drawers in a three-day period in August. Big differences can be seen for the PMT block and the Interface card.*

Nevertheless it is a future goal to decrease those differences.

4.7 Effects of ambient temperature on non-isolated pipes

So far all the pipes used in the cooling tests were isolated to avoid any influence of the ambient temperature. In the final ATLAS detector setup there won't be enough space for isolated pipes therefore other solutions have to be found.

A favoured possibility is the so called MEPLA tube which was tested on the dependence of the ambient temperature.

4.7.1 Mepla tube

The MEPLA tube (figure 4.24) is a product of the European company GEBERIT. It consists of three layers polyethylene-aluminium-polyethylene and combines the advantages of plastic and metal pipes. The major advantages are:

- Fast and easy installation

- No soldering, brazing, thread cutting

- Flexible

- Dimensionally stable

- Corrosion & UV resistant

- Diffusion tight

- Complete range of pipes and fittings

The tube also satisfies TIS [1] requirements. Because of those properties the tube seems to be suitable for installation in the final ATLAS detector. The only open question that remained was the influence of ambient temperature on the non-isolated MEPLA tube. This test is explained later.

The MEPLA tube was also used in the real size cooling project in building 185.
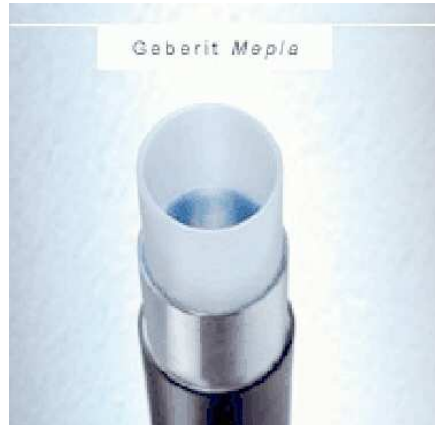
Figure 4.24: *The MEPLA tube is a three layer pipe (polyethylene - aluminium - polyethylene) and combines the advantages of plastic and metal pipes. The layer structure can be seen very clearly in this picture*

4.7.2   The MEPLA tube test

In the final ATLAS detector setup an ambient temperature gradient of 5°C is expected between the lowest and the highest module. The distance between those two modules is approximately 10 m. As all the cooling water temperatures at the entrance of the modules should be as close as possible it is important that the temperature pick up due to the 10 m of non-isolated MEPLA tube is negligible. If this temperature pick up is not sufficiently small it would result in different cooling water temperatures in different drawers and therefore also different temperatures of the electronic components which has to be avoided. To equalise the input temperatures for the modules, a system of re-heaters was under discussion. Placed at the entrance of each module they could have regulated the water temperature individually. But several points made this concept doubtful, for example the limited space, the layout of the re-heaters, their control or the additional cabling.

Figure 4.25 gives an overview of the situation in the pit.

---

[1]Technical Inspection and Safety division
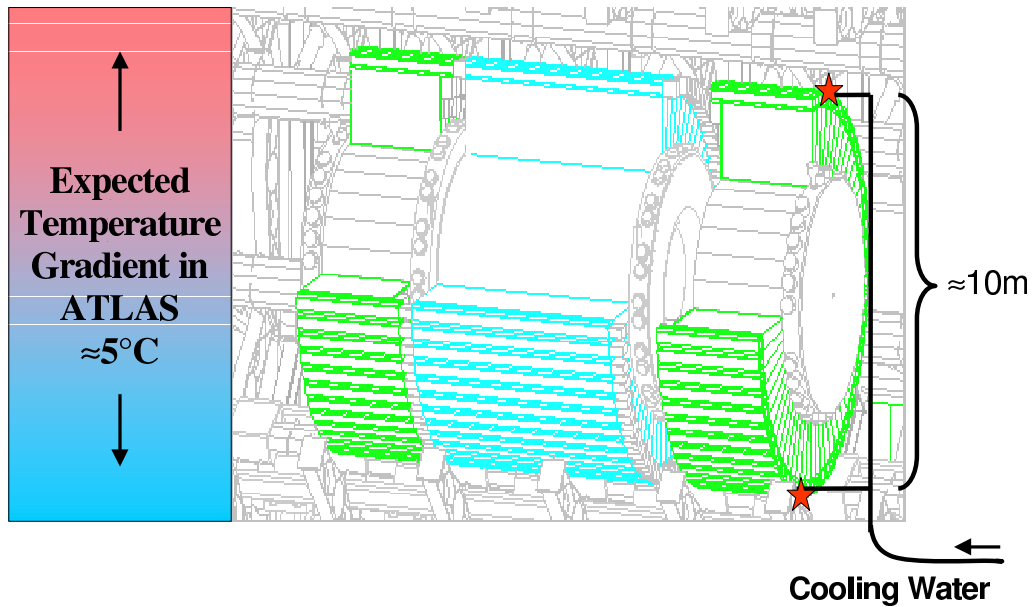
Figure 4.25: *Sketch of the Tile Calorimeter in the final ATLAS setup. There will be an ambient temperature gradient between highest and lowest module of approximately 5°C. Despite this gradient the cooling water temperature at the entrance of the modules should be as close as possible.*

For the test, the piping of the cooling system in the test-beam area was modified. The isolated inlet pipe of circuit number 4 was replaced by a 10 m long non-isolated MEPLA tube. The water temperature at the beginning and the end of the tube was measured for changing ambient temperature and the results were compared with the isolated tube of circuit number 1. Any ambient effects on the cooling unit have been removed by calculating the difference between the exit and input temperature of the tube.

In figure 4.26 this temperature difference is shown for the isolated tube versus the ambient temperature. A dependence of

$$0.01°C/°C(ambient) \tag{4.11}$$

was found and is explainable with the non-perfect isolation of the tube.

Figure 4.27 shows the same measurement for the MEPLA tube. As expected the slope is a little bit steeper, to be more precisely it is

$$0.04°C/°C(ambient). \tag{4.12}$$

73
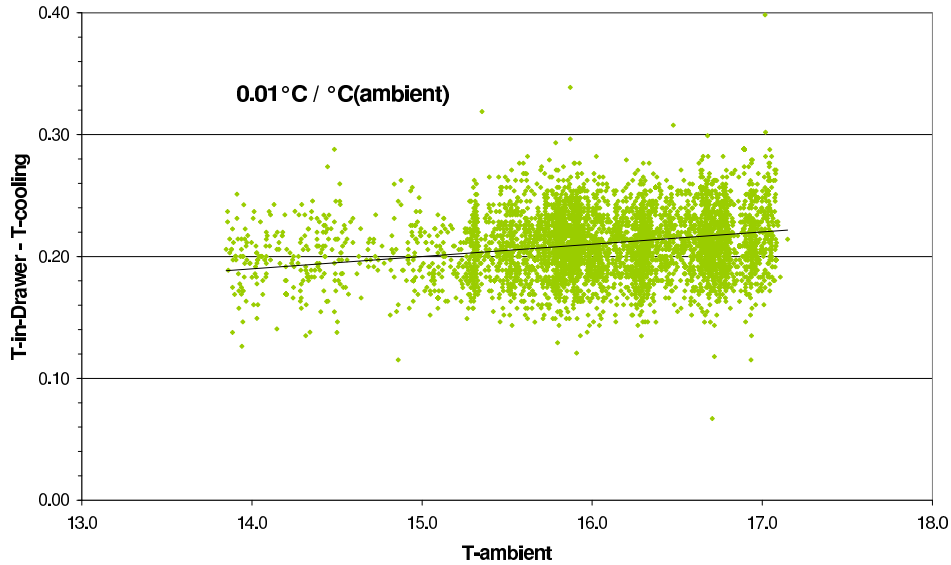
Figure 4.26: *Temperature difference between exit (T-in-Drawer) and input (T-cooling) of the isolated tube versus the ambient temperature. Building this difference removes any ambient effects on the cooling unit and makes it possible to evaluate the temperature pick up between the two points. The slope of 0.01°C/°C(ambient) can be explained with the non-perfect isolation of the tube.*

Nevertheless this dependence is negligible small in our case. For the expected temperature gradient of 5°C in the pit it would mean less than 0.2°C temperature difference of the cooling water between the lowest and the highest module. This difference would cause a change of the PMT temperature of only 0.1°C. "Less than 0.2°C" because the temperature gradient of 5°C in the test between day and night affected the whole length of the tube whereas in the final detector setup the temperature gradient will be between the two ends of the tube.

$$0.04°C/°C(ambient) \ \& \ 5°C \text{ gradient} \Rightarrow 0.2°C \tag{4.13}$$

Calculations

Calculations regarding the heat transfer for a MEPLA tube have also been performed. As boundary conditions a temperature difference of 5°C was used and the manufacturer specifications for the tube were taken. All the following formulas and used numbers are collected in [35]. First of all it was important to decide whether the flow was laminar or turbulent. In turbulent flow the heat absorption of the cooling liquid is much higher than in laminar flow because the liquid is

74
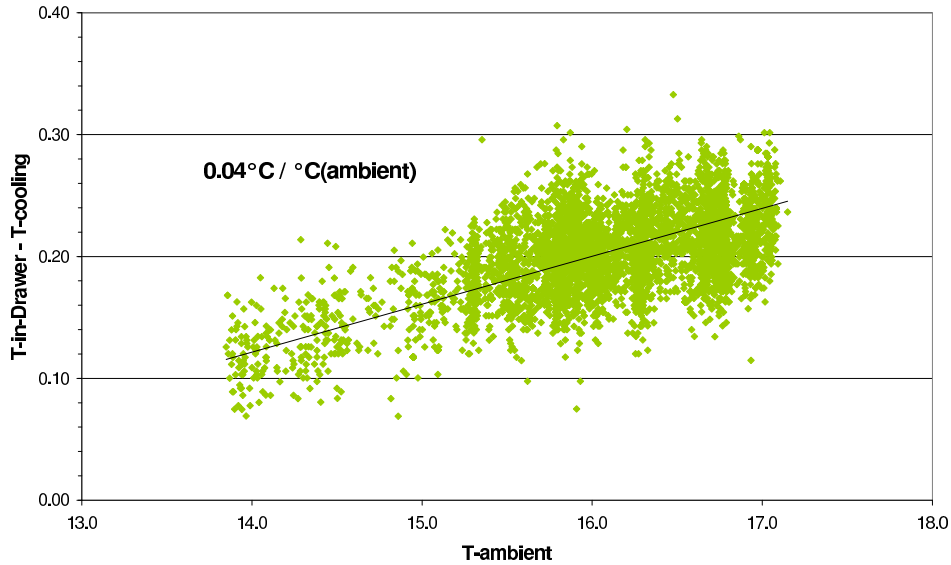
Figure 4.27: *Temperature difference between exit (T-in-Drawer) and input (T-cooling) of the MEPLA tube versus the ambient temperature. As expected the influence of ambient temperature is slightly higher than for the isolated tube. Nevertheless the influence of 0.04° C/° C(ambient) is absolutely negligible in our case.*

constantly mixing. Warm liquid is transported from the tube walls to the centre and cold liquid is transported from the centre to the tube walls. In laminar flow there is much less mixing of the liquid and therefore less heat can be transferred from the walls of the tube to the liquid. The two modes, laminar and turbulent are shown in figure 4.28. To distinguish the two modes the Reynolds-number (Re) is computed. It depends on the density (ρ), the velocity (u), the tube diameter (D) and the viscosity (μ). For the MEPLA tube and water at a temperature of 18°C it gives

$$Re = \frac{\rho * u * D}{\mu} \simeq 1900 \tag{4.14}$$

Since the boundary value between laminar and turbulent is around Re = 2300 we are still in laminar flow.

To calculate the water temperature at the end of the 10 m MEPLA tube, the whole length is divided into n segments, each Δx m long, as it can be seen in figure 4.29. Then a recursive formula is used to calculate the actual temperature of each piece until the last segment is computed. This procedure is very similar to a finite element calculation and can be easily carried out using a spread sheet
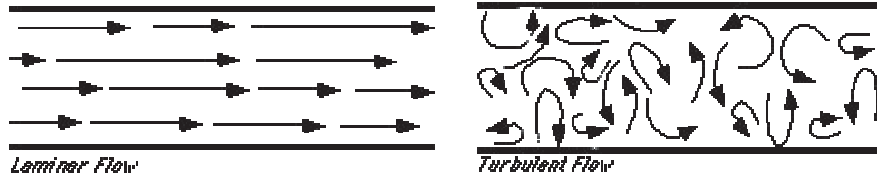
Figure 4.28: *Two general flow modes of liquids and gases are shown. The Reynolds-number can be used to identify the flow regime the system is in.*
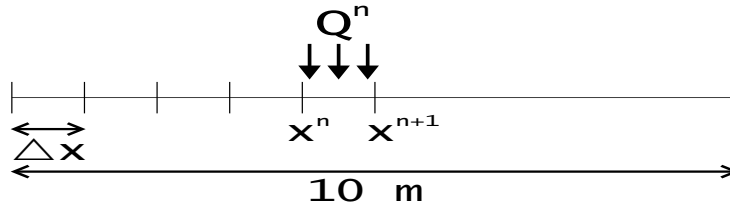
Figure 4.29: *To compute the water temperature at the end of the MEPLA tube, it is divided into n small segments. Using the recursive formula 4.17 it is possible to calculate the temperature of each piece.*

program.

We start with the basic formula of calorimetry which gives an expression for the absorbed power (Q [W])

$$Q = \dot{m} * C * (T^{n+1} - T^n) \tag{4.15}$$

($\dot{m}$...mass flow [kg/s], C...specific heat capacity [J/(kg*K)], T^n...water temperature of the actual segment T^{n+1}...water temperature of the successive segment) Transforming the equation and substituting Q with help of Newton's law for external heat transfer

$$Q = \frac{T_{ambient} - T^n}{R} \tag{4.16}$$

we get

$$T^{n+1} = \frac{T_{ambient} - T^n}{R * \dot{m} * C} + T^n \tag{4.17}$$

(R ... thermal resistance [K/W]) Formula 4.17 is the desired recursive formula which can be used to compute the water temperature in the end of the 10 m MEPLA tube. R, the thermal resistance, consists of three terms as shown in formula 4.18.

$$R = \frac{1}{h_i * \pi * \Delta x * D_i} + \frac{\ln \frac{r_o}{r_i}}{2 * \pi * \Delta x * K_M} + \frac{1}{h_o * \pi * \Delta x * D_o} \qquad (4.18)$$

(h_i...inner heat-transfer coefficient, Δx...lenght of segment, D_i...inner diameter, r_i...inner radius, r_o...outer radius, K_M...heat conductivity of MEPLA tube, h_o...outer heat-transfer coefficient, D_o...outer diameter)

The first term represents the thermal resistance between the cooling water and the inner wall of the tube, the second term describes the resistance of the tube itself and the third term represents the transition from the outer tube wall to the surrounding air. The heat conductivity for the MEPLA tube is given by the producer (0.43 [W/(m*K)]). The heat-transfer coefficient, h, has to be calculated according to the environmental conditions. In our case a h_i of 208 W/$(m^2$*K) and a h_o of 4.7 W/$(m^2$*K) was found.

After inserting all the values in formula 4.17 and computing the value for the last segment of the 10 m MEPLA tube, we found the value of

$$T_{10m} = 18.16°C \qquad (4.19)$$

Finally the result of the calculation can be compared with the performed measurement. In the calculations a difference between the cooling water temperature and the ambient temperature of 5°C was assumed. For this assumption the measurement result 4.12 gives an increase of 0.2°C of the cooling water temperature and therefore an absolute value of 18.2°C. Obviously the measurement is in very good agreement with the calculation.

4.7.3   Conclusion

The tests showed that using the MEPLA tubes the temperature pick up is negligible for the expected temperature gradient in the final ATLAS detector. Based on this results the idea of installing re-heaters for the different sections of the Tilecal detector to provide equal temperatures was abandoned by the collaboration. In addition samples of the MEPLA tube were given to the TIS division and passed the safety requirements (fire, radiation, etc.).

4.8   Total dissipated power of the final super-drawers

The two main sources of heat production in the Tilecal modules are the electronics of the superdrawer and the low voltage power supply in the fingers. As it can be seen in figure 4.30 they both build a unit from the cooling point of view and are fed by one cooling channel which delivers cooling water in series first to the

superdrawer and then to the finger. As already mentioned the cooling system was designed to extract a total of 300 W per cooling channel and to keep a Δ T between input and outlet of the module of 2°C. 200 W are expected to be dissipated by the electronics in the superdrawer and 100 W by the low voltage power supply in the finger.
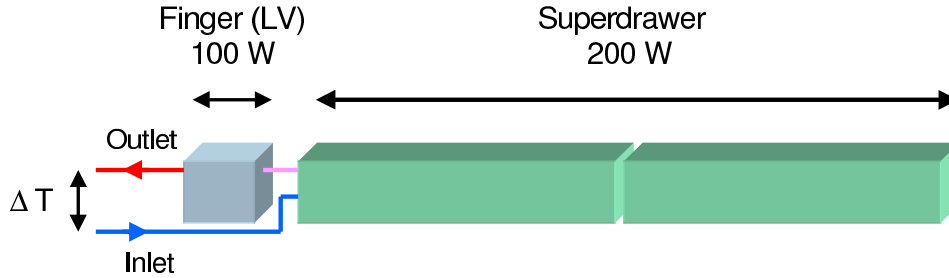
Figure 4.30: *The cooling for the superdrawer and the LV power supply inside the finger. The cold water first enters the superdrawer and then the finger. The ΔT is measured between inlet and outlet of the module. The design values for the cooling station are also given: 200 W for the superdrawer and 100 W for the LV power supply.*

The cooling unit had to be designed before the final superdrawers and low voltage power supplies were constructed and therefore the design was based on theoretical values and measurements of electronic prototypes. This circumstance made it necessary to measure the power dissipation of the final components used for the production in order to verify or to disprove the current cooling system design.

Hence a dedicated measurement of the consumed power of the electronics in the superdrawers has been performed. Since the final low voltage power supplies for the fingers are not yet available, the different components in a superdrawer are powered by external power supplies each providing a different voltage according to the powered component. The voltage and the current were measured with an external multimeter and the consumed power was calculated with Joule's law:

$$P = I * V \tag{4.20}$$

P ... power [W], I ... current [A], V ... voltage [V]

The amount of electronics in the extended barrel and the barrel superdrawers are different and consequently they have a different power dissipation. Consequently both types of superdrawers had to be measured. In total two extended barrel and three barrel module superdrawers were checked. The results are collected in table 4.6.

	measured value	with safety factor 1.5
Ext.Bar. - IFA 38	129 W	194 W
Ext.Bar. - ANL 8	135 W	202 W
Barrel - JINR 18	166 W	249 W
Barrel - JINR 34	173 W	260 W
Barrel - M0-	182 W	273 W

	average value	average with safety factor 1.5
Extended Barrel	132 W	198 W
Barrel Module	174 W	261 W

Table 4.6: *The measured values for the total consumed power (without and with a safety factor of 1.5) for two extended barrel superdrawers and three barrel superdrawers are presented. The average consumed power for both types of superdrawers are also given. Additionally the design values for the cooling system are presented.*

The measured values for both types of superdrawers are within the design values of the cooling unit (200 W). But due to the effects of ageing and radiation damage the electronics are expected to increase their dissipated heat with time. Therefore a safety factor of 1.5 was introduced for the total consumed power.

Even with this factor the cooling works sufficiently well to maintain the desired ΔT of 2°C for the superdrawer.

Applying the safety factor for the extended barrel modules we get a average total power dissipation of 198 W which is still within the assumptions for the design. For the barrel module we get a power dissipation of 174*1.5 = 273 W which is above the design value of 200 W.

Nevertheless the ΔT below 2°C will still be maintained for the superdrawer. In the LV power supply, which is not sensitive to temperature, it will be higher, probably at 3°C.

4.8.1 Remote control and monitoring of the LV power supply

In the July and August 02 period of test beam calibrations a new remote control and monitoring system was implemented. From time to time, specially while debugging the electronics, it is necessary to reset the boards by means of a power-cycle. But it is not always possible to have access to the LV power supplies that are located beside the modules, for example when the particle beam is on. Thus a remote control for the power supplies was developed based on the already presented DCS systems in chapter 3 and 4.2.2, particularly the ELMB and PVSS-

II. With a dedicated interface panel it is now possible to switch the power supplies on and off with a simple mouse click.

Additionally the monitoring of the voltages and currents of one LV power supply was enabled by means of a specially adapted ELMB and again the PVSS application. For the next testbeam the monitoring of all 6 power supplies is planned.

4.9 Flow test

In April 2002 a flow test has been carried out in building 185 to determine the amount of heat that is extracted by the cooling system. During the test the water flow was varied from 20 - 82 l/h and the Δ T between input and outlet of the superdrawer was measured. With those values it was possible to calculate the extracted heat per second.

Since there were only a few modules already equipped with electronics the test was carried out in one of the Tilecal storage areas in building 185. The used module was the extended barrel module IFA 38 which was calibrated in the summer period 2001. Building 185 housed the second cooling station which is mobile but otherwise similar to the one in the testbeam area. The mobile cooling station will also be used for future Cs calibration of the Tilecal modules.

4.9.1 Scope of the flow test

The flow test was essential to understand if the current conception of the system is sufficient to fulfil its future tasks.

In order to be able to calculate the extracted heat the flow and the Δ T between inlet and outlet of the module (see 4.30) had to be measured and then used in the formula [37]

$$Q = c * m * \Delta T \tag{4.21}$$

Q ... absorbed heat [J/s = W], c ... specific heat capacity [4190 J/(kg*K)], m ... mass flow [kg/s]

Δ T ... temperature difference between input/outlet of the module (°C)

Measurement of the flow

For the measurement of the flow a commercial plastic flowmeter was used. It works based on the suspended float principle where a conical plastic tube with a scale is placed in vertical position. The water flow, coming upwards, raises a little floater placed inside the tube and the flow can be read off the scale.

The accuracy of the flow measurement was better than ± 1 l/h. At lower flow rates, more precisely at rates below 20 l/h, the stability of the whole circuit is

not very good and the flow tends to start to vary with time. Therefore the error of the measurements at low flow rates is bigger than at higher rates.

Measurement of the Δ T

The temperature difference was measured with two NTC sensors placed at the input and at the outlet of the module. The sensors were in direct contact with the cooling water and were well isolated with insulation tape to minimise effects of the ambient temperature.

The readout was implemented in the same way as in the testbeam area. The data was collected and archived by PVSS.

Procedure

During the test the flow was changed successively from the highest possible flow of 82 l/h to 10 l/h. Meanwhile the temperatures of the cooling water at the input and the outlet of the module were measured to be able to compute the extracted heat. To give the system enough time to stabilise, the test was carried out over a few days and a minimum stabilisation time of 4 hours was applied. Throughout the test all the electronics in the superdrawer were powered with their nominal voltage, except the high voltage (HV) supply for the PMT's. The HV could not be used because the light tightness of the modules was not assured since the cover of the modules was partially removed due to reparation work.

To verify that no significant heat dissipation is coming from the HV, testbeam data was checked. The result is presented in figure 4.31. It can be seen that there is no increase of the ΔT between input and outlet of the module, when the HV is switched off. Therefore its heat dissipation can be neglected.

4.9.2 Results and comparison with previous flow tests

The Flow Test in April 2002 substantially validated the two old flow tests from September 2001. This can be seen in figure 4.32 where the symbols of the test in 2001 fit very good together with the newly observed values. The graph shows a plateau at a flow of about 60 l/h. Therefore the previous conclusions regarding the flow in [32] can be confirmed and extended to the final proposition that the flow should not be lower than 60 l/h.

The maximum heat that can be extracted per second with the existing cooling system lies around 92 W for a flow of 60 l/h. Taking into account that the total consumed power by this superdrawer was 129 W it gives a cooling efficiency of 71%. Obviously 37 W are absorbed by the iron mass and have to be extracted by the air condition system of the pit.

It is a crucial point to note that this test was carried out with an extended barrel module which dissipates less heat than a barrel module because it has
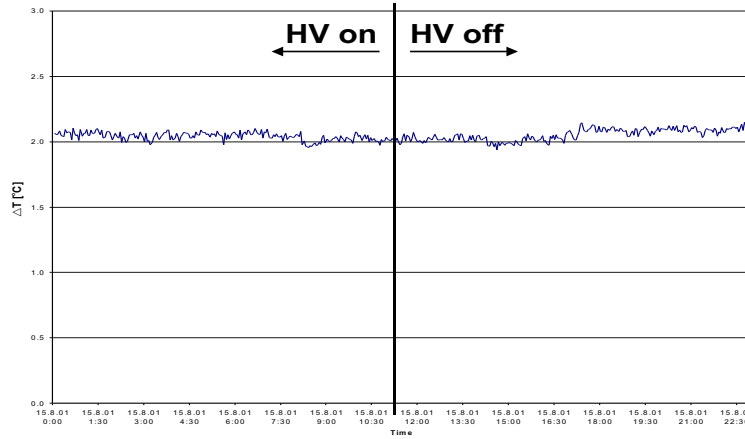
Figure 4.31: *The ΔT between inlet and outlet of the module (see figure 4.30) is shown versus time. At 11:17 the High Voltage was switched off. Since no change of the ΔT is observable, the heat dissipation of the HV can be neglected.*

less electronics inside. Additionally the change of ΔT is shown with respect to different flows in figure 4.33.

4.9.3 Conclusion

It is impossible to extract all the dissipated heat with the cooling system because the superdrawers are not isolated from the surrounding iron mass. And since iron has a very good heat conductivity a significant loss of heat can be expected. This consideration was verified by the flow test.

The cooling system showed an efficiency of 71%. The residual heat is lost trough the iron mass to the surrounding air. This has to be implemented in the conception of the air flow system in the ATLAS pit, in particular for the ATLAS muon spectrometer that is located very close to the Tile superdrawers. In a meeting between Tilecal and the ATLAS Cooling Coordination this problem was presented and currently design studies are going on to implement a dedicated cooling system for the muon chambers which are very close to the Tilecal either using air flow or liquid cooling.

The conclusion of a high cooling efficiency at a flow of 60 l/h was confirmed since a plateau is reached at this flow rate. However 60 l/h should be seen as the minimal required flow. Higher flows like 70 or 80 l/h give a similar or slightly better cooling efficiency but are not necessarily needed.
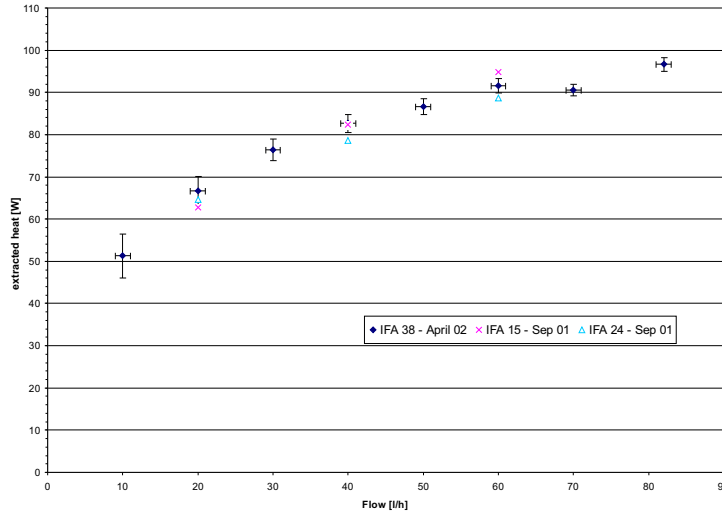
Figure 4.32: *Three flow tests with different modules were carried out. The total extracted heat per second versus different flow values is shown. At a flow of 60 l/h a plateau is reached and the maximum extracted power lies between 90 and 100 W. The results from all the three tests coincide very well and show that the minimum flow applied should be 60 l/h. Note that extended barrel modules were tested which dissipate less power than barrel modules.*

4.10   Temperature development inside the modules without cooling

During the shutdown periods of ATLAS maintenance work on the detector components can be performed. In order to be able to access the barrel part of the detector, the extended barrels will be moved several meters. This movement also has implications on the cooling system since the cooling station is fix installed at the cavern floor and the piping is done with rigid tubes. Therefore it had to be studied if the cooling has to be reconnected after the movement of the extended barrels.

4.10.1   Possible maintenance scenarios for Tilecal

During shutdown periods several tests are envisaged. Two scenarios can be considered:

1. Checks of the electronics and the readout system will be performed but no other measurements that would require normal operating conditions.

2. Additionally to the checks of the electronics and readout, calibration runs
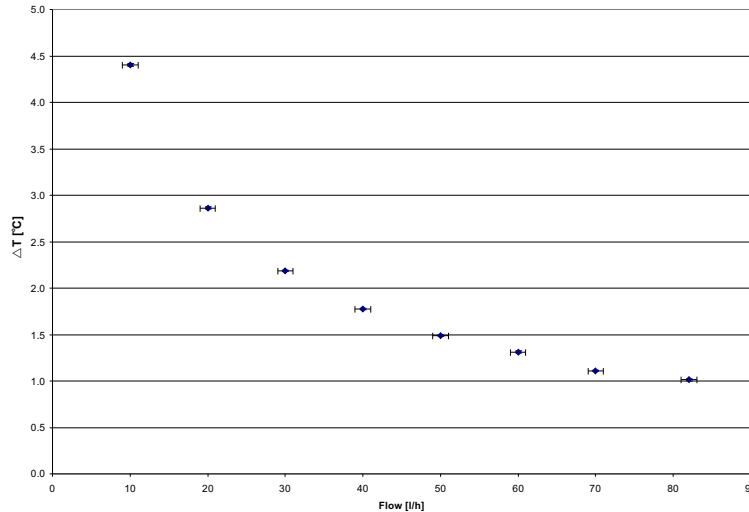
Figure 4.33: *The ΔT is shown versus different flows. For the PMTs in the superdrawer it is important not to exceed the ΔT above $2°C$ because they are sensitive to temperature. The current design of the cooling unit guarantees that even when a safety factor of 1.5 is applied due to ageing and radiation effects of the electronics.*

or other precision measurements will be carried out. Normal operational conditions and therefore also cooling is required.

In the second case the cooling has to stay connected or has to be reconnected after the movement of the extended barrels. The implementation has to be considered in the final cooling system design. Possibilities would be flexible tubes that stay connected or are reconnected after movement. Or fix installed tubes for both positions of the extended barrels, closed and opened, that have to be disconnected before and reconnected after the movement.

In the first scenario it would be sufficient if the electronics and the readout chain stay operational, even if the temperatures are higher than nominal. Then the cooling can stay disconnected if the temperatures in the electronics do not exceed 50°C. To confirm this, dedicated tests have been performed with the cooling unit switched off.

4.10.2 Maximum temperatures inside superdrawers without cooling

Before certification the electronic boards undergo a burn-out test where they are exposed to a heat of 60°C for one week. Only then they are installed on the

superdrawer. The temperature limit for good operation of the electronics was defined at around 45°C [29]. Thus a measurement was carried out to determine the maximum temperatures that are reached inside a superdrawer without cooling.

After the June 2002 calibration period this test was carried out with in total six superdrawers. The cooling had been in normal operational mode during the last few days and all the temperatures inside and outside the modules were nominal. At a certain point the cooling for all six modules was stopped and the increase of temperature inside the superdrawers was monitored. After 4 h 16 m the cooling was turned on again. The measurement for the extended barrel IFA 59 can be seen in figure 4.34, which is representative for all the other modules.
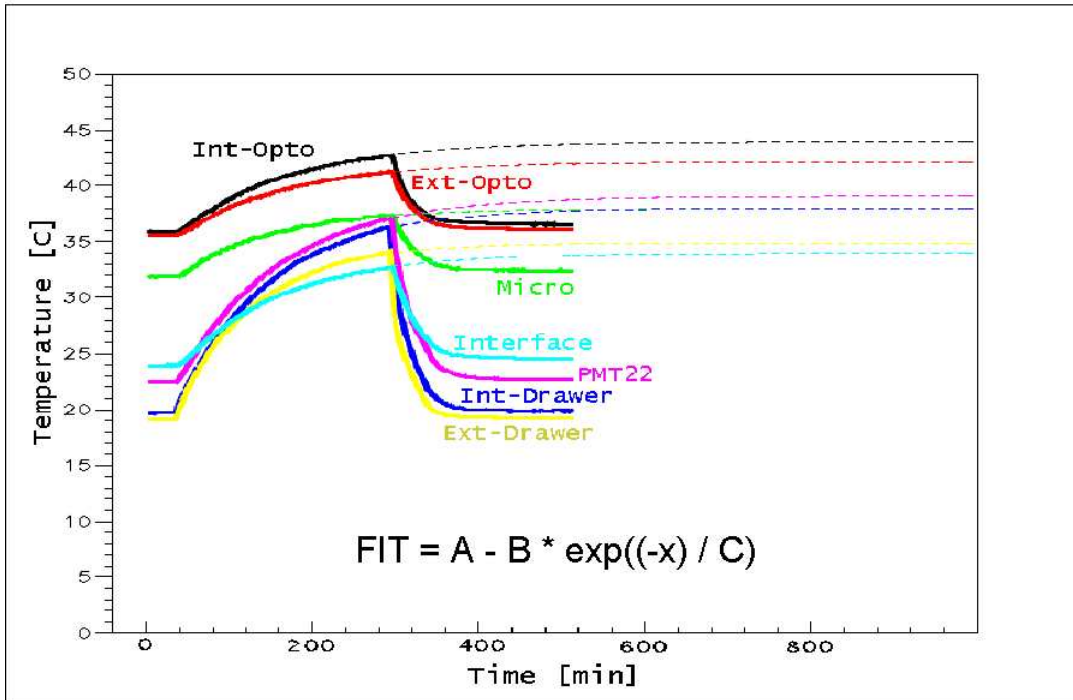
Figure 4.34: *Development of the temperatures inside the superdrawer of IFA 59 after stopping the cooling. The rise is expressed by the given formula. After 4:16 h the cooling was turned on again.*

When the cooling was stopped the temperature of all seven temperature sensors placed inside the superdrawer began to rise. The shape of the curve could be fit by the following expression:

$$T_{electronics} = A - B * exp(-\frac{x}{C})$$

(4.22)

The factor A represents the temperature after an infinite amount of time, factor B gives the difference between the temperature with cooling and without

cooling and the factor C represents the time constant for the gradient of the curve.

With the fit it was possible to estimate the final temperatures inside the superdrawer. The results are summarised in table 4.7. It can be seen that after 4 hours the maximum temperatures are already almost reached. The major temperature rise takes place in the first 2 to 3 hours. On the other hand it takes very long until a stable maximum temperature is reached.

in [°C]	t = 0 h	t = 4:16 h	t = infinity
Int-Opto	35.9	42.7	43.9
Ext-Opto	35.6	41.3	42.2
Micro	31.8	37.4	38
Int-Drawer	19.6	36.3	38
Ext-Drawer	19.1	34.1	34.9
PMT 22	22.4	37.1	39.1
Interface	23.9	32.7	34

Table 4.7: *Summary of the temperatures inside the superdrawer of module IFA 59 with cooling, after 4:16 h of no cooling and the estimated value after a infinite amount of time. It can be observed that after 4 hours most of the increase has already happened.*

Taking these results into account we can conclude that it is possible to operate the electronics for several hours without the cooling because critical temperatures of above 45°C are not reached. Nevertheless a massive temperature increase has to be accounted for. Hence the read out signal cannot be taken as calibrated measurement.

Chapter 5

The full-scale pilot project of the Tilecal cooling system

The ATLAS Tile Calorimeter as well as the LAr Calorimeter are foreseen to use cooling systems based on the Leakless System v.2 which works under sub-atmospheric pressure. Although this system was already running in other experiments, the huge dimensions and the severe environment calls for a full-scale model to check calculations, to test the foreseen components and to develop the control system.

For that reason a full-scale prototype (figure 5.1) was designed and installed in building 185 which also serves as a storage area for Tilecal modules and as pre-assembly site of the barrel and extended barrel cylinders [30].

5.1   Scope of the test

The main goal of the test was to study the Leakless System under the real dimensions of Tilecal. Therefore several hydraulic tests were carried out in order to study the behaviour of the installation and in particular to monitor the pressures at several keypoints in the circuits. Monitoring of temperatures was not foreseen because the water has always ambient temperature in this test.

The system was designed following the calculations presented in the document [38] and the drawings and annex 2 presented in the document [30]. The following points were foreseen to be checked with this installation:

- diameter of the return pipe and the regime of the flow which has a big impact on the pressure drop; additionally operational parameters as well as the pressure control system;

- the general automatic control of the system which includes the setup and implementation of the different control systems: PLC, PID, SCADA, AT-LAS ELMB and interlock for alarms;
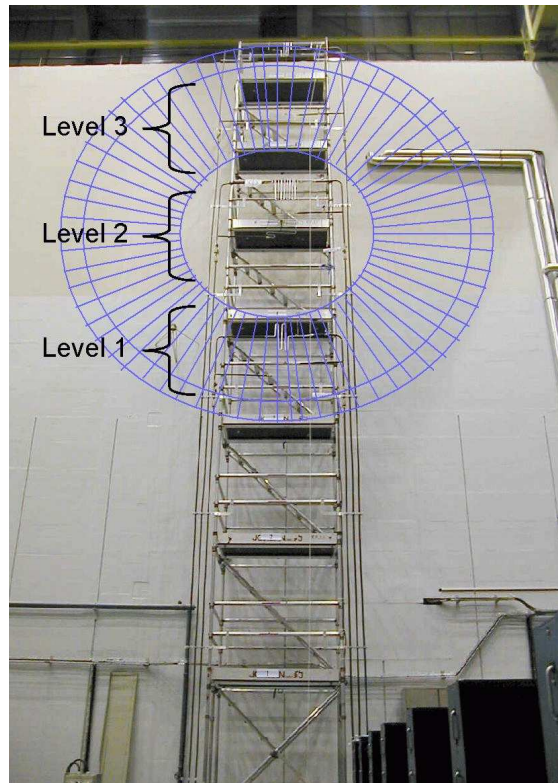
Figure 5.1: *The scaffolding for the full-size test including piping and cabling. Three levels are indicated which represent three sectors in different heights of the final Tilecal cooling layout (∼6.5 m, ∼9.1 m, ∼11.9 m). The round structure shows approximately the size of the Tile Calorimeter (outer diameter 4.23 m) compared to the full-scale installation.*

- the safety of the system; defined alarms and alert handling within the SCADA application but also the definition of a failure mode and the cause analysis; relieve valves and corrosion control; online analysis of the quality of the water;

- the foreseen components of the cooling system (valves, pipes, pressure transmitters, pneumatic system, etc.);

5.2 Layout

In order to simulate the real dimensions of Tilecal in ATLAS, a scaffolding was used to mount the pipes up to a height of almost 15 m. The final calorimeter will be separated into several sectors, each of them fed by an inlet and an outlet tube coming from the cooling station. As already mentioned this separation has to

be done in order to minimise the number of pipes and also to provide a pressure head of less than 3 m for each sector, needed for optimal operation of the Leakless System.

To simulate the sectors which will be at three different heights in the Tilecal, the piping on the scaffolding is divided into three levels at ~6.5 m, ~9.1 m and ~11.9 m. Each level is fed by one inlet pipe and one outlet pipe, hence there are six pipes in total connected to the cooling station.

Each level consists of two inner levels corresponding to the lowest module and the highest module in a sector. Both of these inner levels are equipped with a thinner pipe to simulate the pressure drop inside the modules and a pressure transmitter behind them. The three main levels have a pressure transmitter installed at the entrance to the level as well as a balancing valve and a pneumatic ON/OFF valve at both entrance and exit. The setup is illustrated in figure 5.2.

Level 1 and 3 correspond to sections with 12 superdrawers each, whereas level 2 only to sections with eight superdrawers. Therefore the flow of level 1 and 3 is set to a higher value than in level 2 in order to simulate the different amounts of superdrawers. Additionally, the thin pipe which is used to simulate the pressure drop inside the modules is longer in level 2.

The layout of the cooling station is shown in figure 5.3. Its main components are the storage tank (20), the water pump (24), the pneumatic ball valves (32) which can be used to isolate a circuit, the pneumatic control valve & converter (38) to regulate the pressure of the three levels and the differential pressure regulator (28) in order to maintain a constant pressure drop. All the key components are described in the next section.

5.2.1 Key components

In the following the key components of the full-scale test are presented and described. More details about the components can be found in the annex of the document [30].

Pneumatic ball valve

The valve is used to isolate certain parts of the circuit using a pneumatic system which can be remotely controlled. It is also possible to read out the status of the valve (on or off). (29 & 32 in figure 5.3)

Balancing valve

Balancing valves are used to set a defined flow in the circuit. They are also capable of measuring the flow and reading the pressure. Unfortunately they can only be read out by a special device and monitoring them with the PLC or PVSS is not possible.
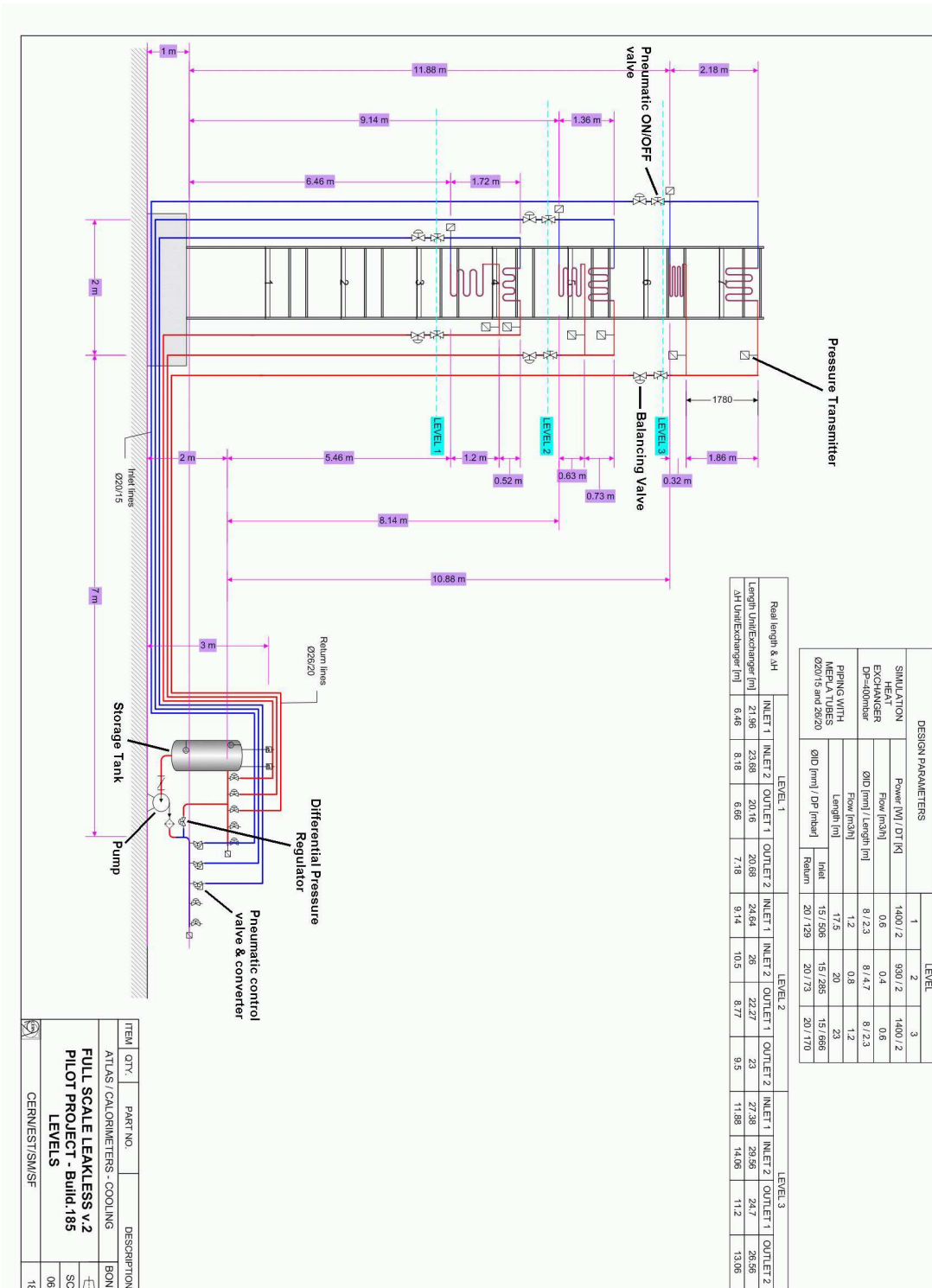
Figure 5.2: *Layout of the piping on the scaffolding for the full-scale test. The dimensions of the setup are given.*

DESIGN PARAMETERS

		LEVEL 1	LEVEL 2	LEVEL 3
SIMULATION HEAT EXCHANGER DP=400mbar	Power [W] / DT [K]	1400 / 2	930 / 2	1400 / 2
	Flow [m3/h]	0.6	0.4	0.6
	ØID [mm] / Length [m]	8 / 2.3	8 / 4.7	8 / 2.3
PIPING WITH MEPLA TUBES Ø20/15 and 26/20	Flow [m3/h]	1.2	0.8	1.2
	Length [m]	17.5	20	23
	ØID [mm] / DP [mbar] Inlet	15 / 506	15 / 285	15 / 666
	Return	20 / 129	20 / 73	20 / 170

		LEVEL 1				LEVEL 2				LEVEL 3			
		INLET 1	INLET 2	OUTLET 1	OUTLET 2	INLET 1	INLET 2	OUTLET 1	OUTLET 2	INLET 1	INLET 2	OUTLET 1	OUTLET 2
Real length & ΔH	Length Unit/Exchanger [m]	21.96	23.68	20.16	20.68	24.64	26	22.27	23	27.38	29.56	24.7	26.56
	ΔH Unit/Exchanger [m]	6.46	8.18	6.66	7.18	9.14	10.5	8.77	9.5	11.88	14.06	11.2	13.06

Pneumatic ON/OFF valve

Pressure Transmitter

Balancing Valve

Inlet lines Ø20/15

Return lines Ø26/20

Storage Tank

Pump

Differential Pressure Regulator

Pneumatic control valve & converter

LEVEL1 LEVEL2 LEVEL3

Figure 5.3: *Layout of the cooling station for the full-scale test.*

Pressure transmitter

Pressure transmitters are used to monitor the actual pressure. They are placed at various keypoints in the circuits and are connected to the PLC. (22 & 26 in figure 5.3)

Water pump

The pump is used to circulated the water in the system. It has to provide enough pressure to move the water up to 15 m. (24 in figure 5.3)

Differential pressure regulator

Sometimes it can happen that only a part of the circuit is running. If in such a case the pump still works with the same speed, the water flow in the running parts is not anymore the nominal one. Usually this problem is solved by automatically varying the speed of the pump but this is not possible in the severe electromagnetic environment of ATLAS. Therefore a mechanical solution was found: a differential pressure regulator will work as a discharge valve in order to maintain a constant pressure drop. (28 in figure 5.3)

Multilayer Mepla tube

The MEPLA tube was chosen for the Tilecal cooling system after a dedicated test was carried out, described in chapter 4.

Pneumatic control valve & converter

The Pneumatic control valve & converter is operated by the PLC and is located at the outlet of the cooling station. It regulates the pressure at the inlet of the three supplied levels. (38 & 39 in figure 5.3)

PID

The PID is used to control the pressures in the circuit and is implemented in the PLC as an algorithm.

PLC

The PLC is the "brain" of the system. It works like a computer and executes programs which are stored in an internal memory. It receives signals from the various sensors in the system, processes the signals and then acts on the components of the circuits according to the predefined programs. (41 in figure 5.3)

Water treatment & control

Corrosion can be a problem in the cooling circuit because Aluminium is used for certain parts of the pipes. Thus is was decided to use demineralised water at a conductivity of ~0.5 μS/cm. A secondary circuit is equipped with a resin filter and a transmitter to control the water quality. According to the quality of the water this secondary circuit will be opened or closed. The corrosion rate will be monitored in intervals with either spectroscopy or electro-chemical analysis. (42 & 43 in figure 5.3)

Tank liquid level transmitter

In order to be able to detect leaks or piping failures, the level of the water in the storage tank will be controlled permanently. Since most of the commercial models are not resistant to magnetic fields, an ultrasonic water level sensor is used. (44 in figure 5.3)

5.2.2 Monitoring of the system

The control of the system is performed by a Schneider Programmable Logical Controller (PLC). A Schneider OPC server is used as interface between the PLC and the PVSS application. Identically to the setup in the H8 test beam area described in chapter 4, the PVSS application will collect all the data and store it in the internal database. The PVSS application for the full-scale test is under development and configuration in this first phase of the project. Nevertheless it was possible to read out the PLC with a special laptop computer provided by the ST/CV group.

5.3 Measurements

5.3.1 Start sequence and run mode

Figure 5.4 shows the start up of the system and different run modes. The behaviour of the pressures at five different points in the installation is presented: the pressure at the pump, inside the storage tank, and at the inlet of each of the three levels.

At first everything is stopped and after some minutes the vacuum pump for the storage tank is activated. During this stand-by period the pressure inside the tank slowly decreases until it reaches a value of approximately -0.3 bar. The pump pressure decreases in exactly the same way (note that there is a different scale for the pump on the right side of the figure). At a certain point the pump is switched on and its pressure increases to 3.2 bar. Consequently also the inlet pressure of the three levels increases. In run mode the control valves are regulated
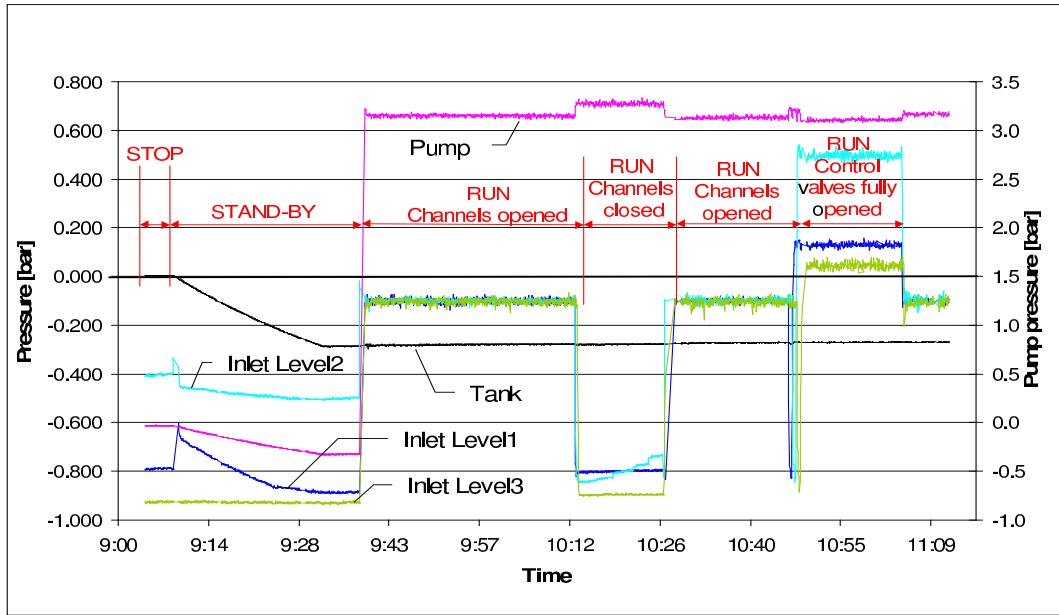
Figure 5.4: *The pressures of the pump, the tank and of the inlet of the three levels at start-up of the system and during several changes of the run mode. Note that the pump pressure is given by the axis on the right whereas all the other pressures are given by the axis on the left.*

in such a way that the inlet pressures are kept at -0.1 bar to provide Leakless mode inside the modules. After some time the inlet pipes of the channels are closed with the isolating ball valves. Due to the pressure drop caused by the height difference between the tank and the three levels, the pressures decrease to -0.8/-0.9 bar. After opening the channels again the system changes back to the nominal pressures. As a last test the control valves were opened completely while the water was flowing. Consequently the inlet pressures rise according to the height and the flow rate of the corresponding level: Level 3 has a lower pressure than level 1 because it is higher. Level 2 has a higher pressure than the other two because its flow is lower.

5.3.2 Characteristics of the Leakless System
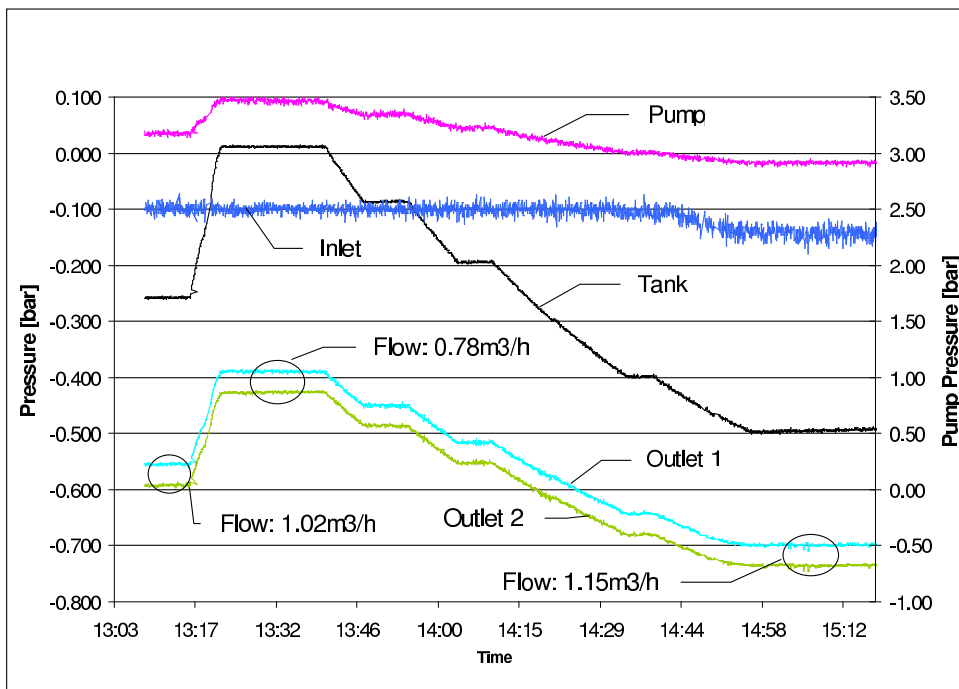
Figure 5.5: *The pressures of the tank, the pump and of the tree sensors in level 1 versus time. The tank pressure was changed in order to simulate a big air intake. Even if the tank pressure rises to the atmospheric level the modules will be always in Leakless mode because of the pressure drop due to the height difference.*

In this test it was studied if the Leakless mode would still be maintained in case of a major leak which would result in big amounts of air entering the system. In such a case the vacuum pump would not be able to maintain sub-atmospheric pressure inside the tank and assuming the worst case it would rise

to atmospheric pressure. Hence the pressure inside the tank was varied from atmospheric to nominal sub-atmospheric pressure and the behaviour of the circuit was monitored. Note that 'Outlet 1' and 'Outlet 2' corresponds to the pressure transmitter located lower respectively higher on the scaffolding.

The results are presented in figure 5.5 where the pressures are shown for the tank, the pump and the three sensors in level 1. The test starts with the Leakless System working in nominal mode (tank at sub-atmospheric pressure). Then a leak and the resulting air intake is simulated and the tank pressure raises to zero (atmospheric pressure). Consequently also the pressure inside level 1 raises but obviously sub-atmospheric pressure and therefore also Leakless mode is preserved. Afterwards the pressure in the tank is successively decreased to -0.5 bar and the pressure in level 1 as well as the pump pressure follow this behaviour. Additionally it can be observed that the flow changes with the tank pressure. This can be understood if the flow is seen as a direct consequence of the pressure difference between inlet and outlet of the circuit. If the pressure difference increases also the flow increases.

The test showed that the Leakless mode will be maintained inside the modules even in the case of a major air intake and resulting increase of the tank pressure. The reason is the height difference between the tank and the levels which creates a large pressure drop.

For the two higher levels it was found that they are less influenced by the successive pressure changes in the tank. It seems that their pressure is already very low due to the big height difference and is not very much influenced by the tank pressure.

5.3.3 The pressure control system

The inlet pressure of the levels is set by three pneumatic control valves located at the cooling station. They are controlled by the PLC and keep the pressure stable around -0.1 bar. Without these valves the pressure in the levels would exceed atmospheric pressure and Leakless mode would not be ensured.

The control valves are operated pneumatically by an e-p (electrical to pneumatic signal) converter which converts the electrical signals given from the PLC into air pressure. This air pressure is transmitted to the valve via a pneumatic line - a small plastic tube with 4 mm outer diameter. In the final ATLAS setup the converter will be placed in a side cavern, specially built for services of the detector. Hence the pneumatic lines have to transmit the air pressure from one cavern to the other.

To test the reliability of the pneumatic system working with such long lines a dedicated test was carried out where a 50 m and a 150 m pneumatic line was used to operate the control valve of level 2 and 3.

The measurement can be seen in figure 5.6. Only level 2 is presented because it was stronger affected by the change than level 3.

At first a 50 m line was used to operate the control valve. The pressures were kept stable at their nominal values. Then the system was switched off and the line was changed to a 150 m long one. As a result the fluctuations of the inlet pressure approximately double. The two outlet pressures obviously follow the behaviour of the inlet pressure and their fluctuations also increase by a factor 2.

The conclusion can be drawn that there will be a deterioration of the stability of the regulated pressure. But the effect is relatively small and still acceptable.

In the final ATLAS setup a 150 m long pneumatic line will be needed to connect the control valve in the main cavern with the unit that operates this valve which is situated in a side cavern.
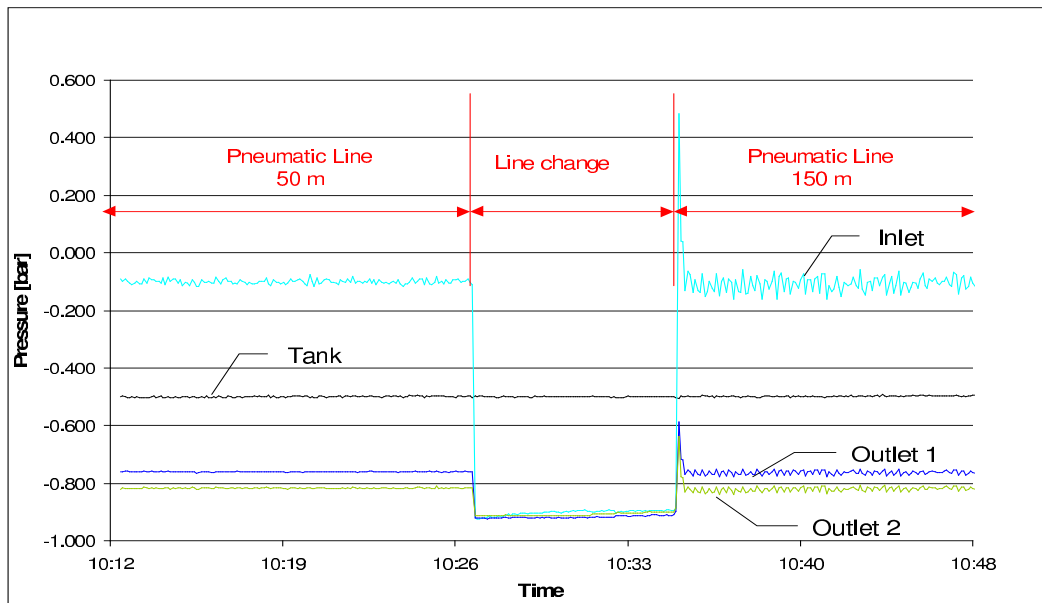
Figure 5.6: *The inlet and outlet pressures of level 2 and the tank pressure versus time. The pneumatic line which operates the control valve that is used to regulate the inlet pressure of the level was changed from a length of 50 m to 150 m. The result was an increase of the fluctuations of the pressures by approximately a factor 2. In the final ATLAS setup a 150 m long pneumatic line will be needed to connect the control valve in the main cavern with the unit that operates this valve which is situated in a side cavern.*

5.3.4   Comparison of measurements and calculations

For the dimensioning of of the full-scale test the standard equations for pressure and flow, as described in [38], were used. They are based on the assumption of an incompressible liquid and steady flow.

The measurements of the pressure drops in the circuit showed however clear variations from the calculated values. In particular the pressure drop in the return pipes as well as the pressure drop in the thin pipes which simulate the modules did not correspond to the calculated values.

Pressure drop inside the thin pipes

The pressure drop in a pipe has two contributions. First the linear pressure drop inside the pipe due to friction which can be expressed as [38]:

$$\Delta p_{tube} = \rho * \lambda * \frac{L}{D_i} * \frac{v^2}{2} \tag{5.1}$$

(ρ ... fluid density, λ ... friction factor, L ... length of tube, D_i ... inner diameter, v ... fluid velocity)

The friction factor is different for laminar and turbulent flow. In this case the flow is turbulent and the factor is defined as $\lambda = 0.3164 * Re^{-0.25}$ where Re is the corresponding Reynolds number.

The second contribution to the pressure drop comes from the height difference [37]:

$$\Delta p_h = \rho * g * \Delta z \tag{5.2}$$

(g ... acceleration of gravity, Δz ... height difference)

The final pressure drop in the tube is:

$$\Delta p_{tot} = \Delta p_{tube} + \Delta p_h \tag{5.3}$$

The measured values for the thin tubes in the different levels were approximately 45% higher than in the calculation. The values for three representative levels are given in table 5.1

Position	Measured value [mbar]	Calculated value [mbar]
Level 1 Outlet 1	600	410
Level 2 Outlet 1	660	457
Level 3 Outlet 2	760	508

Table 5.1: *The measured and the calculated values for the pressure drop inside the thin pipes which simulate the pressure drop of the modules are given. The measured values are approximately 45% larger than the calculated ones.*

Pressure drop inside the return pipe

In a dedicated test the return pipe of level 3 was exchanged with a pipe with smaller diameter. According to the calculations the pressure drop (ΔP_{tube}) in the smaller pipe is 4 times bigger than in the big pipe (see table 5.2). Since the pressure in the tank is fixed, a significant change of the pressure in the outlet of level 3 was expected. But no changes could be observed.

	Inner diameter [mm]	Outer diameter [mm]	Calculated pressure drop ΔP_{pipe} [mbar]
Big pipe	20	26	147
Small pipe	15	20	575

Table 5.2: *The dimensions of the two return pipes and their calculated pressure drop (ΔP_{pipe}). During a dedicated test these pipes were exchanged for level 3 in order to measure the different pressure drops.*

Possible explanation

The height difference between the water level in the tank and the outlet of lowest level is approximately 7 m. Usually the pressure drop for one meter height difference is 0.1 bar. This would mean at least 0.7 bar pressure drop between the lowest level and the water in the tank. Taking into account that the tank is under sub-atmospheric pressure (-0.5 bar) the resulting pressure in the lowest level would be naively -1.2 bar – obviously impossible.

The possible explanation could be that due to the big height difference and the sub-atmospheric pressure in the circuit, the water starts to evaporate and gas bubbles develop in the pipes. The pressure of saturated water vapour is 0.023 bar at a temperature of 20°C [37]. This means that the water starts to boil if the pressure drops below this value. As a consequence of the gas bubbles the flow becomes unstable, the liquid becomes compressible and the equations used loose their validity.

In order to understand what happens with the pressure once the standard equations are invalid, the formula for the pressure of an ideal gas at a given height can be considered [37]:

$$p = p_0 \exp\left(-\frac{\mu g h}{kT}\right) \tag{5.4}$$

(p_0 ... pressure at $h = 0$, μ ... molecular mass, h ... height, k ... Boltzmann constant, T ... temperature)

According to the formula the pressure approaches absolute vacuum slower and slower with increasing height. A similar effect happens in the full scale

installation that can be seen in figure 5.7. The pressures for level 1 and level 3 are shown as well as the pump and the tank pressure. At a certain point the pump is switched off but all valves are kept open. The pressure in the pump resembles the pressure in the tank because they are on the same height. But the pressures of level 1 and 3 are all approximately at -0.92 bar regardless of their height difference of roughly 5 m. It seems that a minimum achievable pressure is reached for both levels.

The effect of water evaporation could cause increased corrosion of some components due to cavitation. For that reason also the corrosion is studied with the full scale prototype as explained later. If the evaporation occurs in the thin pipes of the system which simulate the modules then the efficiency of the cooling would rise because evaporation consumes heat.
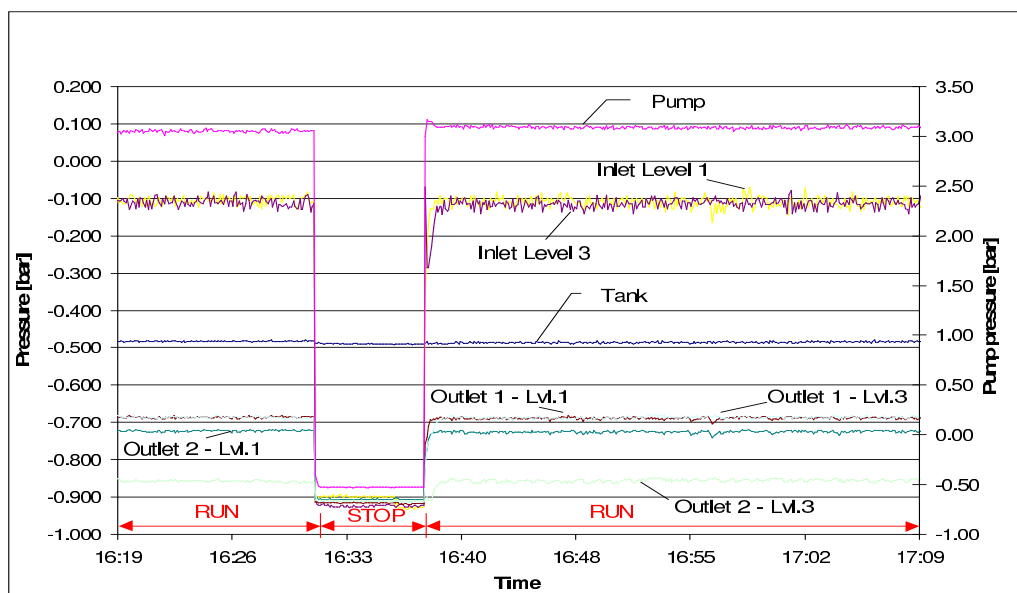
Figure 5.7: *The pressures of level 1 and 3 as well as the tank and the pump pressure. At a certain point the pump is stopped and the pressures of the different level reach the same value (∼-0.92bar). The pressure of the pump is similar to the tank because they are on the same height.*

5.3.5 Corrosion

The corrosion of components is an important factor in a cooling system which is also studied with the full-scale prototype. Demineralised water is used in order to decrease the conductivity and the subsequent corrosion of components like brass

valves or aluminium pipes. A water treatment unit, implemented in the circuit, keeps the water quality on a constant level.

The operation of the full-scale prototype during several months gives the possibility to evaluate effects arising due to corrosion. The final results will be available only after the end of the test, in spring 2003.

Chapter 6

Conclusions

This chapter gives a summary of the most important tests. Results and conclusions are presented.

6.1   Tests with the prototype cooling stations for module calibration

The prototype cooling station has been built in order to provide a cooling system during the calibration of the Tilecal modules. In total 12% of the modules will be calibrated with a particle beam and the rest with a Cs source. Hence two almost identical cooling stations have been built which were successfully operated starting from summer 2001.

6.1.1   Calorimeter response at different temperatures

The calorimeter response was measured for different temperatures with a particle beam of 180 GeV. It was found that the measured energy decreases with the temperature of the PMT following the formula

$$\frac{\Delta E}{E} = 0.2\%/°C_{PMT} \tag{6.1}$$

The result confirmed previous measurements of PMT characteristics. Combined with another measurement concerning the influence of the cooling temperature on the temperature of the electronics inside a superdrawer, a relation between cooling temperature and gain of the PMTs could be found:

$$\frac{\Delta G}{G} = 0.15\%/°C_{cooling} \tag{6.2}$$

Finally it could be concluded that in order to ensure a PMT gain stability of 0.5% the cooling water temperature has to be stable within 3.4°C, assuming that only the cooling water influences the PMT gain.

6.1.2 Stability of the Cooling system

The temperature fluctuation inside and outside the modules was monitored during several days of operation. A stability of $\pm 0.1°C$ could be observed for the cooling water temperature and the temperature sensors placed in various positions inside the superdrawer which is more than sufficient for the requirements of Tilecal.

In further tests the influence of the ambient temperature on the cooling water temperature was found. Improving the insulation of the sensor which controls the water temperature this dependence could be minimised to

$$\Delta T_{Cooling} = 0.3°C \quad per \quad \Delta 10°C_{ambient} \tag{6.3}$$

All the measured temperature fluctuations are well below the limits found in the test of the calorimeter response.

6.1.3 Evaluation of the foreseen tubes

Since in ATLAS there will be not enough space for insulation of the cooling tubes, a test was carried out to evaluate the suitability of the foreseen tubes. The so-called MEPLA tube was favoured because of several advantages compared to other models (eg. all-aluminium tubes). Additionally it was investigated if re-heaters are needed for the equalisation of the inlet temperatures.

The test showed that the temperature pick-up of the non-isolated MEPLA tube is

$$0.04°C/°C(ambient). \tag{6.4}$$

The estimated temperature gradient in the ATLAS cavern is $5°C$ between the lowest and the highest Tilecal module. The resulting maximum temperature difference is therefore $0.2°C$, which is negligible. Thus the concept of re-heaters could be abandoned.

Additionally calculations were carried out in order to cross-check the experiment with the theory. The results verified the measurements.

6.1.4 Consumed power of the Tilecal modules

The design of the cooling system was based on the theoretical properties of the electronic components. In the summer 2002 calibration period it was possible to evaluate the total consumed power of the electronics and to cross-check the values with the cooling design as shown in table 6.1.

It was found that the measured values suit to the designed values. But introducing a safety factor of 1.5 to correct for estimated ageing and radiation

	measured value	with safety factor 1.5
Ext.Bar. - IFA 38	129 W	194 W
Ext.Bar. - ANL 8	135 W	202 W
Barrel - JINR 18	166 W	249 W
Barrel - JINR 34	173 W	260 W
Barrel - M0-	182 W	273 W

	average value	average with safety factor 1.5
Extended Barrel	132 W	198 W
Barrel Module	174 W	261 W

	superdrawer	LV power supply
Design of Cooling unit	200 W	100 W

Table 6.1: *The measured values for the total consumed power (without and with a safety factor of 1.5) for two extended barrel superdrawers and three barrel superdrawers are presented. The average consumed power for both types of superdrawers are also given. Additionally the design values for the cooling system are presented again.*

damage of the electronic components in 10 years of operation, the real values exceeded the design values of the cooling system. Nevertheless the nominal cooling temperatures (Δ (T_{out}–T_{in})) can still be maintained for the temperature sensitive part, namely the superdrawers. Only the LV power supplies located in the fingers will probably receive cooling water at slightly higher temperatures than designed (Δ (T_{out} – T_{in}) $\simeq$ 3 °C).

6.1.5 Flow test

The flow test was carried out in order to determine the efficiency of the cooling and the optimal water flow. During several days the water flow was varied from 20 to 82 l/h, giving the system enough time to stabilise. After stabilisation the extracted heat for the corresponding flow was evaluated.

The results showed that the extracted heat reached a plateau at a flow of approximately 60 l/h. Hence this value is sufficient for the cooling system. The efficiency at 60 l/h was computed to be 71%. Since the superdrawers are surrounded by conducting iron walls, heat is lost to the outside and a higher efficiency is difficult to obtain. In ATLAS the lost heat finally has to be evacuated by the air conditioning system of the cavern and by the cooling system of the muon chambers which is currently under design.

6.1.6 Temperature increase without cooling

There is the possibility that the cooling will not be connected to the modules during the shutdown of ATLAS. Thus it was evaluated which are the highest reached temperatures inside a superdrawer, if the cooling is not connected. In general a temperature of approximately 45°C should not be exceeded in order to maintain a good performance of the electronics. A dedicated test showed that the maximum temperatures that have to be expected are below this limit and hence it should not be critical to carry out tests of the electronics at least during several hours.

6.2 Tests with the full-scale prototype

The full-scale prototype was built in order to check calculations, to test the foreseen components and to develop the control system for the Tilecal cooling system.

6.2.1 Functionality of the foreseen components

All the foreseen components used in the test worked according to their specifications. It was possible to control the whole system with the PLC. Valves and pressure regulators were tested, the pressures were monitored with pressure transmitters. The system was set into different operational modes and no problems have been observed. The pressure at the inlet of the three different levels was kept sufficiently stable even after the change of pneumatic lines of final length (150 m).

In autumn 2002 the magnetic and radiation tests of the used components will follow. In spring 2003 the results about the effects of corrosion will be available.

6.2.2 Control system

The control system is based on a dedicated PVSS-II application which uses a Schneider OPC server as interface to the PLC of the full-scale prototype. It is not yet completely finished but the implementation is straightforward because similar systems were installed for the prototype cooling stations for module calibration. The control system is planned to be operational end of September 2002.

6.2.3 Calculations

Comparison of measurements and calculations for the pressures in the circuit showed clear differences. It is possible that due to the low pressure which is created by the height and the sub-atmospheric pressure in the tank, water starts

to evaporate and gas bubbles develop inside the pipes. The water becomes compressible and the flow unsteady. As result the standard equations loose their validity.

6.3 Tentative final design recommendations

The prototype cooling stations for module calibration are working well. The temperatures are kept sufficiently stable at 18°C and no major problems have been observed. The only proposition is not to use the same PID controller in the final cooling station as currently used in the testbeam setup. This particular PID is a low cost device and the stability of the system could be improved by the use of a better model.

From the tests presented in chapter 4 the behaviour of the temperatures inside and outside the modules is well understood. Nevertheless it would be desirable to improve the absolute calibration of the seven temperature sensors inside the modules.

A final flow test with the final LV power supplies in the finger is still missing. It has to be clarified if the flow of 60 l/h is still sufficient. Maybe it has to be increased to 70 l/h which should be still achievable with the current layout.

For the full-scale prototype the simulation of a big leak in the inlet to the levels has to be carried out. The ultrasonic water level sensor has to be calibrated and an alarm has to be implemented in the PLC and PVSS. Also the corrosion has to be studied further and possible consequent changes of components have to be evaluated. The control system (PVSS) has to be completed.

The implementation of the control system with PVSS is also well understood. After the experience gained with the full-scale prototype it should be possible to implement the final control system for Tilecal without major problems.

Still missing are radiation and magnetic field tests of the components of the full-scale prototype. They have to be tested for functionality and be approved by TIS.

Appendix A

ATLAS Tile Calorimeter cooling system cost evaluation

ATLAS/TILE COOLING SYSTEM - COST EVALUATION - Draft 20/03/2002

Cooling Unit

		Unit	Quantity	Total
Tank stainless steel 1900l	DEPOSITOS COBALLES SL	2500	1	2500
Pompe CRN 32-40 Tri	GRUNDFOS PUMPEN AG	2450	2	4900
Butterfly valve Lug DN65	Zurcher-Technik	164	1	164
Heat plate exchanger 80kW	SWEP SWISS AG	1800	1	1800
Filtre tout inox DN65	TECOFI	535.46	1	535.46
Diff.pressure regul. SART DN20	Zurcher-Technik	2637	1	2637
Control valve B6R 16m3/h with pneum.actuator	SAUTER SA	828	1	828
Control valve V6R 1m3/h with pneum.actuator	SAUTER SA	603.9	24	14493.6
Filtre à tamis pour eau bronze 1"	40.15.10.116.1	12	1	12
Ball valve 316 - 3/4" with pneumatic simple actuator and position indicator	Zurcher-Technik	364	24	8736
Sight glass Meca-Inox a souder DN15	Zurcher-Technik	385	24	9240
Ball valve 316 - 1/2" with pneumatic simple actuator and position indicator	Zurcher-Technik	344	4	1376
Pressure transmitter -1/+1 bar, 0-10V	Huba Control	237.8	1	237.8
Pressure transmitter -1/5 bar, 0-10V	Huba Control	237.8	1	237.8
Press.Huba -50/-600 - Art.625.64430+105134	Huba Control	79.4	2	158.8
Ultrason liquid level transmit.	DIMAT	1608	1	1608
Manifold 24 channels Stainless steel	CERN mag	1200	2	2400
Piping cooling station Stainless steel	CERN mag	2000	1	2000
Frame cooling station	CERN mag	1500	1	1500
Demineralisation unit 50 liters	AQUAZUR	11347.77	1	11347.77
Accessories cooling station	CERN mag	500	1	500
Check valve 10mbar	40.10.30.106.3	75	2	150
Total Material				67362.23
Manpower ST/CV Piping/Welding	CERN/ST/CV	55	120	6600
Manpower ST/CV Electricity	CERN/ST/CV	55	40	2200
Manpower ST/CV Piping for connecting 52 valves	CERN/ST/CV	55	26	1430
Manpower ST/CV Test	CERN/ST/CV	55	40	2200
Manpower ST/CV for connect. in UX15	CERN/ST/CV	55	40	2200
Total Manpower		55	266	14630
Total cost material + manpower				81992.23

Control Unit

		Unit	Quantity	Total
PLC Premium, 32 Analog, 64 TOR	SCHNEIDER ELECTRIC SA	11254	1	11254
PLC Accessories, rack, cables, etc..	CERN mag	3150	2	6300
Vacuum pump KNF N026 220v	KNF (CH) NEUBERGER AG	366.8	1	366.8
Converter E->P XEP 0-10V	SAUTER SA	324	25	8100
Conductivity trans. Burkert	DIMAT	1258.6	1	1258.6

Description	Supplier/Ref	Unit	Qty	Total
Leakless control accessories	CERN-ST/CV R&D	200	1	200
Pneumatic distributor 3/2	BACHOFEN	140	72	10080
Rack Schroff for pneumatic	CERN mag	1420	1	1420
Total Material				38979.4
Manpower ST/CV Electricity/PLC	CERN/ST/CV	55	120	6600
Manpower ST/CV Test	CERN/ST/CV	55	120	6600
Manpower ST/CV Piping/Welding	CERN/ST/CV	55	40	2200
Total Manpower		55	280	15400
Total cost material + manpower				54379.4

USA15/UX15

Description	Supplier/Ref	Unit	Qty	Total
Electr. Power cable USA15/UX 100m	04.08.21.742.5	650	2	1300
Electr. Signal cable USA15/UX 100m	04.21.51.136.4	710	2	1420
Multitube polyam Ø4/2.7 X 12 - 50m	LEGRIS SA	626.4	20	12528
Connection for pneumatic	LEGRIS SA	10	200	2000
Total Material				17248
Cost for electrical/pneum. cabling	CERN Contract	55	40	2200
Total Manpower		55	40	2200
Total cost material + manpower				19448

Detector

Description	Supplier/Ref	Unit	Qty	Total
Balancing valve STAD1/2"F - Kvs 2.52	RIBAT	55	24	1320
Pneumatic HP valve 3/4"	RIBAT	271	48	13008
Pressure transmitter -1/+1 bar, 0-10V	Huba Control	237.8	12	2853.6
Mepla tube Alu/PE Ø26/20	GEBERIT SA	7.95	1200	9540
Mepla tube Alu/PE Ø40/33	GEBERIT SA	20.9	1000	20900
Mepla fitting mobil Ø26X3/4"M	GEBERIT SA	21	60	1260
Mepla fitting mobil Ø40X1"1/4F	GEBERIT SA	26.7	36	961.2
Mepla Equal Union fitting Ø26	GEBERIT SA	5.5	24	132
Mepla Equal Union fitting Ø40	GEBERIT SA	9.6	200	1920
Mepla Reduc Te fitting Ø26/20/26	GEBERIT SA	10.2	256	2611.2
Mepla Reduc Te fitting Ø40/20/40	GEBERIT SA	14.6	256	3737.6
Mepla Te fitting Ø26X1/2"XØ26	GEBERIT SA	18.3	48	878.4
Mepla Te fitting Ø40X1/2"XØ40	GEBERIT SA	29.5	48	1416
Multitube polyam Ø4/2.7 X 7 - 50m	LEGRIS SA	333	4	1332
Electr. Signal cable USA15/UX 100m	04.21.51.136.4	710	2	1420
Mepla miscellaneous accessories	GEBERIT SA	100	24	2400
Total Material				65690

Description	Supplier	Rate	Hours	Cost
Manpower ST/CV Piping for mepla Ø26 - 1200m	CERN/ST/CV	55	456	25080
Manpower ST/CV Piping for mepla Ø40 - 1000m	CERN/ST/CV	55	460	25300
Manpower ST/CV Piping for fixation mepla 2200m	CERN/ST/CV	55	473	26015
Manpower ST/CV Piping for pressing 976 fittings Mepla	CERN/ST/CV	55	340	18700
Manpower ST/CV Piping for bending Mepla	CERN/ST/CV	55	70	3850
Manpower ST/CV Piping for connecting 72 valves	CERN/ST/CV	55	36	1980
Cost for electrical/pneum. cabling	CERN Contract	55	11	605
Cost for electrical/pneum. connection	CERN Contract	55	13	715
Manpower ST/CV Leak test 8HX24	CERN-ST/CV	55	192	10560
Total Manpower		55	2051	112805
Total cost material + manpower				178495

Whole Cooling System

Description	Supplier	Rate	Hours	Cost
Manpower ST/CV Final test 8HX24	CERN-ST/CV	55	192	10560
Manpower ST/CV Documentation/Training	CERN/ST/CV	55	80	4400
Total Manpower		55	272	14960

Grand Total — CHF 350000

Description	Rate	Hours	Cost
Material			190005
Manpower Piping/Welding/Mechanic	55	2061H	113355
Manpower electricity/PLC/Test/Documentation	55	848 H	46640

Technical characteristics

4 X 64 drawers 300W each (200W in drawer + 10W in LV power supply)
1 cooling unit 77kW with 24 channels
Primary circuit: mixed water 14/16°C - 33 m3/h
Secondary circuit: demineralized water 16/18°C - 33 m3/h

Bibliography

[1] LHC - The Large Hadron Collider - Webpage, http://lhc-new-homepage.web.cern.ch/lhc-new-homepage/

[2] K. Hagiwara et al., Phys. Rev. D 66, 2002

[3] "The European Physical Journal C, Review of Particle Physics", Springer Verlag, 2000

[4] Fernando Varela Rodriguez: "The Detector Control System of the ATLAS experiment at CERN: An application to the calibration of the modules of the Tile Hadron Calorimeter.", doctoral thesis, Universidade de Santiago de Compostela, 2002

[5] ATLAS Collaboration: "ATLAS Technical Co-ordination", CERN/LHCC/99-01, ATLAS TDR 13, 1999

[6] ATLAS Collaboration: "ATLAS Technical Proposal for a General-Purpose pp Experiment at the Large Hadron Collider at CERN", CERN/LHCC/94-43, LHCC/P2, 15 December 1994

[7] CMS Collaboration: "CMS Technical Proposal", CERN/LHCC 94-43, 1994

[8] ALICE Collaboration: "ALICE Technical Proposal", CERN/LHCC 95-71, 1995

[9] LHCb Collaboration: "LHCb Technical Proposal", CERN/LHCC 98-4, 1998

[10] ATLAS Collaboration: "ATLAS Detector and Physics Performance Technical Design Report", CERN/LHCC/99-14, ATLAS TDR 14, 25 May 1999

[11] ATLAS Collaboration: "ATLAS Inner Detector Technical Design Report", CERN/LHCC/97-16, ATLAS TDR 4, 1997

[12] ATLAS Collaboration: "ATLAS Inner Detector Technical Design Report", CERN/LHCC/97-17, ATLAS TDR 5, 1997

[13] ATLAS Collaboration: "ATLAS Liquid Argon Calorimeter Technical Design Report", CERN/LHCC/96-41, ATLAS TDR 2, 1998

[14] ATLAS Collaboration: "ATLAS Tile Calorimeter Technical Design Report", CERN/LHCC/96-42, ATLAS TDR 3, 1998

[15] ATLAS Collaboration: "ATLAS Muon Spectrometer Technical Design Report", CERN/LHCC/97-22, ATLAS TDR 10, 1997

[16] ATLAS Collaboration: "ATLAS Magnet System Technical Design Report", CERN/LHCC/97-18, ATLAS TDR 6, 1997

[17] D. Fortin et al.: "Performance of the ATLAS Hadronic Endcap Calorimeter Modules to electrons and pions from 1999 Beam Test Data", ATL-LARG-01-nnn, HEC-Note-104, University of Victoria, Canada, 2001

[18] C. Fabjan et al.: "Grundlagen der Teilchendetektoren", Vorlesungsskriptum Teil 2, 2000

[19] A. M. Henriques Correia: "Development of a Lead/Scintillating-fibre Calorimeter for jet detection at LHC. Study of the Z' Vector Boson in the jet decay mode.", doctoral thesis, University of Lisbon, 1993

[20] T. Davidek: "Optimisation of the Light Collection from Scintillating Detectors", diploma thesis, 1995

[21] ATLAS Collaboration: ATLAS Calorimeter Performance Technical Design Report, CERN/LHCC 96-40, ATLAS TDR 1, 1996

[22] ATLAS collaboration (Calorimetry and Data Acquisition): "Results from a combined test of an electromagnetic liquid Argon calorimeter with a hadronic scintillating-tile calorimeter", CERN/PPE/96-178, 1996

[23] ALICE Collaboration: ALICE Technical Proposal, CERN/LHCC 95-71, 1995

[24] LHCb Collaboration: "LHCb Technical Proposal", CERN/LHCC 98-4, 1998

[25] C. Fabjan, T. Lundlam: Ann. Rev. Nucl. Part. Sci. 32, 1982

[26] ATLAS Collaboration (Calorimetry and Data Acquisition): "Results from a new combined test of an electromagnetic liquid argon calorimeter with a hadronic scintillation-tile calorimeter", Nucl. Instrum. Methods Phys. Res., A:449 (2000) no.3, pp.461-477, 2000

[27] J. B. Budagov: "The e/h ration of the ATLAS Hadronic Tile Calorimeter", ATL-TILECAL-2001-001, 2001

[28] S. Nemecek: "Npe from muon response of Sep01 data", Talk during ATLAS week, February 2002

[29] P. Bonneau et al.: "Cooling system for the TILECAL hadron calorimeter of the ATLAS detector", ATL-TILECAL-98-139, 1998

[30] G. Blanchot et al.: "ATLAS Cooling System LCS v.2 Full Scale Test", ATLAS Project Document ATC-TL-ES-0001, 2001

[31] H. Boterenbrood et al.: "Vertical Slice of the ATLAS Detector Control System", 7th Workshop of Electronics for LHC Experiments, Stockholm Sweden, 2001

[32] P. Bonneau, P. Grenier, A.M. Henriques Correia, **G. Schlager**, F. Varela Rodriguez, G. Montrou, M. Vassent: "Performance and tests of the cooling system for the ATLAS Tile hadron calorimeter modules calibration",ATL-TILECAL-2001-006, 2001

[33] D. Acosta et al.: "Electron-Pion Discrimination with a Scintillating Fiber Calorimeter", CERN-PPE70-172, 1991

[34] R. Chadelas et al.: "High Voltage Distributor System for the Tile Hadron Calorimeter of the ATLAS Detector", ATLAS internal note, ATL-TILECAL-2000-003, 2000

[35] Frank P. Incropera, David P. DeWitt: "Fundamentals of Heat and Mass Transfer", Wiley, 5th edition, 2002

[36] N. Bouhemaid et al.: "Characterisation of the Hamamatsu 10-stages R59000 photomultipliers at Clermont for the TILE calorimeter", ATL-TILECAL-97-108, ATLAS internal note, 1997

[37] C. Nordling et al.: "Physics Handbook for Science and Engineering", Studentlitteratur, 1999

[38] P. Bonneau: "Leakless Cooling System V.2; Pressure drop calculations and assumtions", CERN ST/CV, 2001